Molecular and Structural Insights into *Chironex fleckeri* Venom

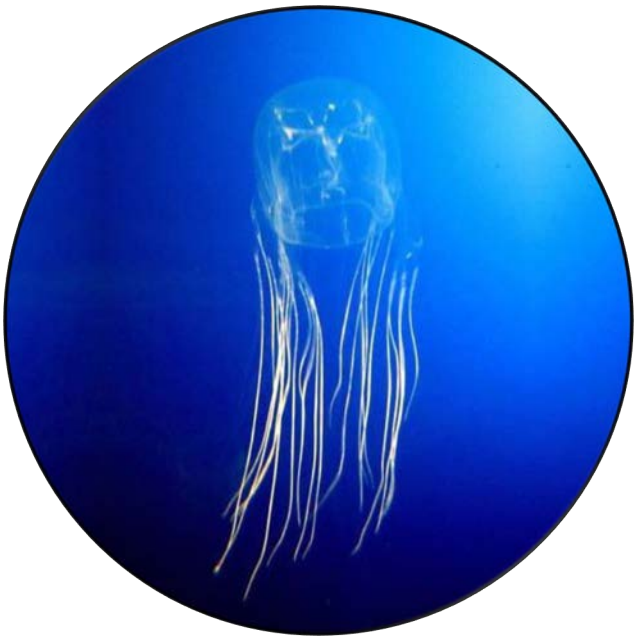

Athena Andreosso

M.Sc. Marine Biology

B.Sc.Biology

For the degree of Doctor of Philosophy in Medical and Molecular Sciences

College of Public Health, Medical and Veterinary Sciences

James Cook University, Cairns, Australia

1st February 2019

Acknowledgments

A PhD in Science has been my dream since before I even fully understood its meaning. It has been a long and incredible journey, that has led me through many countries with countless beautiful souls. To those countless souls I am ever so grateful. It was your laughter, the adventures and comfort we shared, that have helped me stay on track with my dreams and recognise opportunity when it knocks on the door. And what an opportunity it was! A PhD in the midst of tropical rainforests, creeks, sunshine, floods… and all the venomous creatures. Cairns, your ruthless nature is magnificent.

For this opportunity, I wish to express my deepest gratitude to my University and the College of Public Health, Medical and Veterinary Sciences. Thank you, for letting me become a Doctor in Medicinal and Biological Science, thank you for the scholarships that made this dream come true.

I would like to continue by expressing how profoundly grateful I am to my primary supervisor, **Prof. Norelle Daly**. I do not quite have the words to adequately describe the value of your guidance. The crisp, precise, strategic and thorough approach of your work had all the strengths I had yet to gain. Thank you for sharing your scientific knowledge and experience, your patience, your foresight, your diligence, your continuous support and, thank you, for the integrity of that support. Hands-down, the best supervisor I have ever had. I know the team agrees.

I would also like to thank my secondary supervisor **Dr. Michael Smout** for teaching me a good bulk of my skills, for always being there to stop science-tragedies from unfolding and for the odd geeky joke. It was delightful learning from you, thank you.

I wish to extend my gratitude also to my advisor, **Prof. Jamie Seymour,** for I have not forgotten how the prospect for my PhD came about. Thank you for introducing me to the spectacular world of venomous animals and for helping me in my quest to become PhD-candidate. I have certainly learned more than I had bargained for; thank you.

Now, a special thank you to **Dr. Paramjit Bansal**. Learning from you was marvellous! Between the jokes and the punches, the utter lack of instruction, you somehow taught me everything I needed to know about peptide synthesis. Thank you for all of it. You made my most dreadful days in the lab just a little bit brighter, with your outrageous, and yet sharp, running commentary on the flaws of human kind. You are a tremendous chemist and fabulously hilarious.

I also would like to thank **Dr. David Wilson, Dr. Paul Giacomin** and **Mr. Jeremy Potriquet** for their teaching, contribution and technical support. Dave, thank you for teaching me the ropes of the HPLC/mass spec. and for helping me troubleshoot, well… everything. Paul, thank you for your help designing the flow cytometry experiments as well as for your support with the data collection. Jeremy, thank you for your help with the identification of the venom proteins and for the many informative conversations about mass spectrometry. I have gained so many new skills in my PhD and it is all thanks to the great support I have received from the **AITHM-team**, thank you.

I would like to also express my gratitude to **Ms. Mohadeseh Dastpeyman** and **Dr. Claudia Cobos**, who on many occasions offered their help and support in the lab. Further I would like thank **Ms. Martha Cooper**, for assisting me with my statistical analysis and for the many spirited conversations; I have enjoyed them very much, thank you.

Also, I would like to thank the quirky members of the Tropical Australian Stinger Research Unit, in particular **Dr. Robert Courtney**, for helping with the jellyfish collection, **Ms. Jessica Sleeman**, **Mr. Richard Fitzpatrick** and **Ms. Sally Turner** for their feedback and friendship. This journey was a lot more fun with you lot in it.

My deepest gratitude goes out to **Ms. Imogen DaSilva**. If something had to happen quickly, you were the go-to person. Many PhD students will say Amen to that. But beyond that, I have gained a true friend (and a half – we mustn't forget Barnaby the Beagle) and your candid friendship has been refreshingly welcome.

Also, many thanks to the administrative staff of AITHM: **Ms. Mel Campbell** and **Mrs. Trilby Butcher,** thank you for your assistance and the occasional banter and **Mrs. Julie Woodward**, for your help, your encouraging smile and words.

Thank you very much for the help and opportunities that my College of Public Health, Medical and Veterinary Sciences. A special thank you to: **Mr. Tina Cornell, A/Prof Kerrianne Watt, Mrs. Kerry Knight and Mr. Shane Walker.**

Finally, and most importantly, a big warm thank you to **my family**. Thank you for your love and support and thank you, for letting me embark on my own adventures, over and over again, and yet always welcoming me back with open arms. To the fiercest woman I know, **my mum,** thank you for always believing I could achieve anything I set my mind to, for being tough when I needed you to be and for giving me the privileged life I have been lucky to have. Thank you to my **nonna,** for your unconditional love, the incredibly amazing food and the pride you have for me as your grandchild. You have thought me what it means to be a decent human being. To my **nonno**, my inspiration, for I have not met anyone with your tenacity,

endurance and your cheeky sense of humour. May you rest in peace, **nonno**. To my stepdad, **Raouf,** thank you, for you made sure there was always laughter in the house and for always lending me an ear when I needed it. To my **baby sister, Rachel,** you are my reason to keep going. I want to be better for you. I want to prove to you, that we can achieve anything we set our minds to, so that if you find yourself stuck one day, you can find hope in my path. Thank you, **Teresa, Flora, Claudia and Maggie** for always having an open door and for being the best aunts/stepmom anyone could hope for. You all deserve to be lived up to. Thank you, **Carlos**, my cousin, thank you for your advice and for sharing your experiences; they have guided many of my decisions. You have always been an inspiration, even if you haven't always felt like one. I feel nothing but love for you, brother. To everyone in my family, thank you for loving me with all my imperfections, for supporting me, embracing me. Thank you for the beautifully heated and ardent lunch time conversations that have turned me into the curious, critical and passionate human being I am today.

I would also like to thank my two extended Aussie families who have opened their doors to me without hesitation and given me a home away from home. To my **Kroombit family**, no words will ever express the gratitude I have for you. With genuine appreciation, you have thought me the value of a good work ethic, silence and patience. You are my happy place. To **Erryn, Jarred** and **Taleigha**, thank you for making me part of your family when I needed one. Without you, starting a life here in Cairns would have been a lot harder, infinitely more boring and a lot less homely. You are an extraordinary bunch.

Finally, to my gorgeous **wife**, **Katherine Elisabeth Mason.** You are my person. Thank you for your love, compassion and for hauling me over the finish line when I needed a little nudge. Thank you for listening to my frustrations, fears and occasional foolishness and for loving me despite of them. Every day is made more wonderful, any challenge is made easier and I am made a better human with your presence. Be mine, always.

This for you, **Caterina Pettinella**, my sister from another mister. I made it.

May I have the courage to live life just a little more like you did.

Rest in peace, *Chiappa mia*.

"Whatever it is you are seeking; won't come in the form you're expecting"

Haruki Murakami

Statement of The Contribution of Others

During my PhD candidature my thesis work has included:

1) Fluorescence microscopy
2) Fractionation and identification of complex venom samples (FPLC, mass spectrometry)
3) Biological assays (xCELLigence, Flow cytometry)
4) Peptide synthesis (synthesis, purification, mass analysis)
5) Structural analysis of peptides (NMR spectroscopy)
6) Thesis write-up

I have had great support from the AITHM team, a JCU scholarship and research grants. I have attached a list outlining the contributions from others in the following table.

Nature of Assistance	Contribution	Name and Affiliations
Intellectual support	Project Plan and Development	1) Prof. Norelle Daly, AITHM 2) Prof. Jamie Seymour, AITHM 3) Dr. Michael Smout, AITHM
	Data Analysis Assistance	1) Prof. Norelle Daly, AITHM 2) Prof. Jamie Seymour, AITHM 3) Dr. Michael Smout, AITHM 4) Dr. Paul Giacomin, AITHM 5) Mr. Jeremy Potriquet, AITHM
	Editorial Support	1) Prof. Norelle Daly, AITHM 2) Prof. Michael Smout, AITHM 3) Dr David Wilson, AITHM 4) Dr Paul Giacomin, AITHM
Financial support	Research Costs	1) Fellowship from NHMRC (1020114) 2) Australian Lions Foundation Research Grant
	Stipend	1) James Cook University International Postgraduate Research Scholarship (JCU-IPRS) 2) College Scholarship, College of Public Health, Medical and Veterinary Science, James Cook University
	Conference Travel Assistance	1) College Scholarship, College of Public Health, Medical and Veterinary Science, James Cook University – Stundent Allowance
	Write-Up Grant	1)Doctoral Completion Grant, College of Public Health, Medical and Veterinary Science, James Cook University
Data collection	Research Assistance	1) Dr. Michael Smout (FPLC, microscopy, cell assays) 2) Jeremy Potriquet (mass spectrometry) 3) Dr David Wilson (mass spectrometry) 4) Dr Paramjit Bansal (peptide synthesis)

		5) Dr Paul Giacomin (flow cytometry) 6) Prof. Norelle Daly (NMR)
Technical support	Peptide Synthesis Assistance	1) Dr Paramjit Bansal
	Purification / fractionation	1) Dr. Michael Smout 2) Dr. David Wilson
Biological material collection	*C. fleckeri* tentacles	1) Prof. Jamie Seymour
	Mouse blood	1) Ms Linda Jones (Prof. Alex Loukas-Group)

Published Works by the Author Incorporated into the Thesis

Chapter 4. Structural characterisation of predicted helical regions in the *Chironex fleckeri* CfTX-1 toxin.

Reference:

Andreosso, A., Bansal, P. S., Smout, M. J., Wilson, D., Seymour, J. E., & Daly, N. L. (2018). Structural Characterisation of Predicted Helical Regions in the *Chironex fleckeri* CfTX-1 Toxin. Marine drugs, 16(6), 201. doi:10.3390/md16060201

Author contributions: N.L.D, A.A, M.J.S, and J.E.S conceived and designed the experiments; A.A, P.S.B, and D.W. performed the experiments; A.A. and N.L.D. analysed the data; A.A and N.L.D wrote the paper. All authors analysed the results and approved the final version of the manuscript

Unpublished Works by the Author Incorporated into the Thesis

The following chapter will be submitted for publication shortly.

Chapter 3. Characterisation of cytotoxic proteins from *C. fleckeri* venom

Andreosso A., Potriquet J., Smout M.J., Giacomin P., Wilson, D., Seymour J.E., Daly N.L.

Author contributions: MJS, NLD, JES and AA conceived and designed the study. AA and MJS conducted the venom fractionation and the cell assays. AA and GP conducted the FACS assays. AA and JP carried out the mass spectrometry analysis. All authors analysed the results. AA wrote the manuscript. NLD, MJS and JES edited the manuscript. All authors approved the final version of the manuscript.

Abstract

This thesis focuses on the characterization of the bioactivity, composition, molecular pathways and structural aspects of *Chironex fleckeri* venom proteins. *C. fleckeri* is a box jellyfish that recurrently causes minor to fatal envenomations on the beaches of the northern half of Australia. While there is an antivenom available, its effectiveness is subject to controversy and a rapidly acting treatment has not yet been found. One essential aspect in developing such a treatment is to further the current knowledge regarding the venom components and their effects.

C. fleckeri venom is composed of a complex mixture of proteins which can cause rapid cardiovascular collapse in humans and animals. Two highly cardiotoxic, haemolytic and potentially pore-forming toxins have been previously identified, CfTX-1 and -2, and are thought to be the underlying cause for the cardiovascular collapse. Each of my chapters focussed on different toxinological aspects with the overall aim of shedding some light on the complex nature of *C. fleckeri* venom.

Chapter 2 focussed on the intracellular effects of *C. fleckeri* venom on human cardiomyocytes. While the chosen method, namely fluorescence microscopy, proved inadequate for the intended analysis of *C. fleckeri* venom, the study provided some interesting results. All cells consistently displayed loss of adherence, nuclear condensation and loss of membrane integrity. The nuclear condensation, an event often observed in apoptosis, has not been previously reported in relation to *C. fleckeri* venom.

Chapter 3 focussed on the characterisation of three previously reported bioactive fractions in the venom (CTF-α, CTF-β and CTF-γ). The previously reported cardiotoxic activity of CTF-α and CTF-β, but not CTF-γ, suggested the presence of the toxins CfTX-1 and -2 in the former two fractions. Interestingly, the mass spectrometric analysis revealed the presence of these

toxins in all three fractions, and further these toxins were most abundant in CTF-α, which in the present analysis displayed the least cardiotoxicity. Overall the fractions all contained CfTX-1 and -2, CfTX-A and -B as well as three other cubozoan toxins, CqTX-1, CaTX-A and CrTX-A, in differing proportions. This was reflected in the distinct bioactivity and activated molecular pathways of each of the fractions. Flow cytometry analyses revealed that neither *C. fleckeri* venom, nor CTF-α (top two hits: CfTX-1 and -2), induced apoptosis, whereas CTF-β (CaTX-A, CfTX-A and CfTX-B) and CTF-γ (CrTX-A and CfTX-A) treated cardiomyocytes were in early and late apoptotic stages, respectively. Overall, there was no apparent difference in bioactivity between cardiomyocytes and fibroblasts, whereas the effects of the venom on mouse erythrocytes was significantly higher than on human erythrocytes. This higher potency on mouse cells might explain why haemolysis is a symptom in laboratory animals but not in humans.

Chapter 4 represents the first structural analysis of a *C. fleckeri* toxin. Two predicted helical regions of CfTX-1 were synthesised to assess experimentally whether they had helical structure that may have some relevance in the putatively pore-forming activity of the venom. While complications were encountered in aqueous solutions, both peptides formed a helical structure in the membrane-mimicking solvent SDS. This data represents the first experimental structural data in favour of a pore-forming mode of action.

Overall this thesis has provided insight into the bioactivity of *C. fleckeri* proteins and their mechanisms of action, highlighted the complexity and the difficulty of working with animal venoms and provided some valuable insight for future studies, including those of a structural nature.

Table of Contents

CHAPTER 1

Introduction

1.1. Background on the venomous box jellyfish, *Chironex fleckeri*

Cubozoans, or box jellyfish, are a class of jellyfish that produce some of the most potent venoms in the animal kingdom [1]. While cubozoans inhabit tropical and subtropical oceans throughout the world, *Chironex fleckeri*, the most venomous box jellyfish [2], is found only in Australia. *C. fleckeri* occurs predominantly along beaches and estuaries that are located in the northern half of the Australian continent and its prevalence in shallow waters frequently leads to life-threatening human envenomations that require immediate medical attention [3].

Fortunately, the annual number of deaths due to *C. fleckeri* is low, but the large number of minor envenomations caused by this, and related, species represents a major cost to northern Australian communities in terms of public health, leisure and tourism [3]. Particularly at risk from life-threatening *C. fleckeri* envenomations are children, due to their proportionally increased body exposure, and remote communities, such as the Torres Straight Islands, where *C. fleckeri* is found in high abundance and access to emergency services is limited. Thus far, efforts to minimise or treat the number of victims has often been based on the best available opinion rather than empirical evidence [3-5]. A box jellyfish antivenom is available, although there are controversies over its effectiveness [6]. To find an effective treatment for *C. fleckeri* envenomation it is crucial to expand the currently limited understanding of the mechanism of action of the venom.

1.1.1. *C. fleckeri* envenomation

C. fleckeri envenomations mostly occur in shallow beach waters during Australian summer months. Envenomations are generally the result of the accidental entanglement of bathers with the jellyfish's tentacles. Contact with *C. fleckeri* tentacles triggers the rapid mechanical

discharge of nematocysts (venom capsules) that inject venom into their victim via harpoon-like tubules [7] (Figures 1 and 2). These nematocyst-tubules have the ability to penetrate epithelial layers and vascular walls, which enables the venom to be quickly distributed through the whole body [8]. Envenomation symptoms include instant severe pain (local, systemic and chest pain) as well as local cutaneous inflammation and necrosis [9-11]. *C. fleckeri* tentacles produce a distinct "frosted ladder" pattern on the skin of the victim, which can result in permanent scarring. In severe cases, victims can lose consciousness within seconds, followed by cardiovascular collapse which can result in fatal cardiac arrest less than 10 minutes post contact [10,12,13]. Other documented symptoms include arrhythmias [10,11], peripheral and coronary vasospasm, tachycardia, dilated cardiomyopathy [7,12], both rapid and weak irregular pulse and U-waves in leads I, II, aVR, aVF and chest leads V1 to V6 as well as massive pulmonary oedema with separated lung layers [12] (which indicates a cardiogenic pulmonary oedema [14]).

The cardiotoxic nature of the venom has been confirmed by several *in vivo* studies. For example, rats suffered a transient hypertensive response followed by hypotension and cardiovascular collapse within four minutes of *C. fleckeri* venom administration (0.03 μg/g) [15]. Similarly, after an initial increase in mean arterial pressure, partially purified *C. fleckeri* venom (0.025 μg/g) induced cardiovascular collapse in mice within one minute of administration [16]. However, the molecular mechanisms underlying the cardiovascular collapse remain largely unknown.

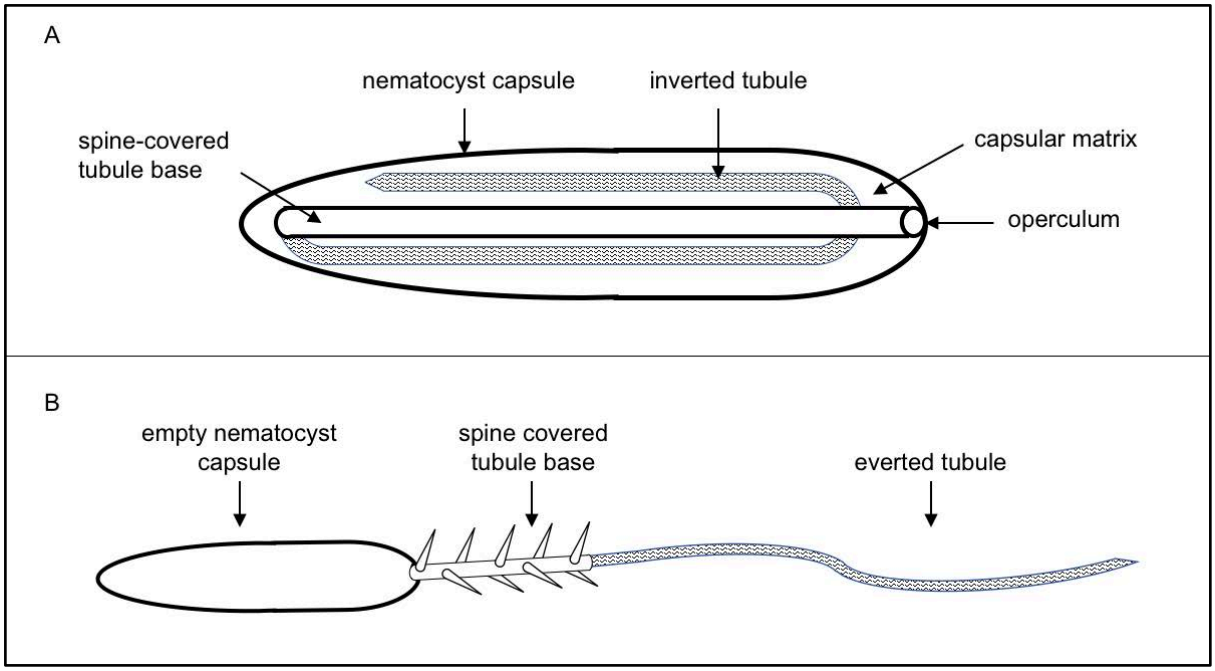

Figure 1: Simplified diagram of an (A) intact and (B) discharged *C. fleckeri* nematocyst.

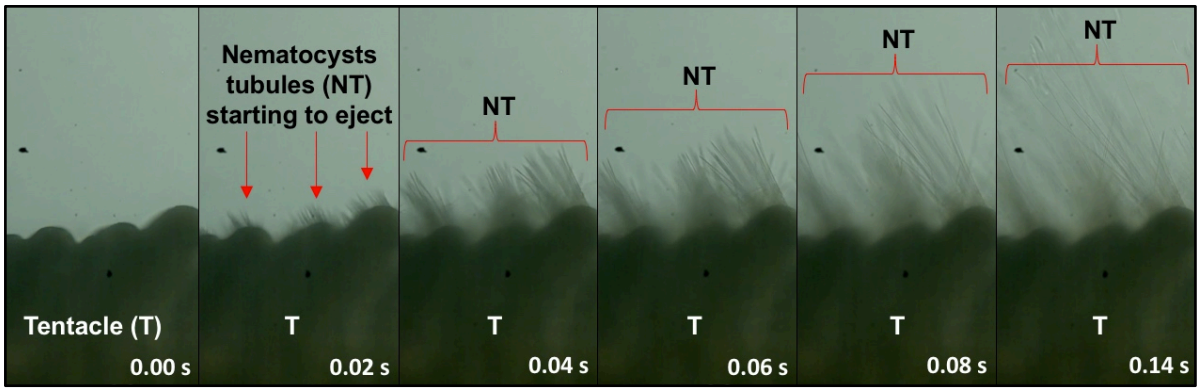

Figure 2: Sequence shots of a live nematocyst discharge time-lapse. The time point of each picture is indicated in the bottom right corner of each image. The dark green area represents the live tentacle (T) and the ejecting nematocysts tubules are indicated by the red arrows and brackets (NT). This image was created from Copyright material of BIOPIXEL.

1.1.2. Treatment for *C. fleckeri* envenomation

No generally effective treatment for *C. fleckeri* envenomation exists. The current first aid guidelines released by the Australian Resuscitation Council are summarized in Figure 3. Vinegar, as mentioned in the guidelines, is present at most tropical beaches and used as the primary local treatment for *C. fleckeri* (and other tropical jellyfish) stings. Vinegar prevents

venom capsules that have not been discharged, from doing so [17]. However, like other previously applied treatments (e.g. pressure immobilisation bandages [4,18] and ice packs [19]), there is no empirical evidence to show that vinegar is safe to use for box jellyfish envenomation. On the contrary, it was shown recently that venom capsules that have already discharged still retain about 40 % of venom within the capsule and, upon vinegar application, the remaining venom is released, and therefore has the potential to do harm when used as a treatment [5].

Current ARC first aid guidelines in tropical* Australia

- Remove victim from water, restrain if necessary
- If victim looks/feels unwell seek medical assistance (000 and lifeguard)
- Commence CPR if victim stops breathing
- Douse sting area with vinegar (30 seconds) and remove remaining tentacles
- If vinegar is inaccessible, remove tentacles, then rinse with seawater
- Do not pour freshwater over sting

* In the non-tropical parts of Australia, the sting may be caused by the 'Blue-bottle' and vinegar is not recommended as it may cause further firing of 'Blue-bottle'-nematocysts.

Figure 3. Summary of first aid guidelines for *C. fleckeri* envenomation as suggested by the Australian Resuscitation Council (ARC) (https://resus.org.au/guidelines)

C. fleckeri antivenom is carried on board Queensland emergency service vehicles. The antivenom is produced by the Commonwealth Serum Laboratories (CSL) in Melbourne from the erythrocytes of sheep treated with *C. fleckeri* venom. As mentioned above, evidence on the effectiveness of the CSL-antivenom is controversial. Antivenom is only effective if given prophylactically [20,21], resulting in difficulties when designing clinically relevant *in vivo* studies. For example, venom injected into chick biventer nerve-muscle preparations reduced the twitch height of the preparation. Antivenom administered after envenoming had no effect on venom-induced reduction in twitch height, whereas prophylactic administration of antivenom (10 minutes prior to venom administration) resulted in significant attenuation of the effect of the venom. Similarly, venom-induced inhibition of cell proliferation was prevented in A7r5 cells preincubated with antivenom (5 U/mL), in contrast to post-venom

antivenom administration [22]. However, *in vivo,* even prophylactic antivenom administration resulted in only 40 % survival in *C. fleckeri* envenomed (0.2 μg/g) rats as opposed to 0 % survival for the control group (no antivenom) [15]. In combination with magnesium sulphate, prophylactic antivenom administration resulted in 100 % survival of envenomed (0.03 μg/g) rats [15]. These results show that the antivenom can mitigate the venoms effects to some extent, but prophylactic administration is not in accordance with a clinically relevant setting.

In general, there are logistical problems with *C. fleckeri* antivenom in terms of timely dose, administration, and production. For instance, lack of knowledge of the amount of venom injected into a victim during an envenomation can prevent an accurate dose from being administered. In the case of a severe envenomation, cardiovascular collapse may occur before emergency services arrive at the scene. Additionally, antivenom is often given intra-muscularly [7]. Yet, the harpoon-like tubule from *C. fleckeri* nematocysts has the ability to penetrate epithelial layers and vascular walls; i.e. the venom is transported through the vascular system [8]. Therefore, intramuscular injection of antivenom at the sting site may be appropriate for local tissue damage; however, whether it is the right approach for neutralising the venom already in the vascular system, is debatable. Additionally, a recent study has shown that the effects of *C. fleckeri* antivenom are both dose and time dependent. Prophylactic doses of antivenom required 70 minutes to unfold their full effect in vitro and the doses required were approximately five times the currently recommended initial dose (max. 3 vials, i.e. 3 x 20’000 units) [23]. Furthermore, the variability of the effectiveness of the antivenom may be related to the geographical [22] and ontogenetic [24] differences in the venom from individual *C. fleckeri* specimens, i.e. the venom used for antivenom production may not be as potent as the venom from other *C. fleckeri* individuals. While some of these logistical problems can be

addressed (e.g. doses and intravenous administration), the timely arrival of emergency services is circumstantial, and the venom used for antivenom production is contingent to availability.

In conclusion, alternative treatments that block the key molecular pathways in the envenomation process may be required instead of, or in combination with, *C. fleckeri* antivenom. Also, given the circumstances, any treatment for severe *C. fleckeri* envenomation would ideally be accessible at the beach and unfold its full effects rapidly in a systemic manner.

1.1.3. *C. fleckeri* venom proteins

The characterisation of *C. fleckeri* venom proteins has been a challenge in terms of specimen collection, venom extraction and biochemical properties of the venom proteins. The protein composition and the potency of the venom vary depending on the size of the animal [24] as well as the geographical location and the year that a specimen is collected [22]. Venom from specimens collected in Weipa, NT showed a different protein composition on a 12 % SDS-page gel than venom collected from specimens in Broome, WA or Mission Beach, QLD [22]. This variation in protein composition was reflected in the activity of the venom, with venom from Weipa eliciting more potent toxicity in cells as well as distinct and more pronounced effects on the cardiovascular system of anesthetised rats than venom from Broome. Further, differences in venom composition were found between juvenile and adult *C. fleckeri* specimens, which correlated with an ontogenetic shift in dietary preference of the animals [24].

The extraction method used for analysis of *C. fleckeri* venom can also impact the proteins present in the samples. Early studies used tentacle extracts [e.g. 25,26] but an 12 %-SDS-Page gel comparison revealed that venom free of tentacular material has a different protein

140 composition than that found in the tentacles [27]. Tentacles are not injected in the
141 envenomation victim, making analysis of venom free of tentacular debris more likely to be
142 clinically relevant. In addition to inconsistent extraction methods, the venom proteins in *C.*
143 *fleckeri* venom have been reported to have a tendency to aggregate and adhere to surfaces
144 [26,28,29], making purification difficult. Further, primary sequence and SDS-PAGE analysis
145 indicated some of the *C. fleckeri* venom proteins are glycosylated which can complicate
146 analysis of the proteins, particularly with mass spectrometry [31|.
147
148 Despite the challenges in isolating *C. fleckeri* proteins, the recent consensus to work with *C.*
149 *fleckeri* nematocyst derived venom has led to the characterisation of several proteins that
150 belong to a family of potent toxins that are unique to cnidarians [16,32,33]. This family of
151 cnidarian venom toxins exhibit several biological activities including cardiotoxicity, pore-
152 formation, cytolysis, dermonecrosis and haemolysis [1,33,34]. Following a phylogenetic
153 analysis these toxins have been divided into Type I and Type II toxins [16]. Both toxin types
154 contain signal peptides, with the distinction that Type II toxins also generally contain an N-
155 terminal pro-region, which is typically a significant modulator in biosynthesis and activation
156 (e.g. transport, correct folding, post-translational modifications, etc.) [16]. Further, mature
157 Type II toxins tend to be shorter in sequence length (thus generally lower in molecular weight)
158 than Type I toxins. Despite these distinct characteristics, both toxin types have been predicted
159 to have similar secondary and tertiary structures [16]. Also, these cubozoan toxins are likely to
160 form dual-domain mature proteins, with a tendency to oligomerize to form large heterogenous
161 Type I or Type II holotoxins [16].
162
163 Thus far, the full cDNA sequences of five *C. fleckeri* venom proteins (CfTX-1, CfTX-2, CfTX-
164 A, CfTX-B and CfTX-Bt – protein sequence determined by Edman degradation) have been

identified and cloned [16,32]. CfTX-1 and -2 were classified as Type I toxins and CfTX-A, -B and -Bt as Type II toxins (Figure 4). Mature CfTX -1 and -2 are 436-residue and 445-residue proteins, respectively, with calculated molecular masses of 49,146 and 49,883 Da, respectively and estimated isoelectric points (pI) of 8.3 and 7.3 respectively [32]. Mature CfTX-A and -B are 429- and 430-residue proteins respectively with theoretical masses of 47,577 (pI 6.3) and 47,655 Da (pI 7.1), respectively [16]. A lower abundance C-terminal truncated form of CfTX-B was also cloned (CfTX-Bt; 296 residues; mol. weight: 31,293 Da; pI: 5.2) as a result of two distinctly identified cDNA populations encoding mature CfTX-B. Although the CfTX-Bt transcript was not found during the transcriptome assembly, a truncated form of CfTX-1 containing a signal sequence and a domain similar to the N-terminal domain was identified [35].

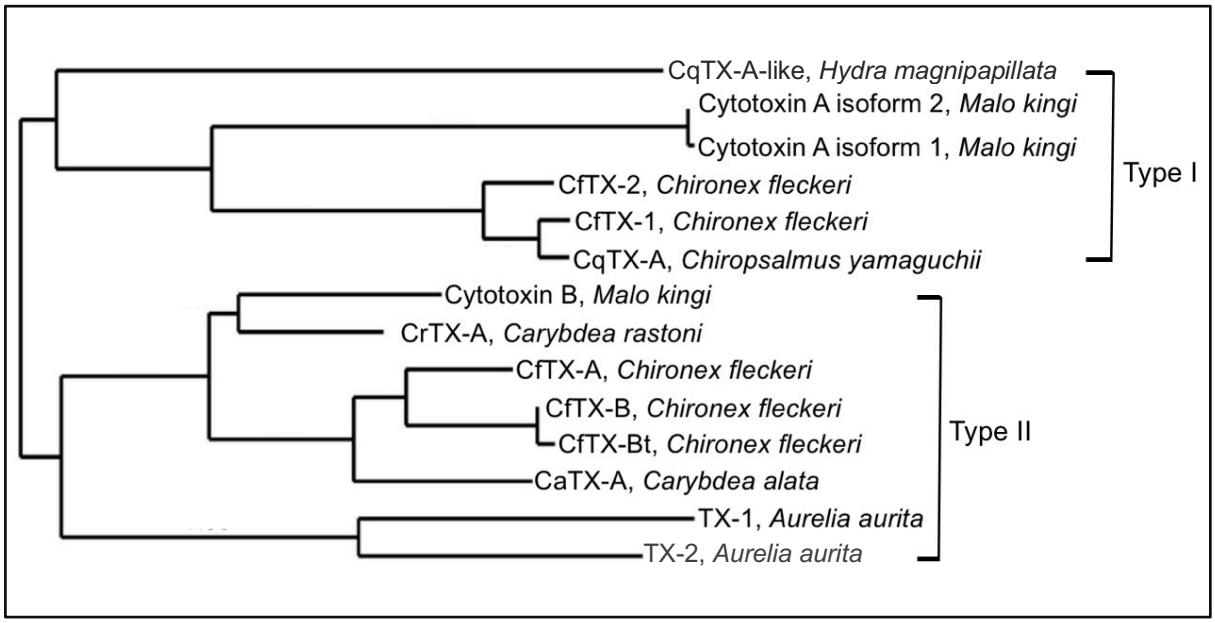

Figure 4: Simplified toxin phylogram as classified into Type I and Type II toxins by [16]. The toxin name is followed by the species name. All species belong to the class Cubozoa, except for *Aurelia aurita* (Scyphozoa) and *Hydra magnipapillata* (Hydrozoa).

Secondary structure prediction indicates that the first 300 N-terminal amino acids of all above-mentioned CfTXs are dominated by α-helices and loop regions, whereas the rest of the sequences were predicted to be dominated by β-sheets and loop structures [16,32]. For CfTX-1 and -2 an amphiphilic α-helix as well as a transmembrane spanning region were also

predicted in the N-terminal region. Because these structures are common in pore-forming toxins [36] and the predicted transmembrane spanning regions consist of a series of conserved amino acids (also found in CqTX-A from *Chiropsalmus yamagucchii*, in CaTX-A from *Alatina alata* and in CrTX-A and -B from *Carybdea rastoni*), pore-formation has been suggested as a potential common property of these cubozoan toxins [32]. Additionally, tertiary structure prediction of CfTX-A and -B suggests structural homology to pore-forming *Bacillus thuringiensis* three domain Cry-toxins (Crystal proteins [36]) [16]. Currently, no experimental structural data exists on full-length *C. fleckeri* venom proteins.

Analysis of the *C. fleckeri* transcriptome has indicated that the venom composition is quite diverse, with more than 170 potential toxin proteins. Seven of these potential toxins have sequence similarity to the previously characterised CfTX proteins and have subsequently been identified using tandem mass spectrometry [30]. Other putative toxins were identified including metalloproteinases, an α-macroglobulin domain containing protein, peroxiredoxin toxins, CRISP proteins, a turripeptide-like protease inhibitor as well as other proteases [35]. However, with only one transcriptome analysis conducted so far, and the lack of genome data, the current *C. fleckeri* venom proteome data is likely to be incomplete.

1.1.4. Mechanism of action of *C. fleckeri* venom

The mechanism of action of *C. fleckeri* venom is poorly understood, but insights have been gained by analysis of crude venom (i.e. the whole complex mixture of biomolecules from the nematocysts) or partially purified venom fractions from chromatographic techniques [6,20,27,37]. Based on the rise in calcium levels upon *C. fleckeri* venom treatment, an interference with transmembranic calcium channels was initially suggested [13]. Analysis of

209 the calcium channel blocker verapamil was controversial due to opposing results from different
210 research papers [13, 40]. Another study testing calcium (nifedipine, Ni2+) and sodium
211 (tetrodotoxin, strophanthidin, amilorides) channel blockers, as well as inhibitors of the
212 sarcoplasmic reticulum (ryanodine), suggested that a rise in sodium due to a non-specific cation
213 leakage through the cell membrane induced an excessive influx of calcium into the heart cell
214 [38]. Electron microscopic analysis indicated that the venom has pore-forming properties [39],
215 consistent with the ion influx into the cell [38]. It has been suggested that this spontaneous and
216 excessive Na+-mediated influx of Ca+ in cardiomyocytes triggers irregular contractions of the
217 single cell, resulting in an overall asynchrony and flagging in communal heart cell contractions,
218 thus causing arrhythmias leading to eventual cardiac failure [38].
219
220 Another hypothesis, suggesting that the envenomation symptoms originate from a
221 hyperadrenergic reaction, was refuted when a *C. fleckeri* venom induced an irreversible
222 contractile response on rat aortas despite prazosin treatment, an α1-adrenoreceptor antagonist
223 [6]. Further, venom induced hypertension and cardiovascular collapse in anaesthetized rats
224 could not be prevented by prasozin or ketanserin, a serotonin 5HT-receptor antagonist [27].
225 Thus, an α1-adrenoreceptor mediated hyperadrenergic response to *C. fleckeri* venom is
226 unlikely [6,27] and consequently, it appears likely that pore-formation is a key factor in the
227 venom induced cardiovascular collapse.
228
229 Based on the structural predictions of the CfTX-toxins it appears likely that these toxins are
230 responsible for the pores observed by electron microscopy [39], but this has yet to be
231 confirmed. For instance, other proteins are present in the crude venom, which could be
232 responsible for pore formation. Additionally, it is unknown what role and consequences the
233 pore formation has in terms of cell death; i.e. do the pores lead to cell death? Which type of

cell death? These questions, as well as how the proteins potentially insert themselves into the cell membrane, remain unanswered and need to be addressed.

1.2. Aims and significance

The present research project addressed *C. fleckeri* venom research gaps in terms of bioactivity, cellular death pathways and experimental structural analysis. Chapter 2 aimed to visualise the effect of *C. fleckeri* venom on the cardiomyocyte by using fluorescence microscopy. Chapter 3 aimed to characterise 3 bioactive venom fractions, two of which are known to be cardiotoxic, as well as a third fraction for comparison, in order to shed more clarity on the cardiotoxic mechanisms of the venom. Finally, Chapter 4 aimed to conduct an experimental structural analysis of two helical regions of the cardiotoxic and hemolytic *C. fleckeri* venom protein CfTX-1. The outcomes provide some clarity on how the venom and its toxins affect different cell types, in particular the cardiomyocyte, and potential mechanisms involved in cell death. Moreover, this project presents the first structural analysis of a *C. fleckeri* venom toxin, which is expected to provide a baseline for future structural studies on *C. fleckeri* venom toxins.

1.3. References

1. Brinkman, D.L.; Burnell, J.N. Biochemical and molecular characterisation of cubozoan protein toxins. *Toxicon* **2009**, *54*, 1162-1173.
2. Endean, R.; Pearn, J.; Covacevich, J. Venom of *Chironex fleckeri*, the world's most venomous animal. *Venoms and Victims. South Brisbane: Queensland Museum* **1988**, 15-24.
3. Bailey, P.M.; Little, M.; Jelinek, G.A.; Wilce, J.A. Jellyfish envenoming syndromes: Unknown toxic mechanisms and unproven therapies. *Medical Journal Australia* **2003**, *178*, 34-37.
4. Little, M. Is there a role for the use of pressure immobilization bandages in the treatment of jellyfish envenomation in Australia? *Emergency Medicine* **2002**, *14*, 171-174.
5. Welfare, P.; Little, M.; Pereira, P.; Seymour, J. An in-vitro examination of the effect of vinegar on discharged nematocysts of *Chironex fleckeri*. *Diving and Hyperbaric Medicine Journal* **2014**, *44*, 30-34.
6. Winter, K.L.; Fernando, R.; Ramasamy, S.; Seymour, J.E.; Isbister, G.K.; Hodgson, W.C. The in vitro vascular effects of two chirodropid (*Chironex fleckeri* and *Chiropsella bronzie*) venoms. *Toxicology Letters* **2007**, *168*, 13-20.
7. Currie, B. Clinical implications of research on the box-jellyfish *Chironex fleckeri*. *Toxicon* **1994**, *32*, 1305-1313.
8. Endean, R.; Rifkin, J. Envenomation involving nematocysts of the box jellyfish *Chironex fleckeri*. *Toxicon* **1983**, *21*, 115-118.
9. Tibballs, J. Australian venomous jellyfish, envenomation syndromes, toxins and therapy. *Toxicon* **2006**, *48*, 830-859.
10. Learmont, S.A. *Chironex fleckeri* (box jellyfish) envenomation: A case study. *Australasian Emergency Nursing Journal* **2006**, *9*, 49-56.
11. O'Reilly, G.M.; Isbister, G.K.; Lawrie, P.M.; Treston, G.T.; Currie, B.J. Prospective study of jellyfish stings from tropical Australia, including the major box jellyfish *Chironex fleckeri*. *The Medical Journal of Australia* **2000**, *175*, 652-655.
12. Maguire, E. *Chironex fleckeri* ("sea wasp") sting. The Medical Journal of Australia **1968**, 2, 1137.
13. Lumley, J.; Williamson, J.; Fenner, P.; Burnett, J.; Colquhoun, D. Fatal envenomation by *Chironex fleckeri*, the North Australian box jellyfish: The continuing search for lethal mechanisms. *The Medical Journal of Australia* **1988**, *148*, 527-534.
14. Ware, L.B.; Matthay, M.A. Acute pulmonary edema. *New England Journal of Medicine* **2005**, *353*, 2788-2796.

15. Ramasamy, S.; Isbister, G.K.; Seymour, J.E.; Hodgson, W.C. The *in vivo* cardiovascular effects of box jellyfish *Chironex fleckeri* venom in rats: Efficacy of pre-treatment with antivenom, verapamil and magnesium sulphate. *Toxicon* **2004**, *43*, 685-690.
16. Brinkman, D.L.; Konstantakopoulos, N.; McInerney, B.V.; Mulvenna, J.; Seymour, J.E.; Isbister, G.K.; Hodgson, W.C. *Chironex fleckeri* (box jellyfish) venom proteins expansion of a cnidarian toxin family that elicits variable cytolytic and cardiovascular effects. *Journal of Biological Chemistry* **2014**, *289*, 4798-4812.
17. Hartwick, R.; Callanan, V.; Williamson, J. Disarming the box-jellyfish: Nematocyst inhibition in *Chironex fleckeri. The Medical Journal of Australia* **1980**, *1*, 15-20.
18. Seymour, J.; Carrette, T.; Cullen, P.; Little, M.; Mulcahy, R.F.; Pereira, P.L. The use of pressure immobilization bandages in the first aid management of cubozoan envenomings. *Toxicon* **2002**, *40*, 1503-1505.
19. Cegolon, L.; Heymann, W.C.; Lange, J.H.; Mastrangelo, G. Jellyfish stings and their management: A review. *Marine Drugs* **2013**, *11*, 523-550.
20. Ramasamy, S.; Isbister, G.K.; Seymour, J.E.; Hodgson, W.C. The in vitro effects of two chirodropid (*Chironex fleckeri* and *Chiropsalmus sp.)* venoms: Efficacy of box jellyfish antivenom. *Toxicon* **2003**, *41*, 703-711.
21. Konstantakopoulos, N.; Isbister, G.K.; Seymour, J.E.; Hodgson, W.C. A cell-based assay for screening of antidotes to, and antivenom against *Chironex fleckeri* (box jellyfish) venom. *Journal of Pharmacological and Toxicological Methods* **2009**, *59*, 166-170.
22. Winter, K.L.; Isbister, G.K.; McGowan, S.; Konstantakopoulos, N.; Seymour, J.E.; Hodgson, W.C. A pharmacological and biochemical examination of the geographical variation of *Chironex fleckeri* venom. *Toxicology Letters* **2010**, *192*, 419-424.
23. Andreosso, A.; Smout, M.J.; Seymour, J.E. Dose and time dependence of box jellyfish antivenom. *Journal of Venomous Animals and Toxins including Tropical Diseases* **2014**, *20*, 34.
24. McClounan, S.; Seymour, J. Venom and cnidome ontogeny of the cubomedusae *Chironex fleckeri. Toxicon* **2012**, *60*, 1335-1341.
25. Keen, T. Interaction of the hemolysin of *Chironex fleckeri* tentacle extracts with lipid monolayers. *Toxicon* **1973**, *11*, 293-299.
26. Keen, T. Surface properties of the hemolytic fraction derived from tentacle extracts of *Chironex fleckeri*. *Toxicon* **1972**, *10*, 587-596.
27. Ramasamy, S.; Isbister, G.K.; Seymour, J.E.; Hodgson, W.C. Pharmacologically distinct cardiovascular effects of box jellyfish (*Chironex fleckeri*) venom and a tentacle-only extract in rats. *Toxicology Letters* **2005**, *155*, 219-226.
28. Olson, C.E.; Pockl, E.E.; Calton, G.J.; Burnett, J.W. Immunochromatographic purification of a nematocyst toxin from the cnidarian *Chironex fleckeri* (sea wasp). *Toxicon* **1984**, *22*, 733-742.

29. Othman, I.; Burnett, J.W. Techniques applicable for purifying *Chironex fleckeri* (box-jellyfish) venom. *Toxicon* **1990**, *28*, 821-835.
30. Brinkman, D.L.; Aziz, A.; Loukas, A.; Potriquet, J.; Seymour, J.; Mulvenna, J. Venom proteome of the box jellyfish *Chironex fleckeri*. *PLoS One* **2012**, *7*, e47866.
31. Sanaie, N.; Cecchini, D.; Pieracci, J. Applying high-throughput methods to develop a purification process for a highly glycosylated protein. *Biotechnology Journal* **2012**, *7*, 1242-1255.
32. Brinkman, D.; Burnell, J. Identification, cloning and sequencing of two major venom proteins from the box jellyfish, *Chironex fleckeri*. *Toxicon* **2007**, *50*, 850-860.
33. Brinkman, D.; Burnell, J. Partial purification of cytolytic venom proteins from the box jellyfish, *Chironex fleckeri*. *Toxicon* **2008**, *51*, 853-863.
34. Brinkman, D.L.; Mulvenna, J.; Konstantakopoulos, N.; Hodgson, W.C.; Isbister, G.K.; Seymour, J.E.; Burnell, J.N. Molecular diversity of box jellyfish toxins. *Toxicon* **2012**, *60*, 148-149.
35. Brinkman, D.L.; Jia, X.; Potriquet, J.; Kumar, D.; Dash, D.; Kvaskoff, D.; Mulvenna, J. Transcriptome and venom proteome of the box jellyfish *Chironex fleckeri*. *BMC Genomics* **2015**, *16*, 407.
36. Parker, M.W.; Feil, S.C. Pore-forming protein toxins: From structure to function. *Progress in Biophysics and Molecular Biology* **2005**, *88*, 91-142.
37. Saggiomo, S.L.; Seymour, J.E. Cardiotoxic effects of venom fractions from the australian box jellyfish *Chironex fleckeri* on human myocardiocytes. *Toxicon* **2012**, *60*, 391-395.
38. Mustafa, M.; White, E.; Hongo, K.; Othman, I.; Orchard, C. The mechanism underlying the cardiotoxic effect of the toxin from the jellyfish *Chironex fleckeri*. *Toxicology and Applied Pharmacology* **1995**, *133*, 196-206.
39. Bailey, P.M.; Bakker, A.J.; Seymour, J.E.; Wilce, J.A. A functional comparison of the venom of three australian jellyfish - *Chironex fleckeri*, *Chiropsalmus sp.,* and *Carybdea xaymacana* - on cytosolic Ca^{2+}, haemolysis and *Artemia sp.* lethality. *Toxicon* **2005**, *45*, 233-242.

CHAPTER 2

Fluorescence microscopy imaging and flow cytometry analyses of *C. fleckeri* venom effects on cardiomyocytes

2.1. Introduction

The rapid cardiovascular collapse observed in severe *C. fleckeri* envenomations has led to research focus on cardiovascular effects of the venom. In their attempts to understand these venom-induced cardiovascular effects on a systemic level, most research was conducted on live animals and animal tissue.

The *in vivo* and animal tissue studies have predominantly provided insight into the physiology of *C. fleckeri* induced cardiovascular symptoms as well as on the effectiveness of potential treatments. For example, *C. fleckeri* venom (0.5-30 μg/kg) caused a transient increase in mean arterial blood pressure followed by cardiovascular collapse within minutes in anaesthetised rats [1-4]. Due to this rise in arterial blood pressure, several blood pressure drugs were tested in combination with antivenom for their capacity to prevent cardiovascular collapse. Antivenom combined with magnesium sulphate prevented cardiovascular collapse only when pre-administered but could not attenuate the transient pressure response [2]. Neither the transient pressure response nor the cardiovascular collapse could be mitigated by antivenom or magnesium sulphate alone, verapamil [2], prazosin or ketanserin [1]. Also, *C. fleckeri* venom caused contractions in rat-isolated small mesenteric arteries, biphasic left atrial responses and decrease in right atrial rate followed by atrial standstill [4]. The effects on the arteries could not be attenuated by arterial blood pressure medications (prazosin, bosentan, calcitonin gene-related peptide ($CGRP_{8-37}$) or tetrodotoxin) and the effect on the atria could not be prevented by propranolol, atropine or $CGRP_{8-37}$, however atrial standstill was prevented by pre-treatment with *C. fleckeri* antivenom [4]. These results suggested that *C. fleckeri* venom acts directly on the cardiac muscle and not via sympathetic nervous system pathways [1,4]. Further, it remains questionable whether *C. fleckeri* antivenom has the capacity to be effective in a clinically

relevant setting (i.e. administration at least 10 minutes post-envenomation) [reviewed in 5] and therefore research has shifted towards understanding the mechanism of action of *C. fleckeri* venom on a cellular level.

The studies on the effect of *C. fleckeri* venom on cell lines are limited, with less than ten published studies, of which only four used human cardiomyocytes [6-9]. These studies on cardiac cell lines have primarily analysed the cytotoxicity of the venom or partially purified fractions. For example, *C. fleckeri* venom was found to be more toxic to cardiac cells than to skeletal muscle cells, and to act in a dose-dependent manner [6,9]. A subsequent study involving fractionation of the venom using size-exclusion chromatography, found that only peak two of the resulting A280 absorbance trace, appeared to be cardiotoxic [7]. Within this peak, fractions termed CTF-α and -β, were primarily responsible for the observed toxicity on human cardiomyocytes, with IC_{50} concentrations after ten minutes exposure to venom of approximately 0.25 μg/mL and 0.6 μg/mL, respectively [8]. The proteins present in these fractions were not determined. While these studies have provided insight into the properties and potency of the venom, none of them focussed on the intracellular effects.

Only one *in vitro* study has analysed *C. fleckeri* venom with a focus on its intracellular cardiotoxic effects. Ventricular rat and ferret myocytes were isolated and analysed post venom exposure with an electrophysiological approach, identifying non-specific ion leakage into the cell, with sodium-mediated spikes of intracellular calcium levels, and thus leading to the suggestion that *C. fleckeri* venom forms pores in cells [10]. However, this study used crushed tentacle extracts and thus it is not clear whether the observed effects on the cells stem from the tentacles, which are known to be cardiotoxic [1], or the venom itself.

As a result of the limited number of studies, very little is known about how *C. fleckeri* venom affects human cardiac cells or the organelles within the cell. Cell survival is related to the proper functioning of its organelles such as the nucleus and the mitochondria. Altered morphology of the nucleus has been implicated in different types of cell death [11] and some unpublished data exists that suggest that *C. fleckeri* venom reduces of the cellular nucleus (pers. communication Dr. Smout). Likewise, mitochondria are of particular importance to the functioning of the cardiomyocyte; heart muscle is a highly oxidative tissue; more than 90 % of the energy for cardiomyocytes comes from mitochondrial respiration [12]. Mitochondria are also involved in calcium cycling [13], which in turn is a key factor in the mechanism of the cardiomyocyte contraction. As such, altered mitochondrial function has been implicated in cardiac dysfunction and heart failure [14], for example, right ventricular failure is associated with increased mitochondrial activity [15]. Analysis of the effects of *C. fleckeri* venom on these organelles might direct future research into the mode of action of the venom.

This chapter assesses the effects of *C. fleckeri* venom on a variety of heart cellular organelles and the integrity of the cell membrane to provide a detailed analysis of the toxicity-induced damage to cardiomyocytes. Fluorescence microscopy and flow cytometry were used to provide a qualitative and quantitative analysis, respectively, of *C. fleckeri* venom on the heart cell and its organelles.

2.2. Methods

2.2.1. *C. fleckeri* venom collection and extraction

C. fleckeri specimens were collected for their venom from Weipa (12.6493° S, 141.8470° E) in March 2015. Nematocyst collection followed the method of Bloom et al., 1998 [16]. In brief, tentacles were removed from the specimens and placed into containers with ocean water at 4 ºC for 3 days. The containers were lightly shaken several times a day to promote autolysis of the nematocysts from the tentacles. On the third day, the solution was run through a fine wire mesh sieve to remove the tentacles and other large debris. The nematocyst solution was then lyophilised for 48 h and stored at -80 ºC until required for venom extraction.

Venom extraction followed the method of Carrette and Seymour, 2004 [17]. In short, approximately 5 µg of lyophilised nematocysts were put into 3 mL vials with approximately 0.5 mL of glass-beads and filled with Milli-Q-water (MQ) (at 4 °C). The mixture was shaken at 5,000 rpm in a Mini-BeadBeater-16 (Glen Mills, Inc., USA) 10 times for 2 min to maximise nematocyst rupture and venom yield. After each time in the beater the vials were cooled in ice slurry for 5 min. The mixture was then centrifuged for 45 s at 20 000 *g*. Finally, the supernatant (i.e. soluble venom proteins) was collected and subsequently lyophilised. The lyophilised venom was stored at -80 °C until required for use.

2.2.2. Cell culture

Human cardiomyocytes (ScienCell Research Laboratories, Inc., USA) were cultured following the manufacturers guideline in 5 mL Cardiac Myocyte Medium (ScienCell Research

Laboratories, Inc., USA), at 37 °C and 5 % CO2 in T25 monolayer flasks. Cells were allowed to grow to 60 % confluence before they were split. At 60 % confluence, cells were washed in 3 mL Dulbecco's phosphate buffered saline (PBS; Thermo Fisher Scientific, Inc., USA) and then detached by incubating for 3 minutes at 37 °C and 5 % CO2 with 1 mL TrypLE (Thermo Fisher Scientific, Inc., USA). The detached cells were then suspended in 5 mL of media, centrifuged at 37 ºC, 150 *g* and the supernatant TrypLE/media solution was discarded. The cell pellet was resuspended in 5 mL of media and introduced into new T25 flasks at approximately 5 % confluence. Cell splitting was conducted at least 4 times to ensure adequate viability of the cells before initiating the experiments.

2.2.3. Fluorescence microscopy

2.2.3.1. Cell transfer into chamber slides

The cardiac cells were transferred into 8-well chamber slides (Nunc™ Lab-Tek™ II Chamber Slide™ System, Thermo Fisher Scientific, Inc., USA; Figure 1) using the same procedure as for cell splitting. After addition of the cells, each well, i.e. chamber, was filled with 500 µL media. The chamber slides are equipped with a lid, allowing for cell incubation in similar conditions to tissue culture flasks. Further, the chambers are removable, turning the chamber slide system into a standard slide for microscopic analysis.

Figure 1: Lab-Tek™ II Chamber Slide™ System with 8 removable chambers and lid for incubation.

2.2.3.2 Optimising cell incubation and confluence in the chamber slides

To identify the shortest incubation period necessary for adequate cell adherence in the chamber slides, the cells were incubated for 24, 48 and 72 h. After the incubation, the cells were visually inspected under a brightfield microscope, then washed and inspected again. Washing entails the removal of old media, addition and subsequent removal of 0.3 mL of PBS (i.e. washing), and re-addition of 0.5 mL of fresh media.

To optimise cell confluence for the experiments; the chamber slides were incubated with concentrations 10,000, 20,000, 30,000, 40,000, 50,000 and 60,000 cells/mL and subsequently inspected under a brightfield microscope.

2.2.3.3. Optimising the staining procedure

Note: Due to the lack of literature for this staining procedure with the use of *C. fleckeri* venom, each step of this method was visually inspected under the brightfield microscope to ensure cells were still adhering to the slide surface or whether a step required optimising.

Following incubation, old media was removed, cells were washed (washing = addition and immediate removal of a solution) in 300 µL PBS (37 ºC) to remove debris and dead (floating) cells and new media (490 µL, 37 ºC) was added. Following the manufacturers guidelines, 10 µL of dye were added to the solution (total volume 500 µL) for 10 min, followed by another washing step in 300 µL PBS (37 ºC) and new media addition (480 µL, 37 ºC). The venom (20 µL) was added to the cell-media solution and allowed to incubate for 10 min (total volume 500 µL).

For the optimisation of the staining procedure, initially an in-well venom concentration of 10 µg/mL was used, as this is approximately the venom concentration that kills 50 % of the cells (IC_{50}) after 10 min in an xCELLigence real-time assay [7] (In 2.2.3.4. a venom concentration

more suited for the fluorescence imaging is determined). The venom-media solution was then decanted, and the chambers were removed.

For each dye three replicates, i.e. three chamber slides, were used. Of the eight chambers on each slide, four were used as control (480 µL of media + 20 µL MQ-water) and four were used for the venom (480 µL of media + 20 µL venom).

2.2.3.4. Venom concentration

The venom concentration was determined via Bradford assay. Seven tenfold dilutions of 285 µg/mL were conducted (lowest concentration: 0.285 ng/mL) and then added to the chambers. One chamber slide per concentration was used. On each chamber slide, four chambers were used for the venom and four were used for the Milli-Q-water-control (MQ-control), following the procedure described in (2.3.). The nuclear stain Hoechst 33342 (Invitrogen™, USA; see 2.2.3.5.1), a common user-friendly nuclear stain, was used to permit for visual inspection of the results under the fluorescence microscope.

2.2.3.5. Fluorescent imaging of the envenomed cardiomyocyte

Three aspects of the effects of *C. fleckeri* venom on the cardiomyocyte morphology were analysed:

2.2.3.5.1 Nuclear morphology

To visualise the effects of *C. fleckeri* venom on the nuclear morphology of cardiomyocytes, cells were incubated for 10 min with 5 µg/mL of the nuclear stain Hoechst 33342 (Invitrogen™, USA). Hoechst 33342 binds into the minor groove of DNA, preferentially to

adenine-thymine (A-T) regions (Invitrogen™, USA). This stain exhibits distinct fluorescence emission spectra that are dependent on dye:base pair ratios (Invitrogen™, USA).

2.2.3.5.2. Cell membrane integrity

Two stains were used for the assessment of the cell membrane integrity, Propidium Iodide (Invitrogen™, USA) and CellMask™ Deep Red (Invitrogen™, USA). Propidium Iodide (PI) is a non-permeant nuclear counter stain that is usually used in combination with a cell permeant dye like Hoechst 33342 to analyse the integrity of cell membranes. Intact healthy cells exclude PI, whereas cells with damaged cell membranes are stained brightly red. Cells were incubated for 10 min with in-well concentrations of 5 µM and 5 µg/mL of PI and Hoechst 33342, respectively. CellMask™ Deep Red is a plasma membrane stain that allows for the visualisation of the entire cell under the fluorescence microscope. Cells were incubated for 10 min with an in-well concentration of 5 µg/mL CellMask Deep Red [18].

2.2.3.5.3. Mitochondrial activity

To assess mitochondrial activity, cardiomyocytes were incubated with for 10 min with 100 nM MitoTracker™ Deep Red FM (Invitrogen™, USA). MitoTracker is a mitochondrion selective stain that is concentrated by active mitochondria. The more active the mitochondria are, the higher the intensity of the Mitotracker stain will be [19].

2.2.4. Flow cytometry

The cells were split and then counted to prepare 200 µL solutions of 500 000 cells/mL. For the first experiment, cells were incubated for 2, 10 and 30 minutes with 3 different venom

552 concentrations (80 ng/ mL, 8 ng/ mL and 0.8 ng/ mL) to determine a venom concentration and
553 incubation period that would allow for a decrease and increase (left- and rightwards shift,
554 respectively, on generated graphs) of the fluorescent signal intensity. Following incubation, the
555 cells were centrifuged at 150 *g*, at room temperature for 5 min, then the supernatant was
556 removed, and the cell pellet was resuspended in 0.2 mL media. The cells were then incubated
557 with propidium iodide for 10 min at a 5 μM.
558
559 All following experiments were prepared in the same manner, i.e. with the above chosen venom
560 concentration and with the corresponding dyes. Dye incubation times and concentrations for
561 Hoechst and MitoTracker™ Deep Red FM were 5 μg/mL for 10 minutes and 100 nM for 30
562 minutes, respectively, according to the manufacturer's guidelines. Following incubation with
563 the dye, the cells were centrifuged again at 37 °C, 150 *g* for 5 min and resuspended in 200 μL
564 of fresh media.
565 The cells were loaded onto a BD FACSCanto™ II flow cytometer (BD Biosciences) with the
566 BD FACSDiva™ software (BD Biosciences). For each sample, 10,000 cells were counted and
567 analysed. Fluorescence was measured in the FITC, Pacific Blue and PerCP-Cy5-5 channels
568 with excitation and emission wavelengths as follows: Propidium Iodide (493/636 nm),
569 Hoechst (361⁄497), MitoTracker™ Deep Red FM (581/644 nm). Statistical analysis was
570 carried out in GraphPad Prism 7.0; the data was tested for normality and then analysed via
571 One-way ANOVA with a Dunnett's multiple comparison test.
572

2.3. Results

To analyse the effects of the venom on cardiomyocytes a range of organelle specific fluorescent dyes were used. However, before these experiments could be carried out several parameters were assessed to guide the design of the staining experiments. These parameters included analysis of cell adherence to the chamber slides, incubation time of the cells with venom, the number of wash steps required to remove dead cells, dye or venom solution. Furthermore, the optimal venom concentration had to be identified, i.e. a concentration that would allow visualisation of the effects on the cells without a large percentage of cell death, or cells detaching from the surface of the chamber slides.

2.3.1. Fluorescence microscopy

2.3.1.1. Cell attachment, incubation time and cell confluence

Cell adherence, incubation time and cell confluence were assessed to ensure the cells were evenly spread across the wells and would not detach due to mechanical disturbances such as media or treatment addition or removal. Even distribution of the cells is also important for imaging purposes in order to facilitate focussed imaging and allow for systematic analysis.

Cardiomyocyte adherence to Lab-Tek® II Chamber slides was tested by incubating 30,000 cells/mL in 500 µL of cardiomyocyte medium for 24, 48 and 72 hours at 37ºC and 5 % CO_2. Visual inspection of the wells under a brightfield microscope showed that the cells were not adhering even after the longest incubation period of 72 hours (not shown). The experiment was repeated with Lab-Tek® II – CC2™ Chamber Slide™ System slides with a specialised CC2

coating for fastidious cells. Visual inspection showed that the cells were adhering well for all incubation periods, and subsequent experiments were carried out with these slides. However, when the cells were washed to test if they were still adhering after physical disturbances (i.e. adding and removing new media etc), cells incubated for less than 72 hours resulted in more than approximately 20 % cell detachment.

Using the Lab-Tek® II – CC2™ Chamber Slides the influence of cell confluence on photographic imaging was tested by incubating the chambers with a range of cell numbers (10,000, 20,000, 30,000, 40,000, 50,000 and 60,000 cell/mL) in 500 µL of media for 72 hours at 37ºC and 5 % CO_2. 20,000 cells/mL resulted in approximately 80 % confluence, which is recommended by the cell line manufacturer for ideal viability, whereas 30,000 cells/mL or more resulted in 100 % confluence and thus cell clustering, leading to difficulties in achieving adequate focus with the camera (Figure 2). Using 10,000 cells/mL was adequate for the purpose of imaging but resulted in only approximately 50 % confluence (Figure 2). Consequently, the concentration of 20,000 cells/mL incubated for 72h was used for all further experiments.

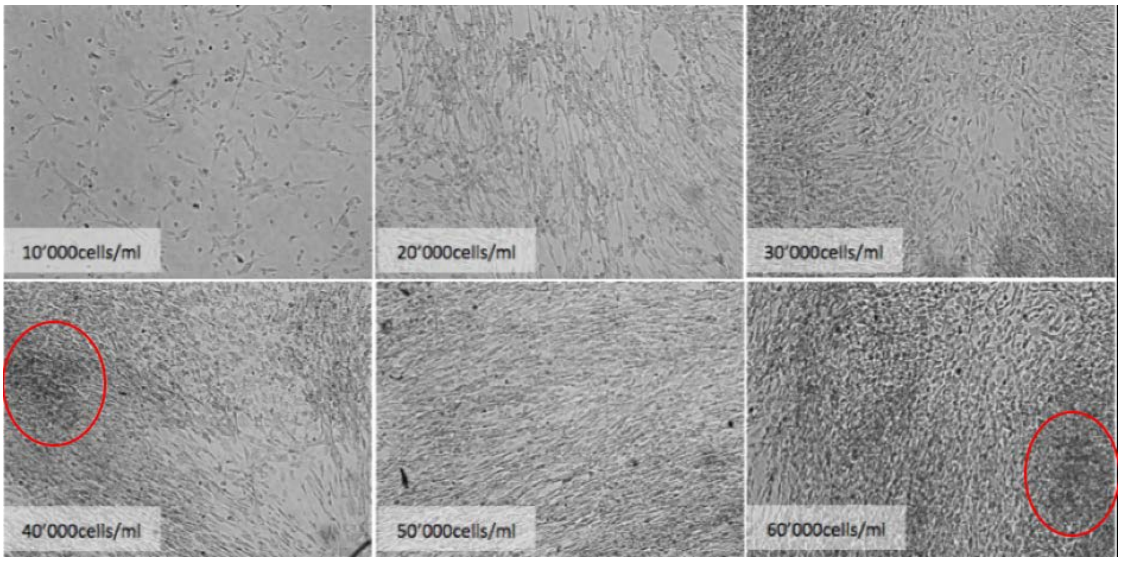

Figure 2: Brightfield images of different cell concentrations incubated for 72 h in Lab-Tek® ii-CC2™ Chamber Slide™ System (8-well chamber slides; 0.5mL/well). Cells with 30,000 cells/mL or greater resulted in overgrowth and clustering of the cells (see dark patches circled in red) making them unsuitable for systematic imaging. 20,000 cells/mL were chosen as the most suitable conditions for the following experiments.

618 ***2.3.1.2. Development of the staining procedure***

619

620 The chamber slide system is a method for the analysis of fixed cells, but the aim of the current
621 experiments was to study the effects of the venom on live cells, and therefore the
622 manufacturer's protocol had to be modified. The protocol recommended in the Lab-Tek® II –
623 CC2™ Chamber Slides protocol (without the fixation step), involves the following steps: 1)
624 cell wash, 2) dye addition, 3) cell wash, 4) treatment addition (i.e. venom), 5) chamber removal.
625 Because the original application of the slides differs from the current experiment, each step
626 was evaluated by visual inspection and adjusted (if necessary), as outlined below:

627

628 1) Wash

629 To remove dead or unhealthy cells (i.e. floating cells) from the chambers, old media
630 was decanted, the cells were washed in 300 µL pre-warmed (37ºC) PBS (with
631 subsequent removal of the PBS) and then 490 µL of new pre-warmed (37ºC) media was
632 added. However, based on visual inspection this procedure resulted in the cells
633 detaching from the bottom of the chamber slides. Replacing the PBS with media
634 resulted in only approximately 20 % cell detachment. A further improvement was
635 obtained when the media was applied very slowly and resulted in only approximately
636 5 % detachment of the cells.

637

638 2) Dye addition

639 Initial experiments were carried out using the nuclear stain Hoechst 33342 as it has a
640 simple staining protocol. Following the manufacturer's guidelines, cells were incubated
641 in the cell-media solution (490 µL) with 10 µL of dye for 10 minutes at 37 ºC (total
642 volume 500 µL). Visual inspection did not reveal any cell detachment, suggesting this
643 stain was appropriate to use.

3) Wash

To remove excess dye, another wash step was conducted with media (added gently) instead of PBS as described in step 1) of the experimental procedure. After the wash, 480 µL of new, pre-warmed media was added. Visual inspection indicated minor cell detachment with approximately 5 % of the cells floating in the fresh media solution, which was deemed acceptable for the experiment and consequently the effects of the venom were analysed.

4) Addition of venom and MQ-water control

The venom concentration initially chosen was 10 µg/mL, as this concentration has previously been shown to cause approximately 50 % cell death after 10 minutes when added to wells loaded with 3000 cells and incubated for 12 hours [7]. The venom concentration was optimised in a separate experiment, after the experimental procedure was established (See section 2.3.2.1). 20 µL of venom and 20 µL of MQ-water control were added to four chambers each and incubated for 10 minutes at 37ºC. Following incubation, the venom/media solution was removed. Visual inspection was carried out after chamber removal (see step 5).

5) Chamber removal

The chambers were removed following the manufacturers guidelines. Visual inspection after chamber removal revealed that the venom had leaked from adjacent chambers into the control chambers. This was identified by the presence of nematocysts and cell detachment in the control wells (i.e. wells without venom) (see Figure 3). This presence of nematocysts revealed two problems with the experiment. Firstly, it suggested that the venom used here was not free from larger debris; therefore, an additional filtration

step with a 45 µm filter was included in the venom extraction method used to remove any macromolecular debris, i.e. unruptured nematocysts from the venom. Secondly, there should not have been any leakage from one well across another, i.e. venom should not leak into control wells, which indicated that an additional wash was required after the venom addition and before the chamber removal. However, adding another wash to the staining procedure would have increased the risk of cell detachment yet again. Therefore, to keep the number of wash steps in the staining procedure low (i.e. two washes), it was decided to add venom and dye simultaneously, thus eliminating the wash step between dye and venom addition.

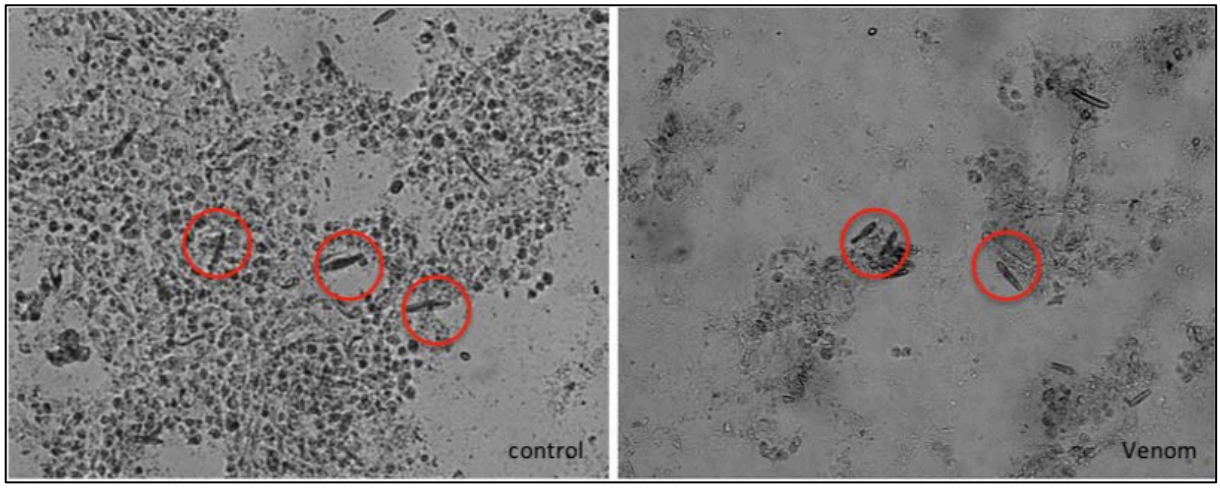

Figure 3: Two brightfield images (magnification 10x) showing leakage of venom to the neighbouring well. On the left is the control well (20 µL MQ-water) and on the right is a neighbouring well with *C. fleckeri* venom (20 µL at 10 µg/mL). Nematocysts (circled in red) were present in both the control and the venom wells, suggesting there was leakage across wells.

Consequently, the staining procedure was altered as follows:

Step 1: Wash

Step 2: Venom (or control) and dye addition

Step 3: Wash

Step 4: Chamber removal

With this modified staining procedure, upon visual inspection of the controls, only approximately 10 % of the cells detached in total during the two wash steps. However, the wells containing the venom showed significant cell detachment (data not shown), suggesting the venom concentration was too high and needed to be adjusted (see section 3.3).

2.3.1.3. Venom concentration

C. fleckeri venom can cause rapid cell death and detachment [7,8]; cell death and detachment occurring in under 20 minutes would have hindered the feasibility of the experiments as this is approximately the period required from the time point of envenomation to the time of microscopic analysis. Therefore, a concentration had to be identified that would cause enough damage to the cell to see the effects under the microscope without resulting in complete cell detachment from the surface of the chamber slides.

Seven concentrations (10-fold dilutions) between 285 µg/mL and 0.285 ng/mL were tested, following the experimental procedure established above and using the same fluorescent dye (nuclear stain Hoechst 33342). Visual inspection under the fluorescence microscope showed that the venom concentrations did not appear to display a typical dose-response-like effect on the cells (Figure 4). For example, there appeared to be more cell detachment at a concentration of 2.85 ng/mL (Figure 4F) than at 2850 ng/mL (Figure 4C). Secondly, in most replicates, this cell detachment resulted in large cell-less patches as well as clusters of floating cells which hindered clarity and focus during imaging; rendering the replicates unusable. While no images were taken of the unusable chambers, the lack of camera focus can be seen in nearly all the images (Figure 4A-G), including the Milli-Q-water-control (Figure 4H). Thirdly, each venom

chamber had a great level of variability within itself, i.e. in one area of the chamber, imaging was easily feasible while in another area of the same chamber cells were completely detached and lumped up on the edge of the chamber and/or images would appear blurry or completely out of focus.

Overall, it was difficult to systematically photograph the same section in each chamber across all samples. In addition, it was not feasible to have 7 samples in triplicates (1 replicate being 1 chamber slide with 8 chambers/wells) and triplicates of the control; the time required between the removal of the chamber housing and the capturing of the image was too extensive. Finding a usable area in a chamber and adjusting the focus to that area, often required up to 10 min; leading to fading of the fluorescent dye within that chamber, as well as in neighboring chambers. Figure 4A-H shows one image of the stained cells for each concentration.

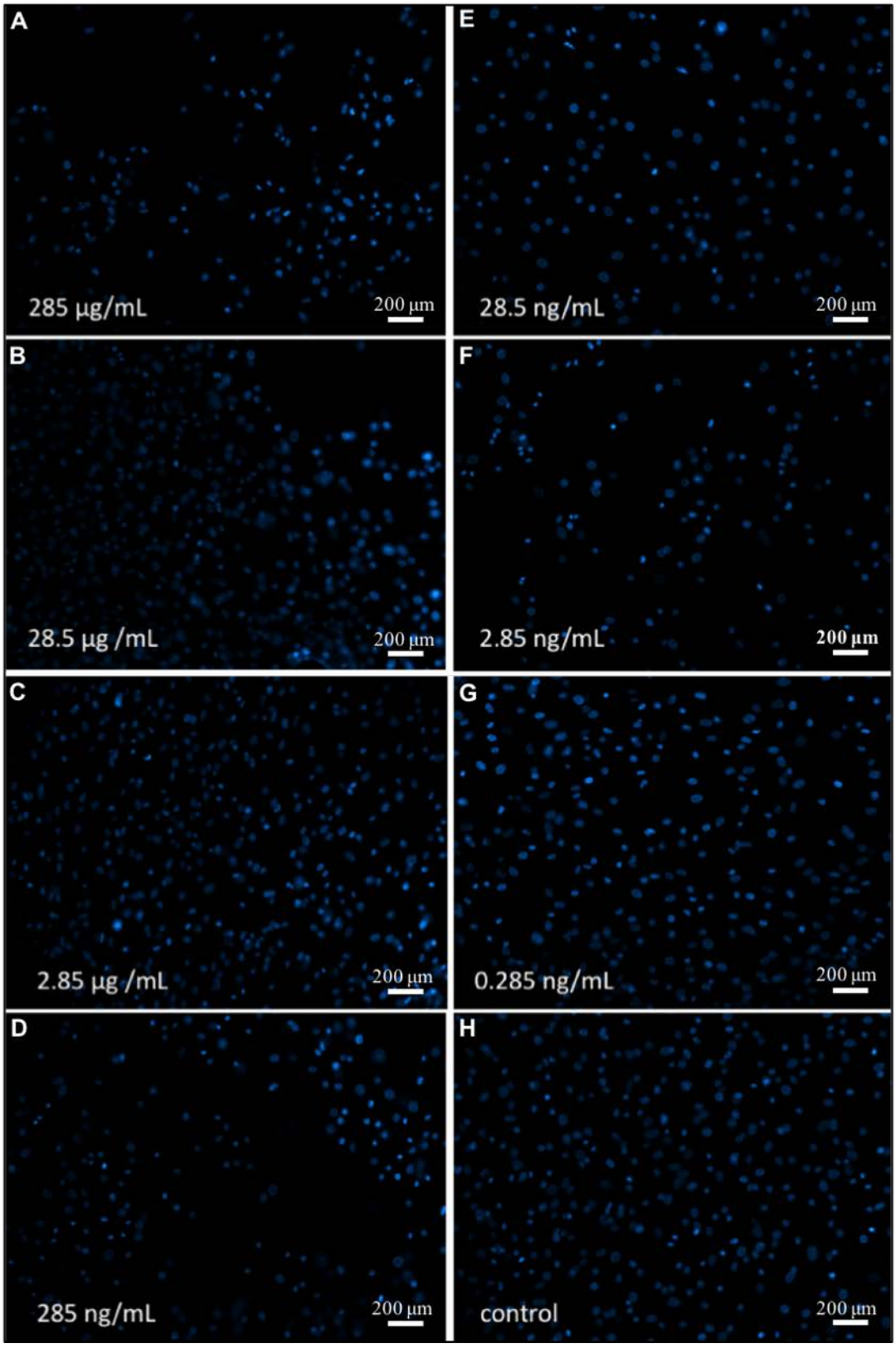

Figure 4: Imaging of the effect of different *C. fleckeri* venom concentrations on human cardiomyctes at a 20x magnification (scale bar: 200 µm) with a Zeiss Axio Imager M1 microscope (Carl Zeiss AG, Germany) and the Nuance Multispectral Imaging System FX (Perkin Elmer, Inc., USA). The cells were stained with the nuclear stain Hoechst 33342. Venom concentrations are indicated on each image (images A-G). The negative control with no venom added is shown in image H.

2.3.1.4. Fluorescence microscopy imaging of envenomed cells

Due to the complications encountered during the preliminary experiments, it was decided not to continue with the project to its full extent. Initially, it was anticipated to have three replicates, i.e. three chamber slides per dye, with four control wells and four venom wells per slide. However, since handling a single chamber slide was already logistically challenging, it was decided instead to only use one chamber slide per dye. While a single chamber slide per dye lacks statistical significance, it was concluded that it would provide enough insight to determine whether it was worth pursuing the development of an alternative experimental design and method using these fluorescent dyes (i.e. flow cytometry).

To analyze if fluorescent staining had the potential to reveal some of the effects of *C. fleckeri* venom, four different dyes were tested following the method developed in section 2.3.2. Four wells were incubated with a venom concentration of 0.1 μg/mL and the remaining four wells were used for the MQ-control. The dyes used for this experiment were Hoechst 33342 (nuclear stain), Propidium Iodide and CellMask™ Deep Red (membrane integrity stains) as well as MitoTracker™ Deep Red (mitochondrial stain).

2.3.1.4.1. Cell nucleus

To analyse the effect of *C. fleckeri* venom on the cardiac nuclear morphology, cells were incubated with the cell permeant nuclear stain Hoechst 33342 for a period of 10 minutes. Microscopic analysis showed that the nuclei from the envenomed cells appeared rounder and some also appeared smaller compared to the nuclei from the control cells (Figure 5).

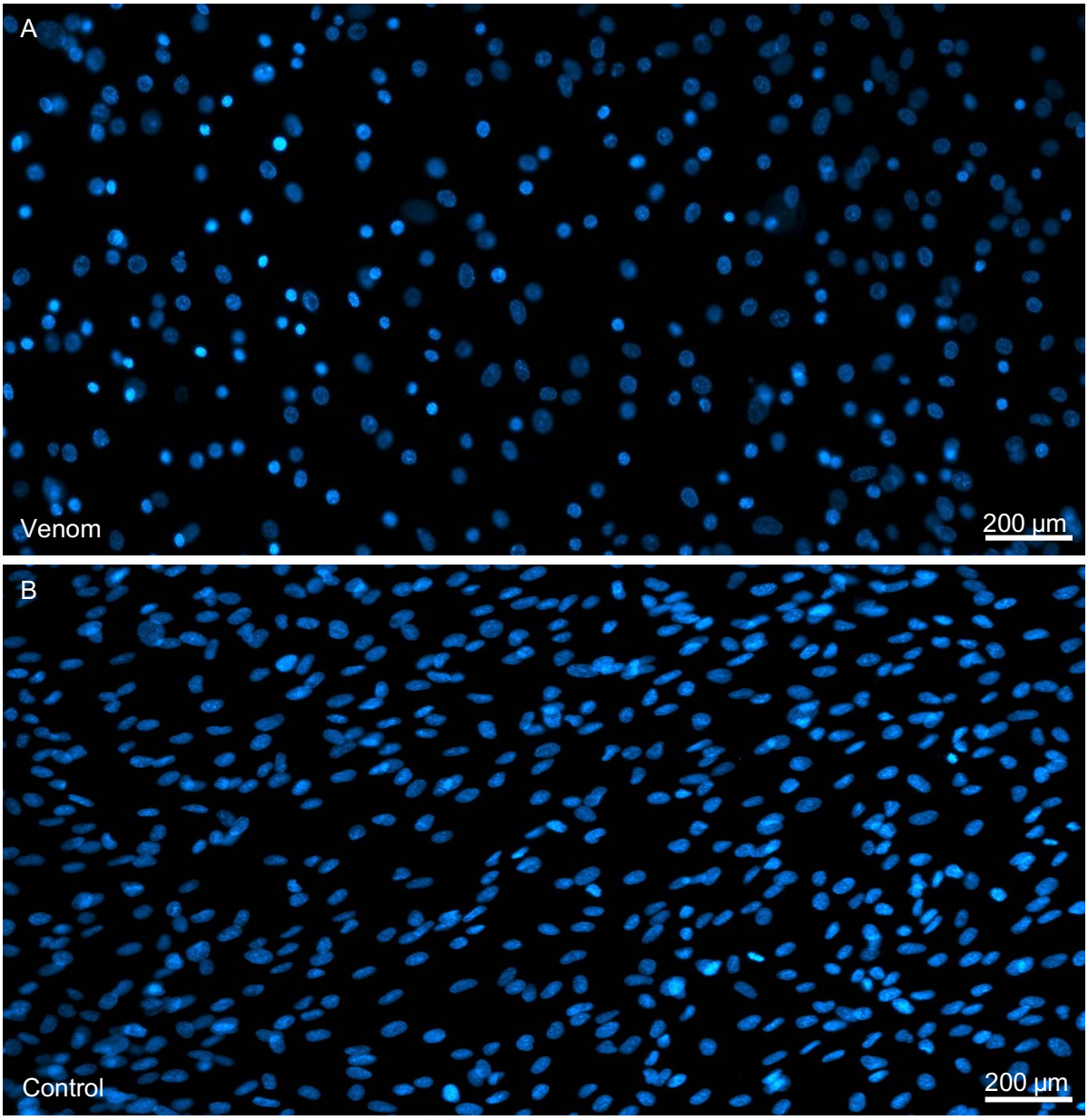

Figure 5: Imaging of the nuclear morphology of cardiomyocytes after *C. fleckeri* venom administration at a 200x magnification (scale bar 200 µm) with a Zeiss Axio Imager M1 microscope (Carl Zeiss AG, Germany) and the Nuance Multispectral Imaging System FX (Perkin Elmer, Inc., USA). Cells were incubated for 10 minutes with the nuclear stain Hoechst 33342 (5 µg/mL) and 0.1 µg/mL of venom (or MQ-water control). (A) Envenomed cells appeared to have a smaller nucleus than (B) the control cells.

758

759

760 *2.3.1.4.2. Cell membrane integrity*

761

762 To assess the integrity of the cardiac cell membrane after *C. fleckeri* envenomation, two
763 experiments were conducted. First, to assess changes in cell membrane permeability, cells were
764 incubated for 10 minutes with the non-permeant nuclear counterstain propidium iodide in

765 combination with Hoechst 33342. The characteristic red fluorescence of the non-permeant
766 propidium iodide counterstain was present in the nuclei of several of the envenomed cells,
767 suggesting damage to the cell wall, whereas the control cells appeared to have intact
768 membranes as only the characteristic blue fluorescence from the cell-permeant Hoechst 33342
769 stain was detectable during the fluorescence microscopy imaging (Figure 6).
770 In a second experiment, to assess changes in the cell membrane morphology, the cells were
771 incubated for 10 minutes with CellMask^{TM} Deep Red, a cell membrane stain. The resulting
772 images showed that compared to the control, cells incubated with venom had undergone
773 morphological changes as they appeared narrower and the cell membranes appeared
774 filamentous (Figure 7). The cellular organization appeared altered as well; in the control wells,
775 the cells appeared to be organized in a parallel pattern, whereas in the treated wells showed
776 disorganized clusters of cells, which is likely associated to the loss of adherence of the cells.
777

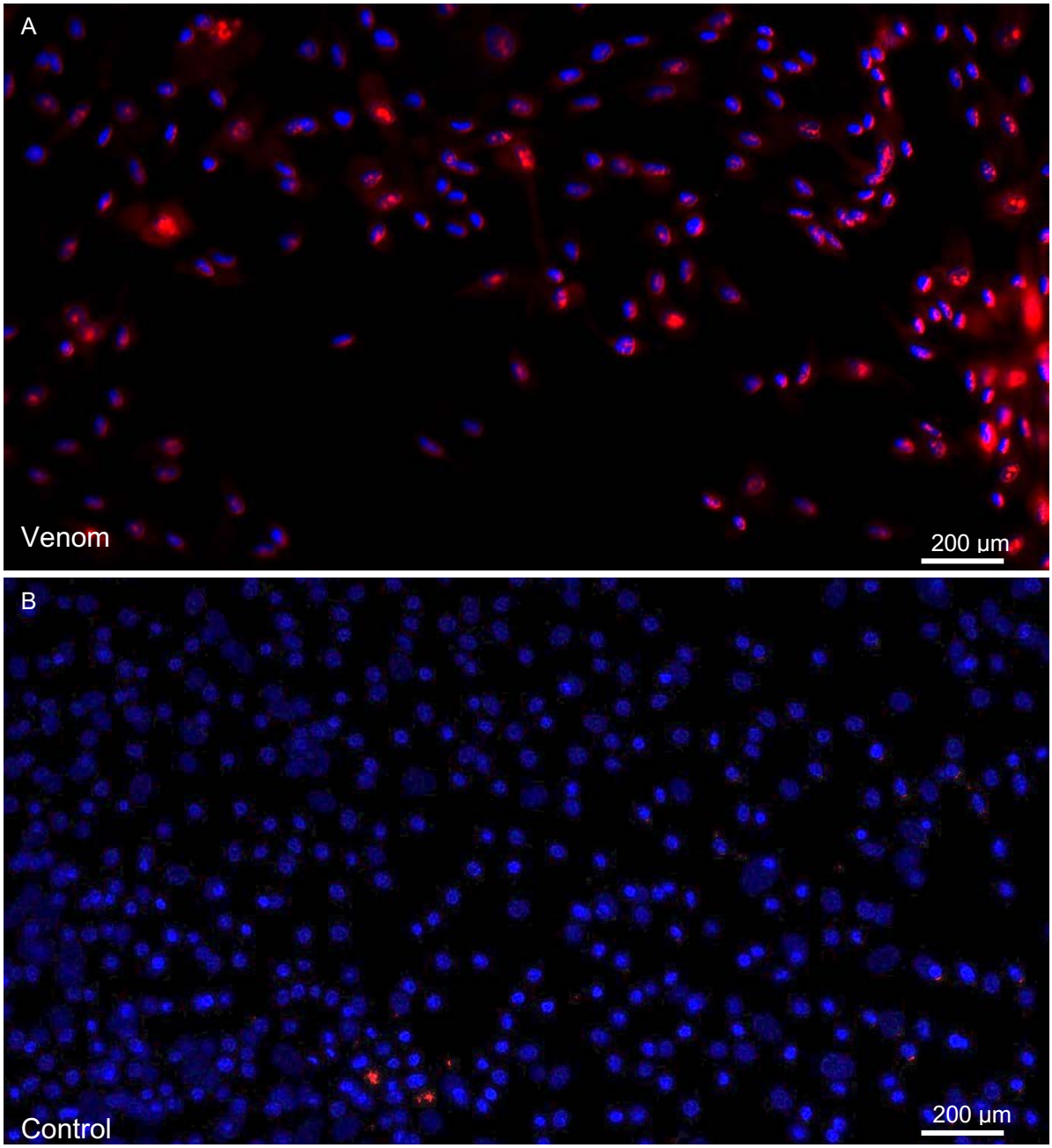

Figure 6: Imaging of the cell membrane integrity after *C. fleckeri*envenomation at a 200x magnification with a Zeiss Axio Imager M1 microscope (Carl Zeiss AG, Germany) and the Nuance Multispectral Imaging System FX (Perkin Elmer, Inc., USA). Cells were incubated for 10 minutes with 0.1 µg/mL venom (or MQ-water) along with the nuclear stains Hoechst 33342 (5 µg/mL) and Propidium Iodide (5 µM). The non-permeant Propidium Iodide counterstained the envenomed cells (A), suggesting loss of membrane integrity, but not but the control cells which emitted only the blue fluorescent signal from the cell-permeant Hoechst stain (B).

778

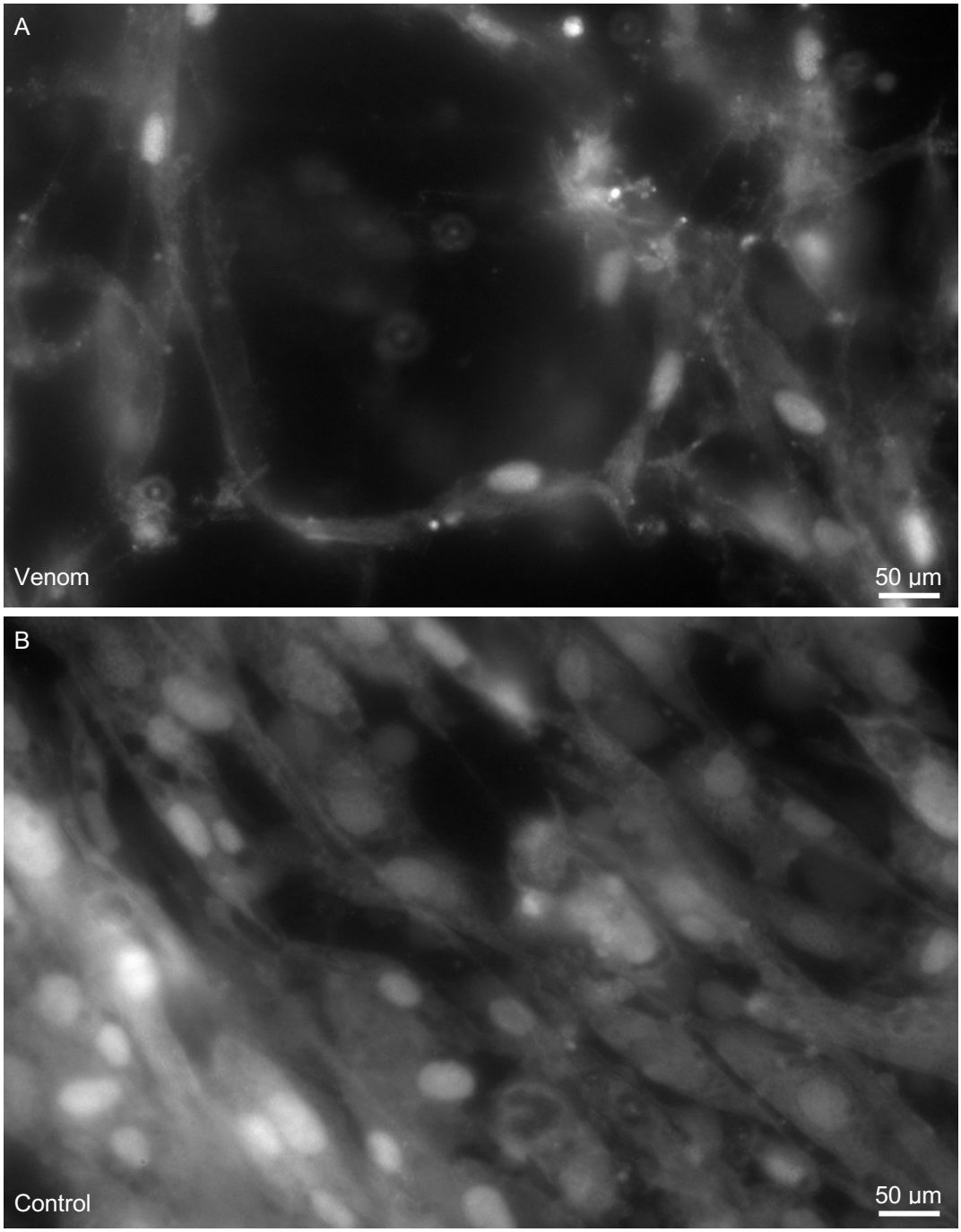

Figure 7: Imaging of the cell morphology after *C. fleckeri* envenomation at a 630x magnification with a Zeiss Axio Imager M1 microscope (Carl Zeiss AG, Germany) and the Nuance Multispectral Imaging System FX (Perkin Elmer, Inc., USA). Cells were incubated for 10 minutes with 0.1 µg/mL *C.fleckeri* venom (or MQ-control) and CellMask DeepRed. The envenomed cells (A) compared to the control cells (B) exhibited a loss of the typical heart cell morphology. The membranes of the envenomed cells appear filamentous and disintegrated as opposed to the control cells.

779

780

781

782

2.3.1.4.3. Mitochondrial membrane potential

To assess the changes in mitochondrial activity during envenomation, the cells were incubated with the MitoTracker™ Deep Red dye for 10 minutes. Changes in mitochondrial membrane potential results in a proportional intensity fluorescent signal from the MitoTracker dye. The cells in the control well appeared to be mostly evenly stained (Figure 8). By contrast, the cells exposed to the venom showed variation in fluorescent signal intensity, with some cells showing a bright fluorescent signal and some cells only showing weak fluorescence. Furthermore, the mitochondria also appeared to concentrate around the nucleus, as opposed to being evenly distributed in the control.

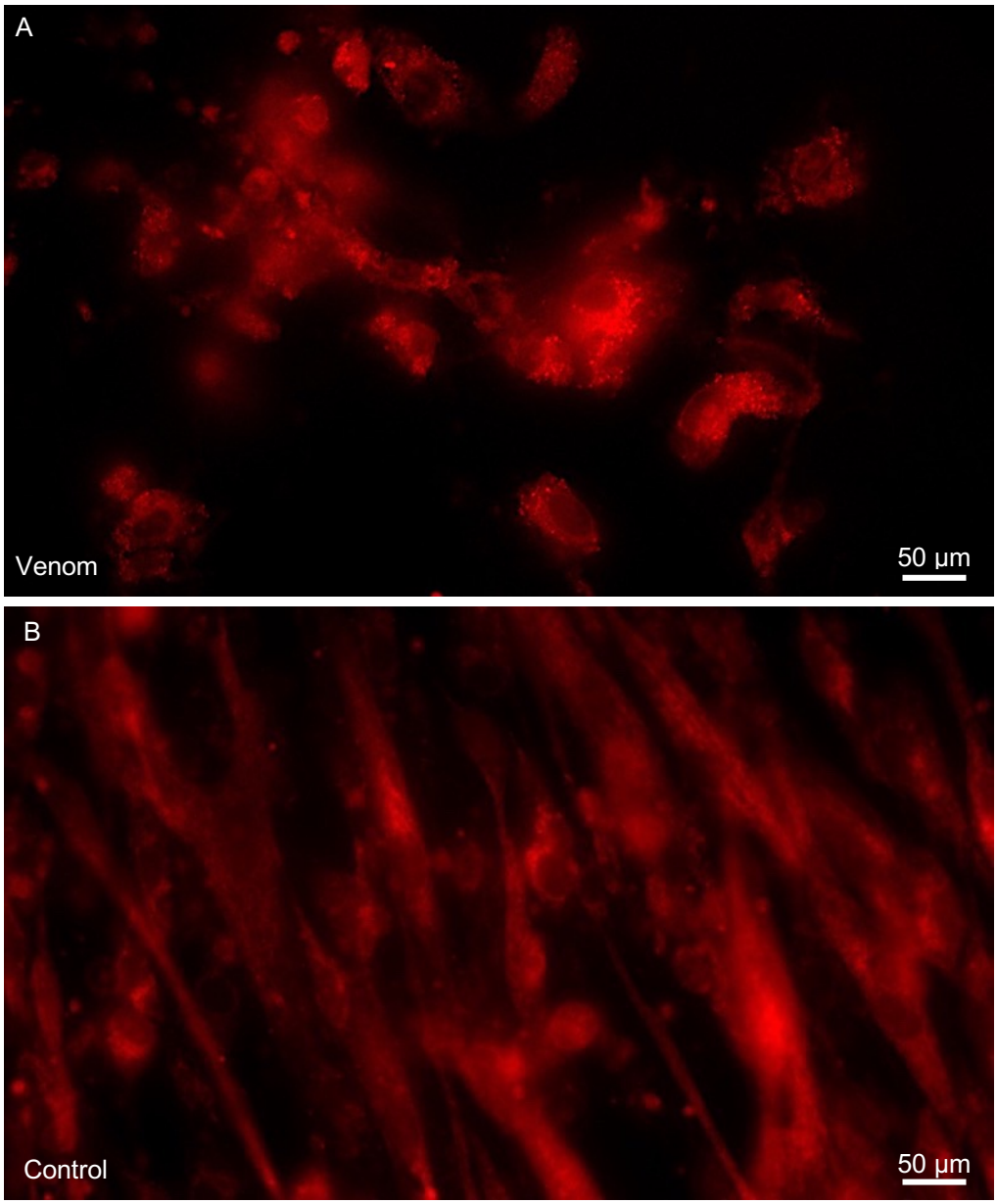

Figure 8: Imaging of the cardiomyocyte mitochondrial membrane potential at a 630x magnification with a Zeiss Axio Imager M1 microscope (Carl Zeiss AG, Germany) and the Nuance Multispectral Imaging System FX (Perkin Elmer, Inc., USA). Cells were incubated for 10 minutes with 0.1 µg/mL *C.fleckeri* venom (or MQ-control) and MitoTracker Red. The image of the envenomed cells (A) shows variable fluorescent signals, as opposed to the more evenly distributed signals of the control cells (B). Increase in fluorescent signal indicates an increase of mitochondrial membrane potential and activity.

793

794

2.3.2. Flow cytometry

2.3.2.1 Venom concentration and venom incubation time

Different venom concentrations (80, 8 and 0.8 ng/mL) and venom incubation times (2, 10 and 30 minutes) were tested to identify a concentration and time that would allow for the detection of a decrease and increase (left- and rightwards shift, respectively) in fluorescent signal on the fluorescence signal intensity histograms generated in the flow cytometry analysis software BD FACSDiva. With 2 minutes of incubation, only 80 ng/mL could be clearly differentiated from the control, whereas concentrations of 8 and 0.8 ng/mL did not seem to affect the cells (Figure 9A). With 10 and 30 minutes of incubation all three concentrations had an effect on the cardiomyocytes, indicated by the dose-dependent rightwards shift of the fluorescent signal trace on the histograms (Figure 9B and 9C). Concentrations that allowed for a left- and rightward shift were 8 and 0.8 ng/mL at both 10 and 30 minutes, and thus it was decided they were suitable, at either of the two mentioned incubation periods, for the following experiments. While for the latter incubation periods, 80 ng/mL resulted in fluorescent signal intensities that were shifted too far right to allow for further right shift within the sensitivity tolerances of the flow cytometer, this concentration was also used for the following experiments. 30 minutes was chosen as incubation period, as it allowed for more experiment preparation time than 10 or 2 minutes and was, thus, logistically favourable. In summary, for all following experiments, cells were incubated for 30 minutes with all three tested concentrations, to ensure the recording of concentration-dependent effects.

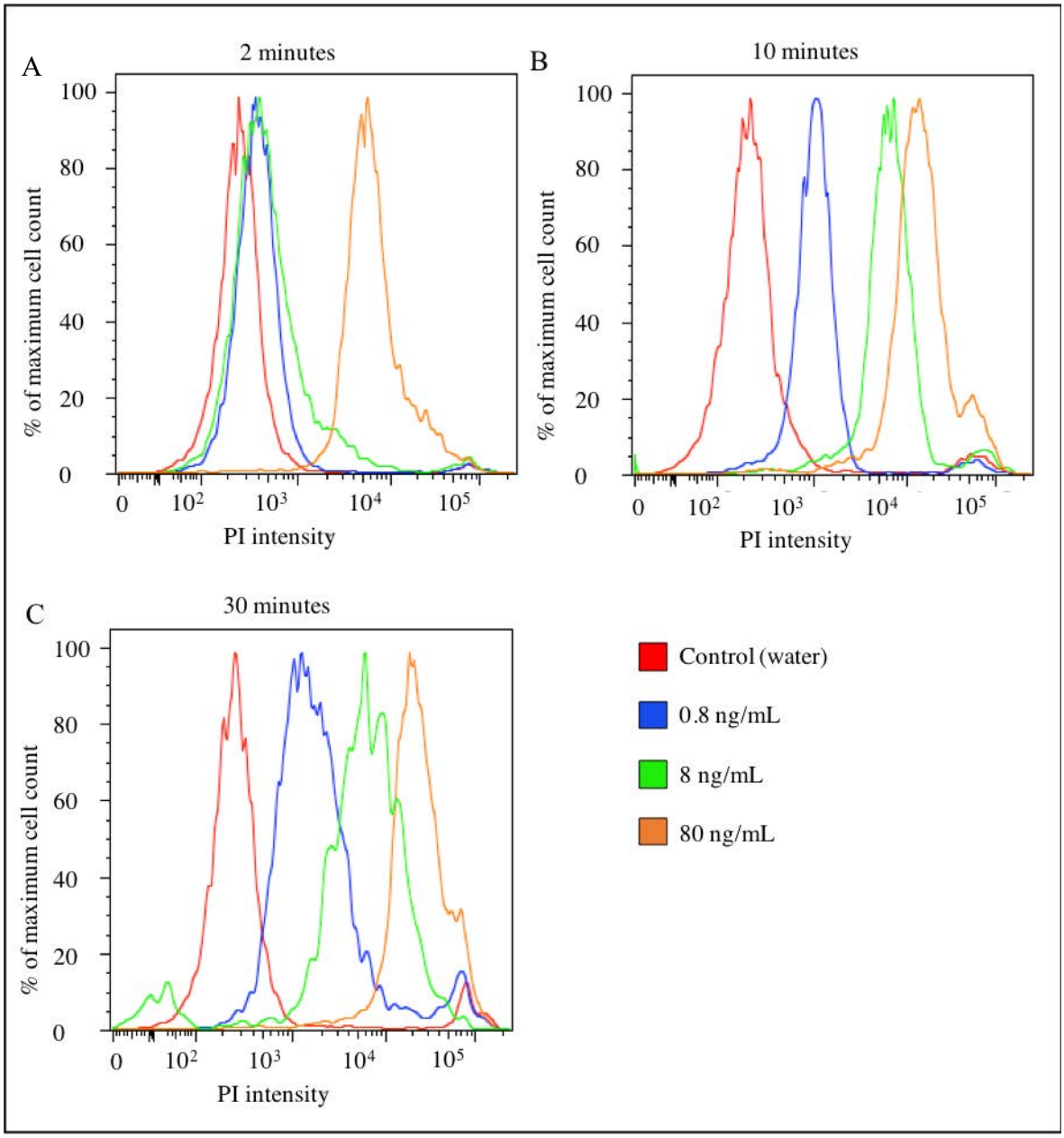

Figure 9: Fluorescent signal intensity histograms of incubation time and concentration dependent effects of *C. fleckeri* venom on Propidium Iodide (PI)-stained cardiomyocytes. The x-axis represents the dye intensity and y-axis represents the percentage of cells of the maximum cell count. The incubation periods are indicated above each graph and the concentrations are listed on the legend.

2.3.2.2. Nuclear and mitochondrial stain

To assess whether *C. fleckeri* venom had a quantifiable effect on the cardiomyocyte nucleus and/or mitochondria, cells were exposed for 30 minutes to concentrations of 80 ng/mL, 8 ng/mL and 0.8 ng/mL. *C. fleckeri* venom did not induce a significant change in the intensity of the fluorescence of the nuclei compared to the control, despite an observable concentration-dependent increase of the peak height in the fluorescent signal intensity histograms (Figure 10). Cardiomyocyte mitochondria were significantly affected by concentrations of 80 ng/mL, showing a significant ($p < 0.001$, $F_{Dfn,\ Dfd} = 16.53_{3,8}$) decrease in geographical mean of the intensity of the fluorescent signal (i.e. leftward shift) compared to the control (Figure 11). Similar to the Hoechst experiments, at 80 ng/mL the cells appear dead (decrease in forward scatter). The other two concentrations did not elicit an observable effect and the data is summarised in Figure 11C.

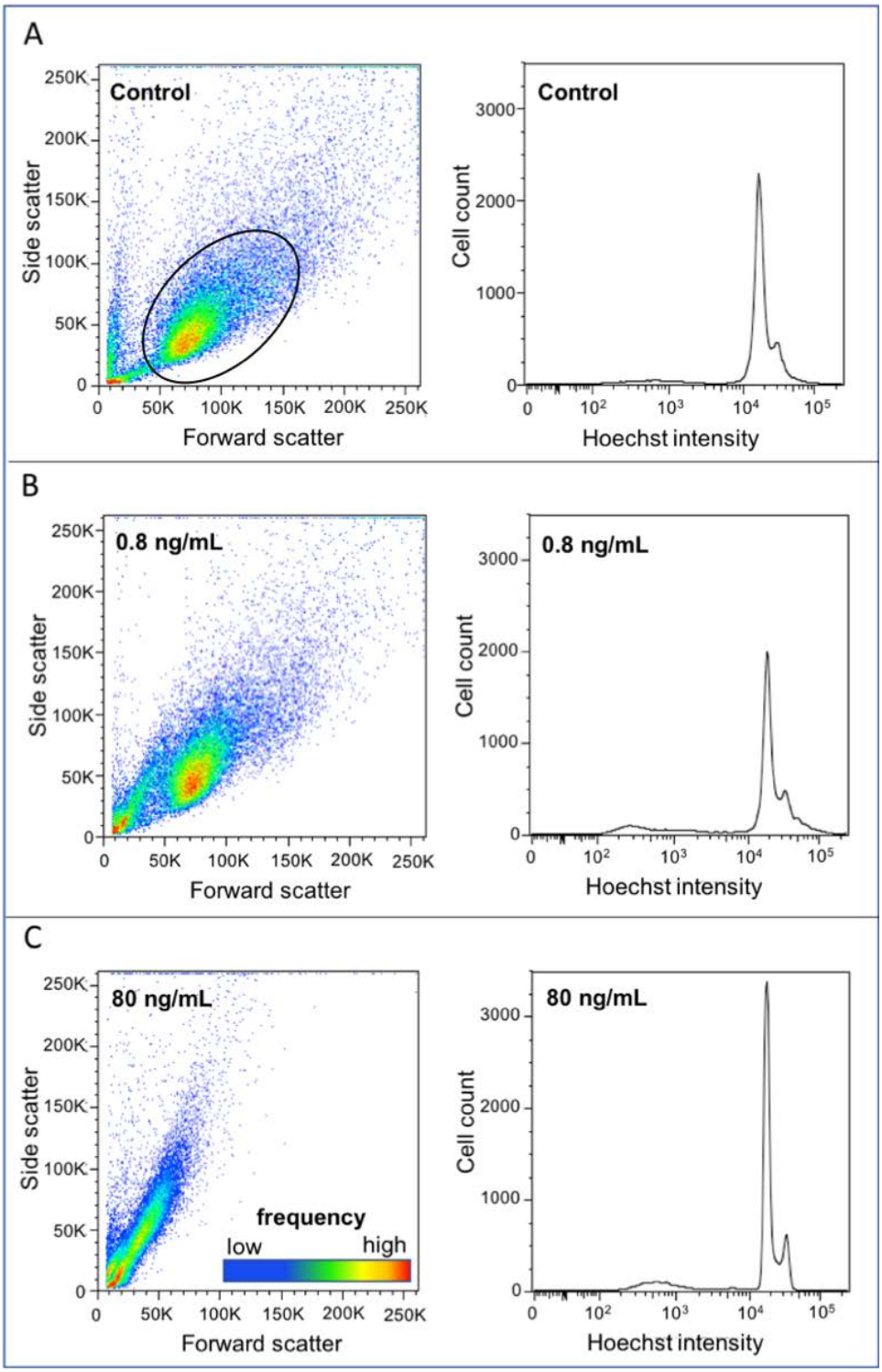

Figure 10: Nuclear dye (Hoechst 33342) experiments: Cell density charts (left) and fluorescent signal intensity histograms (right) for nucleus-stained cardiomyocytes exposed to (A) no (control), (B) 0.8 ng/mL, (C) 80 ng/mL) *C. fleckeri* venom. The x- and the y- axis for the cell density charts indicated the forward and the sideward scatter, respectively, of each counted cell, with a legend provided in panel (C). The x- and the y-axis for the intensity histograms represent the cell count and the intensity of the fluorescent signal, respectively. The circled data in panel (A) represents a healthy population of cardiomyocytes. The cells exposed to 80 ng/mL venom display a decreased forward scatter compared to the control, suggesting that these cells have died. The data for 8 ng/mL *C. fleckeri* venom is not shown as, similar to 0.8 ng/mL, it did not differ significantly from the control.

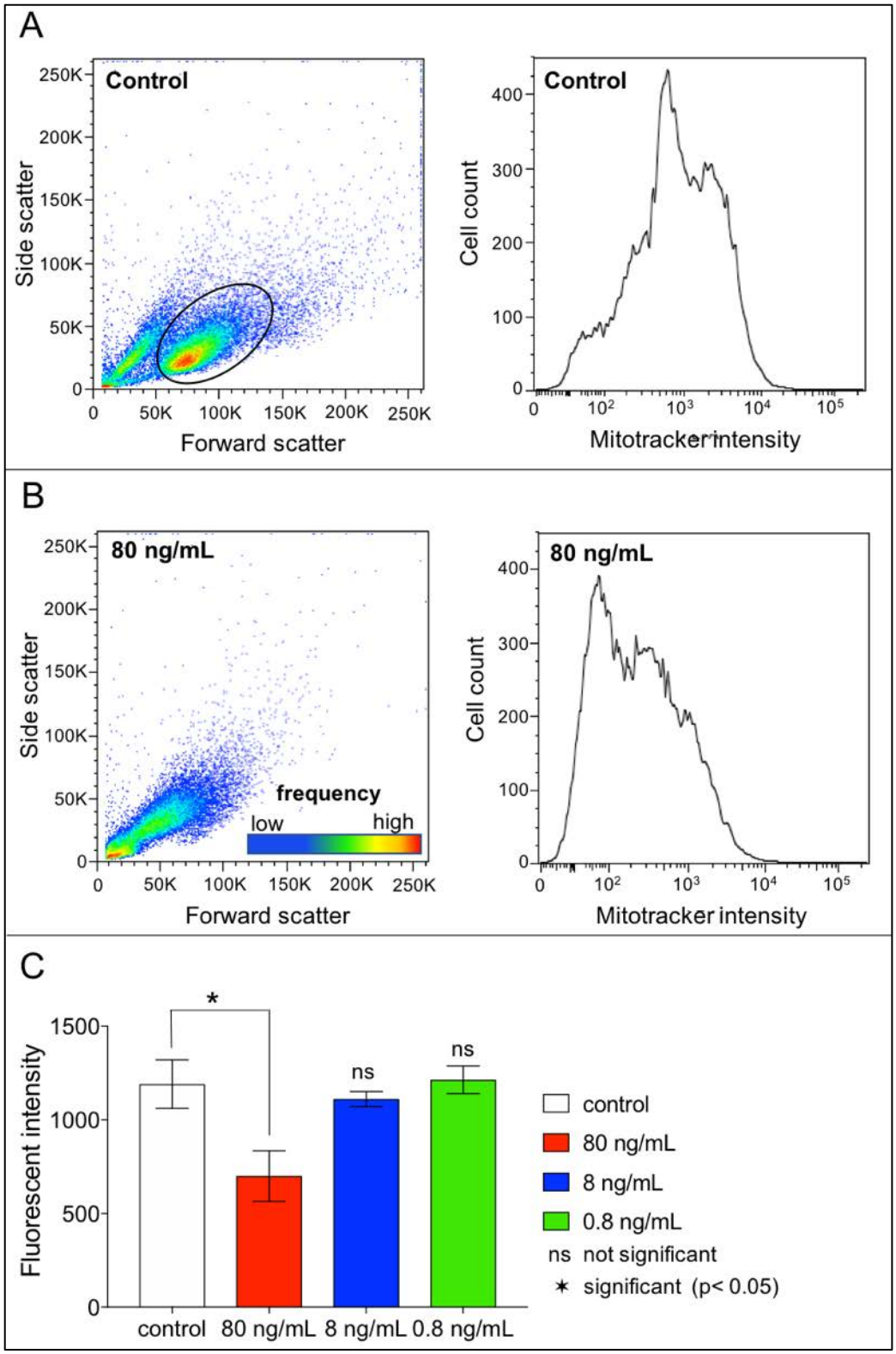

Figure 11: MitoTracker experiments. Panel (A) and (B) show the data density charts (left) and the fluorescent signal intensity histograms (right) for the control as well as cardiomyocytes exposed to the highest concentration of venom (80 ng/mL). The other concentrations are not shown as they did not differ from the control. The circled data in panel (A) represents a healthy population of cardiomyocytes. Panel (C) shows the geographic mean of the fluorescent signal intensity (y-axis) for each of the tested samples (x-axis). Statistical significance with $p < 0.05$ is indicated by *. 80 ng/mL induced a significant decrease in the intensity of the fluorescent signal from the mitochondria compared to the control as well as an increase in dead cells (reduced forward scatter).

2.4. Discussion

2.4.1. Effect of *C. fleckeri* venom on cellular components of the cardiomyocyte

This study presents a fluorescence microscopy imaging assay to visualise and a flow cytometry assay to quantify the effects of *C. fleckeri* venom on different cellular components of the cardiomyocyte. Two of the three types of cellular components assessed in this study, the nucleus and the cell membrane, exhibited distinct morphological changes after *C. fleckeri* administration. The morphological changes of the cell membrane were quantified by flow cytometry, but the changes to the nuclei were not quantifiable with the present method. Further, the cellular distribution of the mitochondria was altered upon administration of venom, which was accompanied by a significant decrease in the geographical mean of the fluorescent signal intensity for the highest concentration tested. Albeit the lack of statistical robustness of the fluorescence microscopy experiments due to only testing one chamber slide per dye, the results, discussed in detail below, provide some context for the effects of *C.fleckeri* venom on cardiomyocytes.

The *C. fleckeri* envenomed cardiomyocytes displayed a reduced nuclear size. Many of the nuclei of the envenomed cells analysed by fluorescence microscopy appeared to “condense”; apart from becoming smaller in size, their shape also appeared rounder, similar to the nuclear condensation seen in apoptotic cells [e.g. 11]. The flow cytometry analyses could not quantify this observation; it is possible that this “condensation” does not affect the dye binding mechanism and is therefore not quantifiable in this manner. Hoechst binds to the minor grove in double-stranded DNA [20], thus the lack of effect in the flow cytometry assay suggests that

882 *C. fleckeri* venom does not degrade DNA into single strands nor does it alter the DNA content
883 of the cells, at the concentrations tested.
884
885 *C. fleckeri* venom caused loss of plasma membrane integrity and loss of adherent properties
886 compared to the control cells. During the fluorescence microscopy imaging most of the
887 envenomed cells detached, floating in the suspension, while many of the still adhering cells
888 appeared filamentous and narrower than the control. The plasma membranes of the envenomed
889 cardiomyocytes became permeable to propidium iodide, indicating the loss of membrane
890 integrity. *C. fleckeri* venom can create pores the size of approximately 50 nm in diameter [21],
891 thus it is not clear if the propidium iodide entered the cells through the pores or whether the
892 membranes ruptured as a result of mechanical cell death, such as necrosis.
893
894 *C. fleckeri* venom also appeared to alter the activity of cardiomyocyte mitochondria. The
895 microscopic analysis showed that the mitochondrial dye had a distinctly different distribution
896 in the envenomed cells than in the control cells. In the control cells, the MitoTracker dye was
897 evenly distributed throughout the cardiomyocyte, while in the envenomed cells the dye
898 appeared to aggregate around the nucleus. The flow cytometry experiments showed a
899 significant decrease in the fluorescent signal intensity emitted from the mitochondria of cells
900 exposed to the highest venom concentration, but not for the other concentrations. It is not clear
901 if this loss of fluorescence is the secondary result of an increased number of dead cells (and
902 therefore dead mitochondria) or the direct result of decreased mitochondrial functioning. The
903 MitoTracker dye is cell permeant and works by binding to thiol-reactive chloromethyl moieties
904 in, and then being metabolised by, the mitochondria (Invitrogen™, USA). Therefore, in dead
905 cells, this dye does not work adequately and a loss of fluorescence, as observed here, is to be
906 expected. In terms of the aggregation of the mitochondrial dye observed during the microscopic

study, this could be the secondary result of the altered cell shape of the envenomed cardiomyoctyes. However, as mentioned above, the envenomed cardiomyocytes appeared narrower and filamentous in shape (compared to the control), while the mitochondrial dye aggregated in a rounded pattern around the nucleus.

2.4.2 Limitations of this study

The fluorescence microscopy imaging assay developed here posed several challenges and limitations relating to the preparation of the slides and the analysis of the data. A key factor for the success of this assay is the adherence of the cardiomyocytes to the chamber slides. Adequate adherence is necessary to prevent cells from being flushed away during the preparation of the slides and to ensure even distribution of the cells on the slides to enable systematic analysis with fluorescence microscopy. To counteract the problem of lack of adherence, the LabTek II Chamber slides that were initially used were replaced with LabTek CC2 coated chamber slides. This alleviated the problem to a degree, likely because the CC2 coating was developed to mimic the polystyrene surface of tissue culture flasks, as opposed to the standard glass surface of the LabTek II slides. However, as soon as venom was added to the cardiomyocytes, they started to detach regardless of the CC2 coating. This resulted in problems of repeatability of the experiments. Generally, during fluorescence microscopy imaging experiments a set number of defined areas are selected for analysis, and those areas are systematically analysed on each slide, or in the present case, in each chamber. Here this type of systematic analysis was not possible, as most of the cells detached and floated away, resulting in large cell-less patches. Further, detached cells were floating above patches of attached cells, hindering the achievement of adequate focus and thus resulting in extensive

delays in finding a photographable area. This further hindered systematic analysis through the dyes fading due to prolonged exposure of the cells to the fluorescence lasers.

While the flow cytometry experiments were suitable in terms of logistics, repeatability and statistical robustness, the experimental questions, i.e. whether or not the venom reduces the size of the nucleus or alters mitochondrial activity, could not be quantified adequately. Perhaps, a more extensive analysis that includes the analysis of different nuclear dyes or, for example, mitochondrial depressants, could provide more insight into the mechanism of *C. fleckeri* venom.

Lastly, alternative imaging methods such as automated cell imagers could be explored for the visualisation of *C. fleckeri* venom effects. Automated cell imagers have similar features to fluorescence microscopes, without requiring the expertise of the latter. In addition to being more user-friendly, automated cell imagers can be used for qualitative and high-throughput quantitative analyses which would potentially alleviate the problems of statistical robustness encountered in this chapter.

2.4.3. Conclusions

While the presented data did not answer the questions originally posed in regard to *C. fleckeri* venom, repeated exposure of the cardiomyocytes to the venom resulted in three consistently recurring effects: cell detachment, nuclear condensation, loss of membrane integrity. *C. fleckeri* venom induced cell detachment of adherent cells, such as cardiomyocytes or skeletal myocytes, is a common observation and therefore myocyte adherence has often been used as a measure of cell viability [e.g. 8,9,22]. Yet, cell death as such has not been analysed. Currently

there is no evidence for the type of cardiomyocyte death induced by *C. fleckeri* venom, i.e. apoptosis, necrosis or other. Necrosis of the skin has been observed in envenomation victims [23], however, not in cardiac myocytes. In the present microscopic analysis, the cell walls of the envenomed cardiomyocytes were ruptured, indicating a mechanical cell death such as necrosis. On the other hand, it has previously been shown that detachment of adherent cells can lead to a programmed cell death, such as apoptosis [24]. This is supported by the "condensation" of the nuclei, which is commonly observed in apoptotic cells. Given the complexity of *C. fleckeri* venom, it is possible that both types of cell death (i.e. mechanical or apoptotic or similar) are induced by different toxins in the venom. Further research, perhaps with apoptotic indicators such as Annexin V or Caspase 3, could help clarify the type(s) of cell death (i.e. mechanical or programmed) induced by *C. fleckeri* venom.

2.5. References

1. Ramasamy, S.; Isbister, G.K.; Seymour, J.E.; Hodgson, W.C. Pharmacologically distinct cardiovascular effects of box jellyfish (*Chironex fleckeri*) venom and a tentacle-only extract in rats. Toxicology Letters 2005, 155, 219-226.
2. Ramasamy, S.; Isbister, G.K.; Seymour, J.E.; Hodgson, W.C. The in vivo cardiovascular effects of box jellyfish *Chironex fleckeri* venom in rats: efficacy of pre-treatment with antivenom, verapamil and magnesium sulphate. Toxicon 2004, 43, 685-690.
3. Brinkman, D.L.; Konstantakopoulos, N.; McInerney, B.V.; Mulvenna, J.; Seymour, J.E.; Isbister, G.K.; Hodgson, W.C. *Chironex fleckeri* (box jellyfish) venom proteins expansion of a cnidarian toxin family that elicits variable cytolytic and cardiovascular effects. Journal of Biological Chemistry 2014, 289, 4798-4812.
4. Hughes, R.J.; Angus, J.A.; Winkel, K.D.; Wright, C.E. A pharmacological investigation of the venom extract of the Australian box jellyfish, *Chironex fleckeri*, in cardiac and vascular tissues. Toxicology Letters 2012, 209, 11-20.
5. Cegolon, L.; Heymann, W.C.; Lange, J.H.; Mastrangelo, G. Jellyfish stings and their management: A review. Marine Drugs 2013, 11, 523-550.
6. McClounan, S.; Seymour, J. Venom and cnidome ontogeny of the cubomedusae *Chironex fleckeri*. Toxicon 2012, 60, 1335-1341.
7. Saggiomo, S.L.; Seymour, J.E. Cardiotoxic effects of venom fractions from the Australian box jellyfish *Chironex fleckeri* on human myocardiocytes. Toxicon 2012, 60, 391-395.
8. Chaousis, S.; Smout, M.; Wilson, D.; Loukas, A.; Mulvenna, J.; Seymour, J. Rapid short term and gradual permanent cardiotoxic effects of vertebrate toxins from *Chironex fleckeri* (Australian box jellyfish) venom. Toxicon 2014, 80, 17-26.
9. Pereira, P.; Seymour, J.E. In vitro effects on human heart and skeletal cells of the venom from two cubozoans, *Chironex fleckeri* and *Carukia barnesi*. Toxicon 2013, 76, 310-315.
10. Mustafa, M.; White, E.; Hongo, K.; Othman, I.; Orchard, C. The mechanism underlying the cardiotoxic effect of the toxin from the jellyfish *Chironex fleckeri*. Toxicology and Applied Pharmacology 1995, 133, 196-206.
11. Wang, C.-H.; Monette, R.; Lee, S.-C.; Morley, P.; Wu, W.-G. Cobra cardiotoxin-induced cell death in fetal rat cardiomyocytes and cortical neurons: different pathway but similar cell surface target. Toxicon 2005, 46, 430-440.
12. Ventura-Clapier, R.; Garnier, A.; Veksler, V. Energy metabolism in heart failure. The Journal of Physiology 2004, 555, 1-13.
13. Lukyanenko, V.; Chikando, A.; Lederer, W.J. Mitochondria in cardiomyocyte Ca^{2+} signaling. The International Journal of Biochemistry & Cell Biology 2009, 41, 1957-1971.

14. Hsu, Y.-H.R.; Yogasundaram, H.; Parajuli, N.; Valtuille, L.; Sergi, C.; Oudit, G.Y. Melas syndrome and cardiomyopathy: linking mitochondrial function to heart failure pathogenesis. Heart Failure Reviews 2016, 21, 103-116.
15. Redout, E.M.; Wagner, M.J.; Zuidwijk, M.J.; Boer, C.; Musters, R.J.; van Hardeveld, C.; Paulus, W.J.; Simonides, W.S. Right-ventricular failure is associated with increased mitochondrial complex II activity and production of reactive oxygen species. Cardiovascular Research 2007, 75, 770-781.
16. Bloom, D.A.; Burnett, J.W.; Alderslade, P. Partial purification of box jellyfish (*Chironex fleckeri*) nematocyst venom isolated at the beachside. Toxicon 1998, 36, 1075-1085.
17. Carrette, T.; Seymour, J. A rapid and repeatable method for venom extraction from cubozoan nematocysts. Toxicon 2004, 44, 135-139.
18. Monkemoller, V.; Schuttpelz, M.; McCourt, P.; Sorensen, K.; Smedsrod, B.; Huser, T. Imaging fenestrations in liver sinusoidal endothelial cells by optical localization microscopy. Physical Chemistry Chemical Physics 2014, 16, 12576-12581.
19. Gutnisky, C.; Dalvit, G.C.; Thompson, J.G.; Cetica, P.D. Pentose phosphate pathway activity: effect on in vitro maturation and oxidative status of bovine oocytes. Reproduction, Fertility and Development 2014, 26, 931-942.
20. Han, F.; Taulier, N.; Chalikian, T.V. Association of the minor groove binding drug Hoechst 33258 with d(CGCGAATTCGCG)2: volumetric, calorimetric, and spectroscopic characterizations. Biochemistry 2005, 44 (28), 9785-9794 DOI: 10.1021/bi047374f
21. Bailey, P.M.; Bakker, A.J.; Seymour, J.E.; Wilce, J.A. A functional comparison of the venom of three Australian jellyfish - *Chironex fleckeri*, *Chiropsalmus sp*., and *Carybdea xaymacana* - on cytosolic Ca^{2+}, haemolysis and *Artemia sp*. lethality. Toxicon 2005, 45, 233-242.
22. Andreosso, A.; Smout, M.J.; Seymour, J.E. Dose and time dependence of box jellyfish antivenom. Journal of Venomous Animals and Toxins including Tropical Diseases 2014, 20, 34.
23. Currie, B. Clinical implications of research on the box-jellyfish *Chironex fleckeri*. Toxicon 1994, 32, 1305-1313.
24. Caccamo, A.E.; Scaltriti, M.; Caporali, A.; D'Arca, D.; Scorcioni, F.; Astancolle, S.; Mangiola, M.; Bettuzzi, S. Cell detachment and apoptosis induction of immortalized human prostate epithelial cells are associated with early accumulation of a 45 kDa nuclear isoform of clusterin. Biochemical Journal 2004, 382, 157-168.

CHAPTER 3

Characterisation of cardiotoxic protein fractions in *C. fleckeri* venom

3.1. Introduction

Chironex fleckeri is a large chirodropid Australian box jellyfish, with highly potent venom. *C. fleckeri* human envenomation causes agonising pain, local dermonecrosis and a variety of cardiovascular symptoms that may result in cardiac arrest within minutes if the sting area is significant [e.g. 1,2,3]. There is no empirical evidence for effective treatment, which is, in part, related to the lack of knowledge on *C. fleckeri* venom components and their clinically relevant bioactivities. Identifying and characterising the key venom components that lead to the rapid onset of the envenomation symptoms, is essential to improve emergency care of envenomation victims.

C. fleckeri venom is composed of a complex mixture of protein toxins of which only some induce cardiotoxic effects in human cells [4]. Purification of the venom with size-exclusion chromatography resulted in seven main peaks, of which only one peak showed cardiotoxicity in vertebrates [4]. Within this peak, two fractions, termed CTF-α and CTF-β, appear to act synergistically to elicit toxicity on heart cells; CTF-α triggers a rapid but short-term metabolism inhibition while CTF-β toxicity is two-fold slower but causes permanent damage [5]. The synergistic nature of these fractions is potentially the reason for the effects observed on the heart rate of fish exposed to *C. fleckeri* venom [6]. Initially, only stroke volume gradually declines by approximately 50 % until sudden cardiac arrest occurs [6]. However, CTF-α and CTF-β are only partially purified fractions of the venom and the components present have not been identified.

Transcriptomic and proteomic analyses have revealed that *C. fleckeri* venom contains a number of proteins that are unique to cnidarians. These venom proteins display substantial sequence

1066 homology with toxins from the related cubozoans *Carybdea alata, Carybdea rastoni* and
1067 *Chironex yamaguchii* [7]. Based on sequence alignment these cnidarian specific venom
1068 proteins have been phylogenetically grouped into Type-1 and Type 2-toxins [8]. Type 1 toxins
1069 include the highly cardiotoxic and haemolytic proteins CfTX-1 and CfTX-2 [9], whereas Type
1070 2 toxins include the potently haemolytic proteins CfTX-A, CfTX-B and CfTX-Bt [8]. These
1071 toxins are thought to act via pore-formation [8].
1072
1073 Based on the bioactivity reported for *C. fleckeri* toxins [5,8], it appears likely that the
1074 cardiotoxic fractions CTF-α and CTF-β are composed of Type-1 toxins. However, the masses
1075 of these fractions can only be roughly deduced from the FPLC-standards used in that study [5]
1076 and appear to be around 75-85 kDa for CTF-α and 35-45 kDa for CTF-β. Though, it is possible
1077 that the molecular mass in CTF-α is the result of dimerization of CfTX-1 or -2 (approx. 43 kDa
1078 and 45 kDa, respectively) [8,9]. To determine the precise composition and toxin masses of the
1079 CTF-α and CTF-β fractions, further purification and mass spectrometry studies are required.
1080
1081 Rationalising the bioactivity of *C. fleckeri* venom in terms of clinical symptoms has not been
1082 straightforward. It appears likely that the cardiotoxic activity of *C. fleckeri* venom induces a
1083 cardiovascular collapse that results in a fatal cardiac arrest [10-12]. For instance, mice injected
1084 with partially purified cardiotoxic and haemolytic CfTX-1 and -2 toxins suffered from a rapid
1085 cardiovascular collapse whereas mice injected with the haemolytic toxins CfTX-A and -B
1086 suffered less pronounced cardiovascular effects [8]. However, while *C. fleckeri* venom is
1087 potently haemolytic to laboratory animals [13] and human erythrocytes [14], haemolysis is
1088 often discounted because it has not been reported in human victims [1,8,13-15]. There are very
1089 few publicly available clinical or post-mortem reports on box jellyfish envenomations, and

1090 therefore, it is not clear whether haemolysis is not a clinical symptom or whether there is simply
1091 a general lack of available clinical reports.
1092
1093 Alternatively, laboratory animals such as mice, are known to display responses to certain drugs
1094 or toxins that are distinct from humans [16] and this could account for the apparent differences
1095 in haemolytic activity in mice and humans. For example, human beta cells are resistant to
1096 concentrations of sodium nitroprusside, streptozotocin and alloxan that significantly reduce the
1097 viability of rat and mouse beta cells [17]. Another example is that the anti-ulcer drug
1098 Omeprazole, induces CYP1A2 (hemoprotein from the cytochrome P450 oxidase system)
1099 expression in the liver of humans [18], but not mice [19]. Thus, while murine models play an
1100 imperative role in many experimental research studies, differences between mice and humans
1101 must be taken into account [20].
1102
1103 Here we conducted a mass spectrometric analysis of the toxic fractions CTF-α and -β, and -γ,
1104 from size exclusion chromatography of *C. fleckeri* venom to identify the key components.
1105 CTF-γ was included as a comparative fraction because it previously showed very little
1106 cardiotoxicity and was thought to be composed of smaller sized proteins [5] than CfTX-1 and
1107 -2. We analysed the effects of these fractions and crude *C. fleckeri* venom on human
1108 cardiomyocytes and human fibroblasts, and on human and mouse erythrocytes to assess the
1109 presence of species-specific differences. In an attempt to shed more clarity on the mechanism
1110 by which cardiomyocyte death is induced, we also conducted an apoptosis assay. The results
1111 of this study will be useful in directing future research studies towards the identification of the
1112 mechanisms of action involved in *C. fleckeri* envenomation and consequently better treatment
1113 methods.

3.2. Methods

3.2.1. Venom collection and extraction

Large (bell size approx. 30 cm) adult *C. fleckeri* specimens were collected from Weipa, QLD in December 2015. Nematocysts for venom extraction were collected following the method of Bloom et al. [21]. In brief, tentacles were removed from the animal and placed in saltwater buckets, where they were left for 3 days and shaken several times per day to promote autolysis of the nematocysts from the tentacles. To remove the tentacles, the solution was passed through a sieve and subsequently lyophilised and stored at -80 °C until required for venom extraction.

Venom extraction was carried out following the method of Carrette and Seymour [22]. In short, a layer of 0.5 mL of lyophilised nematocysts, followed by a 0.25 mL layer of glass beads was filled into 1.5 mL screw-cap microcentrifuge tubes. The tubes were topped off with Milli-Q-water (MQ-water) and shaken in a mini-bead-beater; 10x for 2 min with 5 min cooling breaks in an ice-slurry. The samples were then centrifuged at 20 000 *g* for 45 sec to separate ruptured nematocyst debris (sinking to the bottom of the tube) from the venom proteins (remaining in the supernatant). The supernatant was then collected, passed through a 0.45 μm filter (to further remove debris), lyophilised and stored at -80 ºC.

3.2.2. Venom fractionation

3.2.2.1. Sample preparation for venom fractionation

Lyophilised venom was suspended in approximately 0.5 mL of MQ to obtain a highly concentrated venom solution of approximately 10 mg/mL. The venom was then passed through

a 0.22 µm filter to remove further debris from the sample and prevent damage to the protein separation instrument.

3.2.2.2. Size exclusion chromatography (SEC)

C. fleckeri venom (350 µL) was loop-loaded and fractionated with the use of a Superdex^{TM} 200 Increase 10/300 GL Column (SD200, GE healthcare), equilibrated at 4 °C with phosphate buffered saline as running buffer (1 x PBS, i.e. 137 mM NaCl, 10 mM Na_2HPO_4, 1.8 mM KH_2PO_4, 2.7 mM KCl, pH 7.4), in a Fast Protein Liquid Chromatography (FPLC) AKTA system (GE healthcare). The eluent was measured at 280 nm, producing a venom profile and was thereby separated into size-specific (range: 600 kDa - 10 kDa) fractions of 0.5 mL. The fractions equivalent to the fractions previously termed CTF-α, -β and –γ, were collected from the wells B1 and B2, B7 and B8 as well as C1 and C2, respectively, as described in [5]. This resulted in a total volume of 1 mL for each of the three fractions. Protein concentration estimates from the FPLC software UNICORN (ÄKTA^{TM}, GE healthcare) were verified by BRADFORD assay and protein concentrations were standardized across samples.

3.2.3. Characterisation of CTF-α, -β and -γ

3.2.3.1. Sample preparation for mass spectrometric analysis

The concentration of the fractions (CTF-α, -β and -γ) was determined from the FPLC and a separate spectrophotometric analysis at 280 nm. The samples were then lyophilised. 50µg of each lyophilised sample was reduced and alkylated and then trypsin digested. Briefly, each sample was resuspended in 240 µL of 50 mM triethylammonium bicarbonate (TEAB) and reduced by adding 0.5 M of dithiothreitol (DTT) to a final concentration of 20 mM and incubated at 50°C for 30 min. The samples were then alkylated by adding 0.5 M iodoacetamide

(IAA) to a final concentration of 50 mM at RT for 30 min in the dark, the reaction was then quenched by adding more DTT to a final concentration of 50 mM.

To concentrate the samples, 30 kDa ultra-4 filtration units (Millipore, Merck KGaA) were washed with 1 mL of 50 mM TEAB at 4,000 x g for 10 min and then the individual samples were loaded onto their respective filtration units and concentrated at 4,000 x g for 15 min. A buffer exchange was performed twice by adding 500 µL of 50 mM TEAB on each of the filtration units and centrifugated at 4,000 x g for 15 min each time. The concentrated samples in 50 mM TEAB (approximatively 50 µL) were then collected from the filtration units and transferred into individual Eppendorf tubes.

Next the samples were trypsin-digested by adding 3 µg of trypsin to each sample and incubated at 37 °C overnight. The next day the digestion reaction was stopped by adding a 10 % trifluoroacetic acid (TFA) solution to the samples to reach a final concentration of 0.1 %. The samples were then lyophilised.

Subsequently, the samples were resuspended in 50 µL of 0.1 % TFA and then desalted using the Zip-Tip® C18 pipette tips (Merck KGaA, Darmstadt, Germany) according to manufacturer's protocol with the following modifications. The tips were washed and conditioned with 80 % acetonitrile (ACN), 0.1 % TFA then 0.1 % TFA in LC-MS grade water. Peptides were then bound to the tips and subsequently eluted with 80 % ACN, 0.1 % TFA and lyophilised before LC-MS analysis.

3.2.3.2. Mass spectrometric analysis

The tryptic fragments from the in-solution digestion were resuspended in 50 µL of 0.1 % formic acid (FA) in LC-MS grade water and were separated by an Eksigent nanoLC 415 system (AB Sciex) using a 15 cm long Eksigent column (C18-CL particle size 3 µm, 120 Å, 75 µm ID) (AB Sciex) and a linear gradient of 3-40 % solvent B for 60 min followed by 60-80 % solvent

B in 5 min. A pre-concentration step (10 min) was performed employing an Eksigent Trap-column (C18-CL, 3 µm, 120 Å, 350 µm x 0.5 mm) before commencement of the gradient. A flow rate of 300 nL/min was used for all experiments. The mobile phase consisted of solvent A (0.1 % formic acid [aq]) and solvent B (99.9 % acetonitrile/ 0.1 % formic acid [aq]). Eluates from the RP-HPLC column were directly introduced into the PicoView ESI ionisation source of a TripleTOF 6600 MS/MS System (AB Sciex) operated in positive ion electrospray mode at a voltage of 2400 V. All analyses were performed using Information Dependent Acquisition. AnalystTF 1.7.1 (Applied Biosystems) was used for data analysis. Briefly, the acquisition protocol consisted of the use of an Enhanced Mass Spectrum scan with 15 seconds exclusion time and 100 ppm mass tolerance. A cycle time of 1800 ms was used to acquire full scan TOFMS data over the mass range 400–1250 m/z with 250 ms of accumulation and product ion scans using rolling collision energy for 50 ms over the mass range of 100–1500 m/z for up to 30 of the most abundant ions with a relative intensity above 150 and a charge state of +2 − +5. Full product ion spectra for each of the selected precursors were then used for subsequent database searches.

3.2.3.3 Peptides sequences and protein identification

The different datasets were searched for peptide sequences and protein identifications using the ProteinPilot software 5.0.1 (AB Sciex) against three databases:

1) A database generated from *C. fleckeri* transcripts (Dr. D. Brinkman's transcripts assembled by M.Sc. J. Portiquet, personal communication M.Sc. J. Potriquet (20,562 proteins).

2) A database generated from *Carukia barnesi* (Dr. D. Brinkman's transcripts assembled by M.Sc. J. Portiquet, personal communication M.Sc. J. Potriquet) transcriptome (1,426 proteins) for the sake of possible homology matches.

3) An unreviewed Toxin database generated by compiling proteins from UniProtKB database with the "Toxins" annotation consisting of 26,142 proteins.

All searches were conducted employing the following search parameters: trypsin as digestion enzyme, precursor ion mass tolerance ± 0.05 Da, fragment ion tolerance ± 0.1 Da, Iodoacetamide with other Cys mods possible for Cystein alkylation and ID focus set on Biological modifications and FDR analysis was enabled.

Peptides and proteins identified with less than 1 % global FDR and more than 99 % confidence were considered and the top identified proteins with a minimum of 2 unique peptides were considered in our dataset comparison. Protein hits were order by the semi-quantitative "peptide-hit" method [23, 24] to provide some perspective of their relative abundance.

3.2.4. Cell culture and xCELLigence assay

Human fibroblasts (1BR.3.GN cell line – European cell collection) and cardiodmyocytes (ScienCell, Inc.) were cultured following the manufacturers guideline in 5 mL RPMI media (Gibco) with 10 % Foetal Bovine Serum and Cardiac Myocyte Medium (ScienCell, Inc), respectively, at 37 °C and 5 % CO_2 in 25 cm^2 monolayer flasks. The cells were seeded and incubated in 96-E-well plates at approximately 3000 cells in 150 µL media per well for 24 h at 37 °C and 5 % CO_2 to allow the cells to attach to the bottom of the wells before treatment was applied. Cell adherence to the bottom of the plate, i.e. the cell index, a measure of cell viability was monitored using xCELLigence single plate (SP) system and the Real Time Cell Assay (RTCA) software. The IC_{50}, i.e. the concentration at which 50 % of the cells die, 10 min post-venom addition, was used as a measure of venom toxicity. This time period was chosen to allow for comparison with previously published studies.

3.2.5. Haemolytic activity

To assess haemolytic activity, crude venom as well as the FPLC fractions CTF-α, CTF-β and CTF-γ were tested. These fractions were chosen because there already is cardio- and myotoxicity data available in the literature for comparison. The haemolysis test followed the protocol of the quantitative spectrophotometric assay used by Brinkman et al., 2014 [8] for consistency. In brief, heparinised human (ethics approval number H6838) and mouse blood (donation from the Loukas group, AITHM) was centrifuged (2000x g, slowest deceleration setting, 4 °C, 10 min), and the supernatant was discarded. The sedimented red blood cells (RBC) were washed by resuspending them in cold, sterile PBS (4 °C, pH 7.8) followed by centrifugation (2000x g, slowest deceleration setting, 4 °C, 10 min). This procedure was repeated until the absorbance (540 nm) of the supernatant was 0.2 or less (approximately 5 times). The RBCs were diluted in PBS (4 °C, pH 7.8) to a 1 % concentration and added to a 96-well plate (300 µL / well, i.e. approximately 1.6 x 10^7 cells/ well). Seven dilutions of each venom sample were then added to the plate in triplicates, as well as triplicates of a negative (PBS) and of a positive control (1 % Triton™ x-100, Sigma-Aldrich, now Merck KGaA). The samples were incubated for 30 min at 37 °C and afterwards centrifuged at 3000x g (slowest deceleration setting, 4 °C, 10 min). The supernatant was transferred to a flat-bottom 96-well plate to measure the absorbance (540 nm) of the released haemoglobin. Haemolysis results were plotted as relative percentages from the positive (100 % lysis) and the negative (0 % lysis) control. The graphs were created in Prism 7 (GraphPad, Inc.).

3.2.6. Dual apoptosis assay

To test if *C. fleckeri* venom induces apoptosis in cardiomyocytes, cells were analysed by flow cytometry with the NucView® 488 (caspase-3 detection) and CF®640R (phosphatidylserine detection through annexin-V binding) Dual Apoptosis Assay Kit for Life Cells (Biotium, Inc.). Cardiomyocytes were counted to prepare 200 µL solutions of 10^6 cells/mL and then exposed for 30 min to two concentrations (20 and 100 ng/mL) of crude *C. fleckeri* venom as well as of CTF-α, -β and -γ. Milli-Q water was used as negative control. Each sample was prepared in triplicates. After incubation, the cells were centrifuged at 150 *g* for 5 min at room temperature, the supernatant was decanted, and the resulting cell pellets were resuspended in 200 µL 1x annexin-V binding buffer. Each sample was then incubated in the dark for 30 min with 5 µL of 0.2 mM NucView® 488 Caspase-3 substrate stock solution (resulting in 5 µM final concentrations) and 5 µL of CF®640R annexin-V stock solution (no concentration given). Further, two additional triplicate samples incubated with venom (20 and 100 ng/mL) were stained for 10 min with Propidium Iodide only (permeant to dead cells; Invitrogen™, Thermo Fisher Scientific) to compare the number of dead cells to the number of apoptotic cells. After incubation, 400 µL 1x annexin-V binding buffer was added to each tube and the fluorescence was measured in FITC (excitation/emission 485/515 nm), Cy®5 (excitation/emission 642/662) an PE (excitation/emission 493/636 nm) channels on a BD FACSCanto II (BD Biosciences) with the BD FACSDiva software (BD Biosciences). Statistical analysis (MANOVA and ANOVA with Tukey multiple comparison of means) of the geometric means of the fluorescent signal intensities and graph generation was done in Diva, R (R Foundation) and Prism 7 (GraphPad Software Inc.).

3.3. Results

3.3.1 Identification of major proteins in CTF-α, CTF-β and CTF-γ

C. fleckeri venom was fractionated as previously reported [5] using the same methodology and conditions (Figure 1). To identify the major venom proteins in the fractions CTF-α, CTF-β and CTF-γ, each fraction was analysed by mass spectrometry and the results were matched against three databases (*C. fleckeri, C. barnesi,*and an unreviewed toxins database). Overall, the Type I *C. fleckeri* toxins CfTX-1 and CfTX-2 were both present in all three fractions. The Type II *C. fleckeri* toxins CfTX- A and -B were both present in CTF-β and CTF-γ, but toxin CfTX-A was not present in fraction CTF-α. The two top hits in each fraction were: CfTX-1 and CfTX-2 for CTF-α; CaTX-A (*Carybdea alata*) and CfTX-A for CTF-β; CrTX-A (*Carybdea rastoni*) and CfTX-A for CTF-γ. The top five venom protein hits all came from the *C. fleckeri* database and are given in Table 1, including the sequence coverage at 95 % confidence and the number of unique peptides identified at 95 % confidence. All three CTFs contained all toxins listed in Table 1 (CfTX-1 and -2, CfTX-A and -B, CaTX-A, CrTX-A and CqTX-A (*Chiropsalmus yamaguchii*)), albeit some toxins not making the top five hit list of each fraction. The data presented here are only from the *C. fleckeri* database as the other databases did not result in any higher-ranking hits.

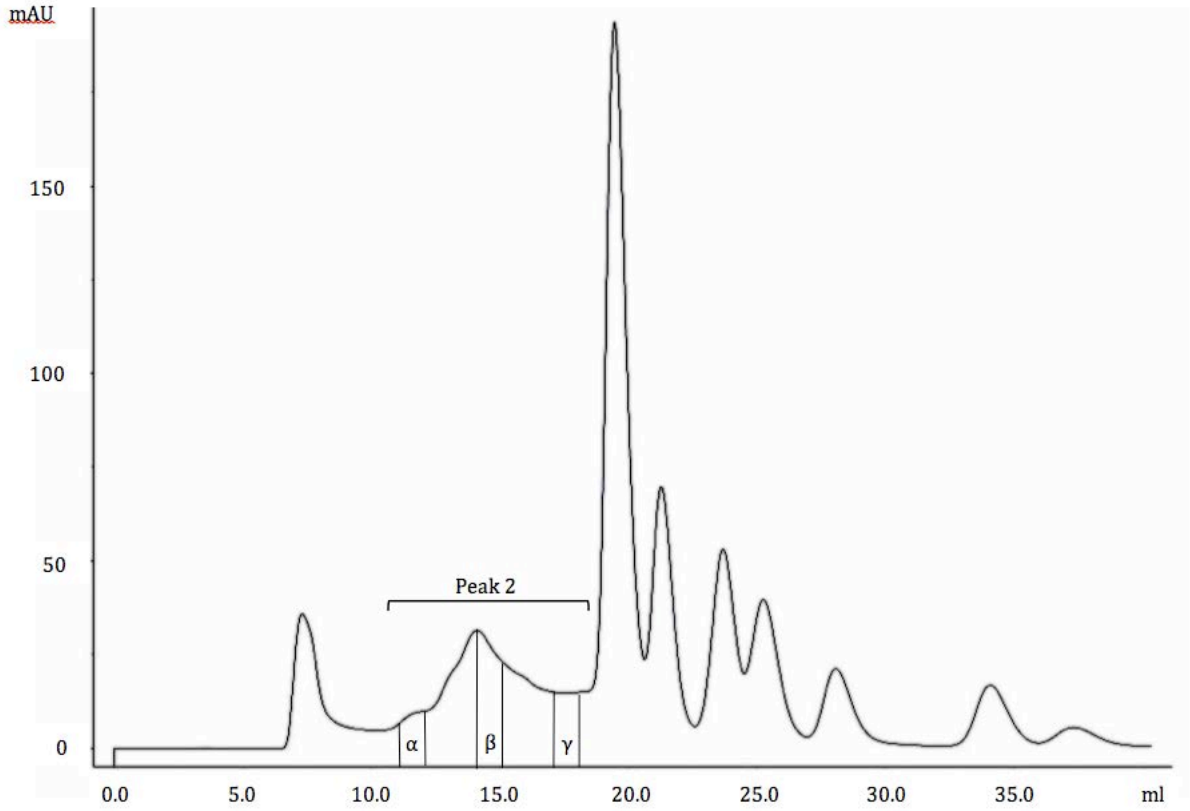

Figure 1: Size-exclusion chromatogram of *C. fleckeri* venom. The x-axis represents the elution volume in mL and the y-axis is a measure of the intensity of the 280 nm absorbance in mAU. CTF-α, CTF-β and CTF-γ are indicated within Peak 2 and are each composed of two 0.5 mL fractions.

Table 1: Top five predicted protein hits for CTF-α, CTF-β and CTF-γ*.

Sample	Top Hits	Species	Unique peptides (95 %)	% sequence coverage (95 %)
CTF-α	CfTX-1 (~ 43 kDa)	*C. fleckeri*	207	81.99
	CfTX-2 (~ 45 kDa)	*C. fleckeri*	180	78.62
	CaTX-A (43 kDa)	*C. alata*	32	53.78
	CfTX-B (~ 42 kDa)	*C.fleckeri*	30	63.77
	CqTX-A (44 kDa)	*C. yamaguchii*	27	77.66
CTF- β	CaTX-A	*C. alata*	412	71.40
	CfTX-A (~ 40 kDa)	*C. fleckeri*	409	66.74
	CfTX-B	*C. fleckeri*	397	75.27
	CfTX-2	*C. fleckeri*	100	78.55
	CfTX-1	*C. fleckeri*	91	77.64
CTF- γ	CrTX-A (43 kDa)	*C. rastoni*	168	66.16
	CfTX-A	*C. fleckeri*	89	64.1
	CfTX-B	*C. fleckeri*	68	70.93
	CaTX-A	*C. alata*	61	70.63
	CfTX-2	*C. fleckeri*	51	70.33

*The hits were ranked by the number of unique peptides (at 95 % confidence). Note, the number of unique peptides is a semiquantitative method to determine relative protein abundances only [23,24]. The size of each protein is lowercased once after the first appearance of that protein. ~ indicates approximate molecular weights due to potential posttranslational modifications. The percentage of sequence coverage was predicted at 95 % confidence.

3.3.2. Realtime cell assay of human fibroblasts and cardiomyocytes

Human fibroblasts and cardiomyocytes were treated with several concentrations of *C. fleckeri* venom and the three fractions CTF-α, CTF-β and CTF-γ, to test if the venom or the fractions had a more pronounced effect on either cell line. Only CTF-γ had a significantly higher effect on cardiomyocytes than on fibroblasts with IC_{50} concentrations of 0.38 µg/mL (95 % CI: 0.26-0.68 µg/mL) and 2.03 µg/mL (95 % CI: 1.55-2.65 µg/mL), respectively (Figure 2D, Figure 3 and Table 2). The effects of the other samples did not differ significantly between cell lines and resulted in similar dose-response curves (Figure 2A, 2B, 2C, 2 and Table 2). *C. fleckeri* venom was 114 times as toxic as the least toxic CTF-α fraction with IC_{50} concentrations on fibroblasts of 0.34 µg/mL (95 % CI: 0.24-0.47 µg/mL) and 38 µg/mL (95 % CI: 22.26-473.12 µg/mL), respectively (See table 3 for detailed statistics). However, CTF-α displayed such low toxicity that the calculation of the IC_{50} calculation is not reliable; this is reflected in the very large 95 % CI. There were no significant differences between the IC_{50} concentrations of *C. fleckeri* venom, CTF-β and CTF-γ on cardiomyocytes; the IC_{50} for CTF-α could not be determined because it did not induce sufficient toxicity at 10 minutes of envenomation (Table 3).

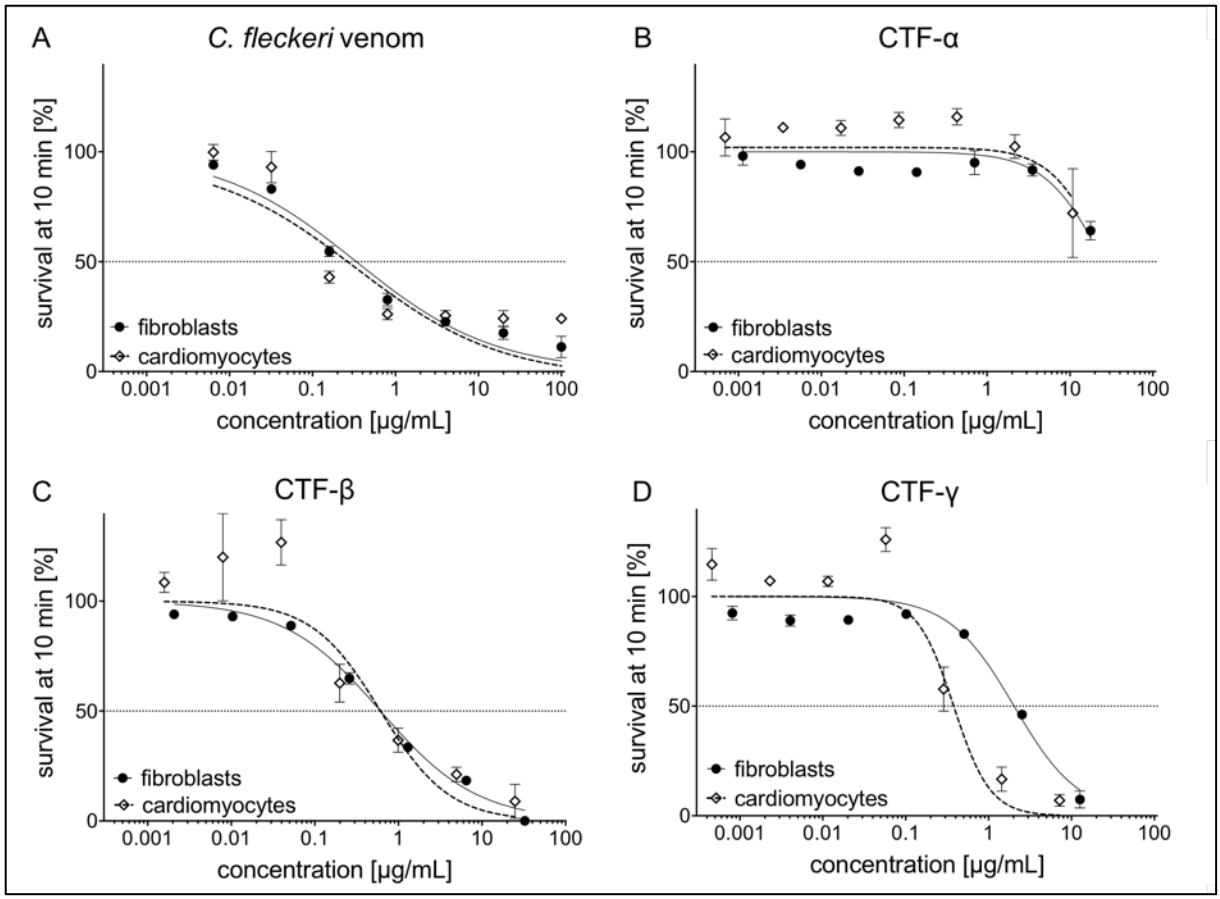

Figure 2: Dose-response curves of (A) *C. fleckeri* venom, (B) CTF-α, (C) CTF-β and (D) CTF-γ on cardiomyocytes and fibroblasts. The x-axis shows the concentration [ng/mL] and the y-axis represents the percentage of cell survival 10 minutes post envenomation. 50 % survival is marked by the horizontal dotted line. Fibroblasts are represented by a continuous line with full circles and cardiomyocytes by a dotted line with clear diamonds. Error bars (standard deviation) are indicated for each data point. Some error bars were smaller than the symbols. All four samples induced a concentration dependent response in both cell lines; cell survival is decreasing with increasing sample concentrations.

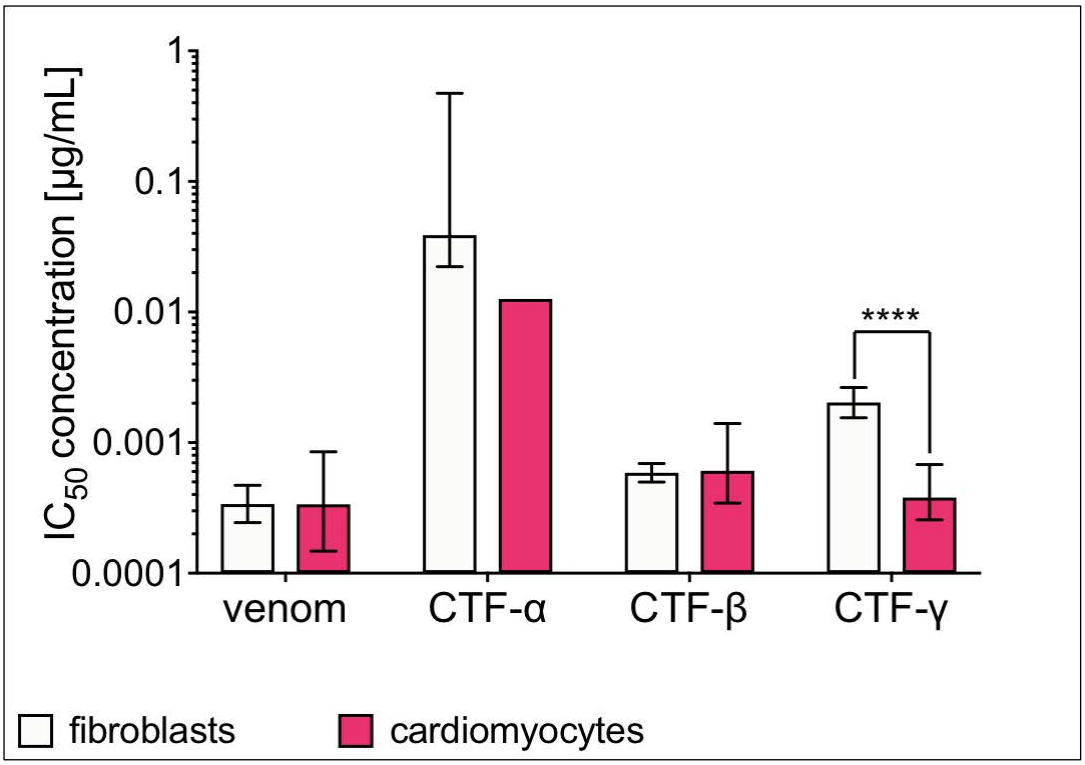

Figure 3: IC_{50} concentrations of *C. fleckeri* venom, CTF-α, CTF-β and CTF-γ for fibroblasts (white) and cardiomyocytes (solid red). The x-axis represents the different samples and the y-axis the IC_{50} concentrations [µg/mL]. The y-axis is represented on a logarithmic scale due to the large differences in sample potency. The error bars represent the standard deviation.

Table 2: Statistical comparison of IC_{50} concentrations between fibroblasts and cardiomyocytes for *C. fleckeri* venom, CTF-α, CTF-β and CTF-γ.

	Fibroblasts		**Cardiomyocytes**		**Cell-line comparison**		
Sample	IC_{50} [µg/mL]	95 % CI [µg/mL]	IC_{50} [µg/mL]	95 % CI [µg/mL]	p-value	F (DFn, DFd)	fold-change
C. fleckeri venom	0.34	0.24-0.47	0.34	0.15-0.85	0.9982	5.18 x 10^{-6} (1,38)	n/a
CTF-α	38.79	22.26-473.12	~12.6[#]	n/a (very wide)	n/a	n/a	n/a
CTF-β	0.59	0.5-0.69	0.61	0.35-1.12	0.8586	0.03219 (1,38)	n/a
CTF-γ	2.03	1.55-2.65	0.38	0.26-0.81	< 0.0001	29.01 (1,38)	5.3

95 % CI indicates the 95 % confidence interval of the calculated IC_{50} concentrations. Statistical output is given as p-value and F-statistic including the degrees of freedom. Significant p-values are highlighted in red. [#] Unreliable calculation due to the extremely low toxicity of CTF-α (None of the tested concentrations resulted in 50 % lysis.)

Table 3: Statistical comparison of IC_{50} concentrations between samples for fibroblast and cardiomyocytes.

	Fibroblasts		Cardiomyocytes	
Compared samples	p-value	F (DFn, DFd)	p-value	F (DFn, DFd)
C. fleckeri venom vs. CTF-α	< 0.0001	347.4 (1,38)	n/a	n/a
C. fleckeri venom vs. CTF-β	< 0.0022	10.8 (1,38)	0.2453	1.4 (1, 36)
C. fleckeri venom vs. CTF-γ	< 0.0001	66.8 (1.38)	0.8204	0.1 (1, 38)
CTF-α vs. CTF-β	< 0.0001	550.0 (1,38)	n/a	n/a
CTF-α vs. CTF-γ	< 0.0001	153.3 (1,38)	n/a	n/a
CTF-β vs. CTF-γ	< 0.0001	58.5 (1,38)	0.2478	1.4 (1, 36)

95 % CI indicates the 95 % confidence interval of the calculated IC_{50} concentrations. Statistical output is given as p-value and F-statistic including the degrees of freedom. Significant below 0.05 p-values are highlighted in red.

3.3.3. Haemolytic activity

The haemolytic activity of *C. fleckeri* venom, CTF-α, CTF-β and CTF-γ was tested on human and mouse erythrocytes to determine if there were differences in sensitivity between the two species. All the samples were more lytic to mouse than to human erythrocytes (Figures 4 and 5). The 50 % haemolytic activity (HU_{50}) concentrations for mouse erythrocytes were significantly lower than those for humans for *C. fleckeri* venom (~ 47 times), CTF-α (~ 37

times) and CTF-γ (~ 5.5 times) than for human erythrocytes; the HU_{50} for CTF-β on mouse blood could not be reliably calculated, as all the concentrations tested induced approximately 100 % haemolysis (Figure 5 and Table 4). The most haemolytic fraction for both human and mouse erythrocytes, was CTF-β (and *C. fleckeri* venom) and the least haemolytic fraction was CTF-α (Figure 5, Table 4 and 5).

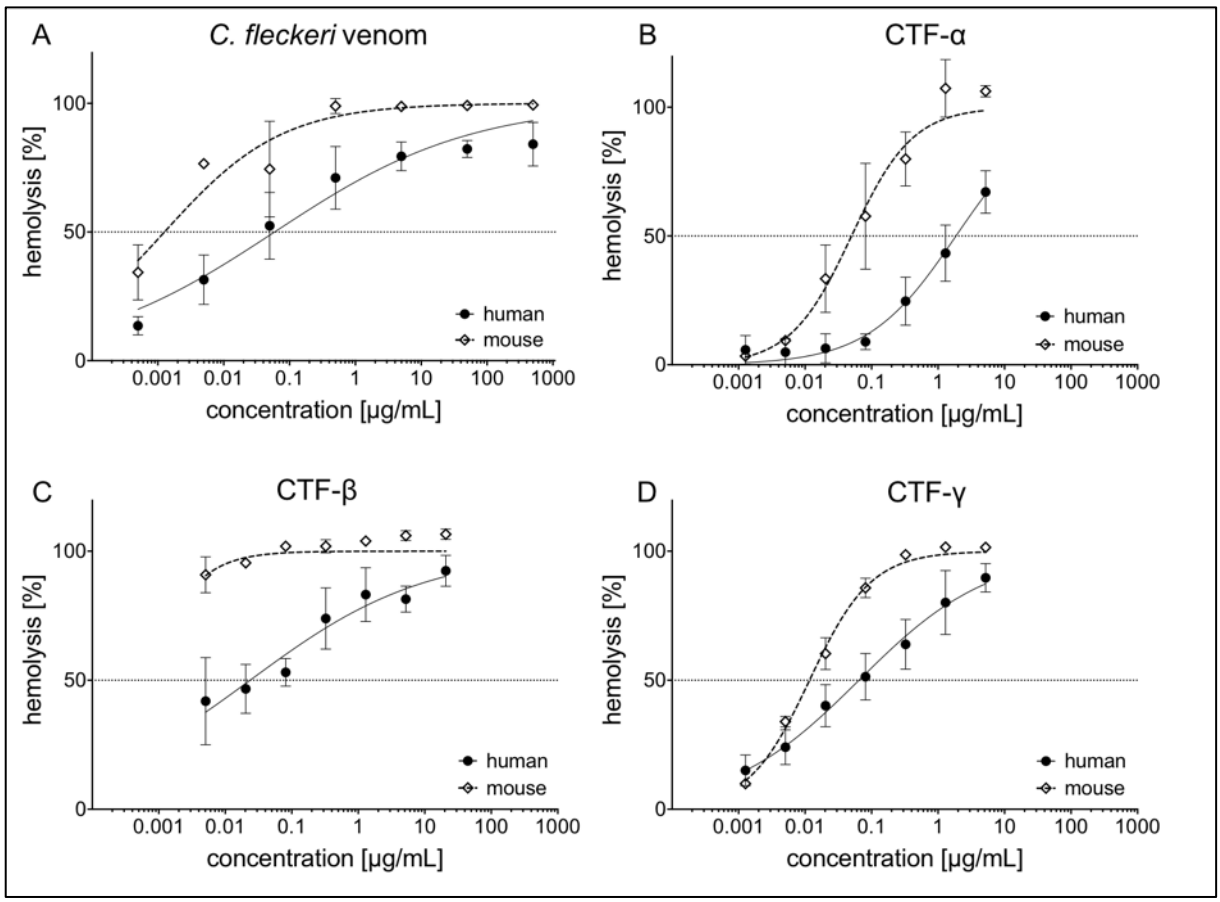

Figure 4: Dose-response curves of (A) *C. fleckeri* venom, (B) CTF-α, (C) CTF-β and (D) CTF-γ on human and mouse erythrocytes. The x-axis shows the concentration [ng/mL] and the y-axis represents the percentage of haemolysis. 50 % haemolysis is marked by the horizontal dotted line. Human erythrocytes are represented by a continuous line with full circles and mouse erythrocytes by a dotted line with clear diamonds. The error bars represent the standard deviation. All four samples induced a concentration dependent response in both cell lines; haemolysis is increasing with sample concentrations.

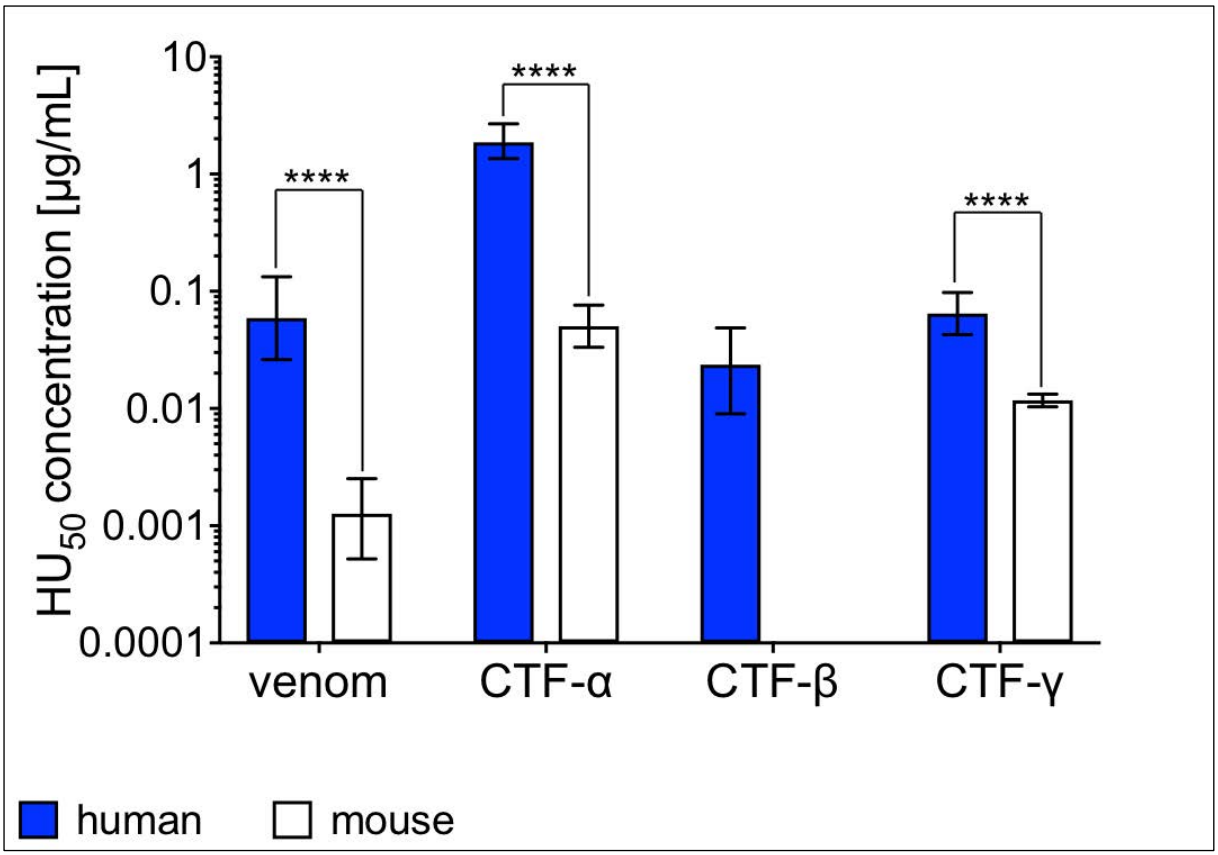

Figure 5: HU_{50} concentrations of *C. fleckeri* venom, CTF-α, CTF-β and CTF-γ for human (solid blue) and mouse (white) erythrocytes. The x-axis represents the different samples and the y-axis the concentration [µg/mL] at which 50 % of the erythrocytes undergo haemolysis (HU_{50}). The y-axis is represented on a logarithmic scale due to the large differences in sample potency. The error bars represent the standard deviation. The mouse erythrocyte IC_{50} for CTF-β was too low to be reliably calculated, as all tested concentrations induced approximately 100 % haemolysis.

Table 4: Statistical comparison of HU_{50} concentrations between human and mouse erythrocytes for *C.fleckeri* venom, CTF-α, CTF-β and CTF-γ .

Sample	Human		Mouse		Comparison of cell lines		
	HU_{50} [µg/mL]	95 % CI [µg/mL]	HU_{50} [µg/mL]	95 % CI [µg/mL]	p-value	F (DFn, DFd)	fold-change
C. fleckeri venom	0.059	0.026-0.133	0.001	0.001-0.003	< 0.0001	45.0 (1,37)	47
CTF-α	1.862	1.353-2.682	50.1	0.033-0.076	< 0.0001	197.4 (1,37)	37
CTF-β	0.024	0.009-0.049	0.001†	n/a	n/a	n/a	n/a
CTF-γ	0.065	0.043-0.098	0.012	0.011-0.013	< 0.0001	80.6 (1,38)	5.5

95 % CI indicates the 95 % confidence interval of the calculated HU_{50} concentrations. Statistical output is given as p-value and F-statistic including the degrees of freedom. Significant p-values are highlighted in red. † Unreliable calculation due to the extremely high toxicity of CTF-β (Each of the tested concentration resulted in approximately 100 % lysis.)

Table 5: Statistical comparison of HU_{50} concentrations between samples for human and mouse erythrocytes.

Compared samples	Human		Mouse	
	p-value	F (DFn, DFd)	p-value	F (DFn, DFd)
C. fleckeri venom vs. CTF-α	< 0.0001	74.2 (1, 38)	< 0.0001	85.4 (1, 36)
C. fleckeri venom vs. CTF-β	0.0913	3.0 (1, 38)	0.7	0.2 (1, 37)
C. fleckeri venom vs. CTF-γ	0.8324	0.1 (1, 38)	< 0.0001	66.0 (1, 38)
CTF-α vs. CTF-β	< 0.0001	168.1 (1, 38)	n/a	n/a
CTF-α vs. CTF-γ	< 0.0001	158.3 (1, 38)	< 0.0001	n/a
CTF-β vs. CTF-γ	0.0129	6.8 (1,38)	n/a	n/a

95 % CI indicates the 95 % confidence interval of the calculated IC_{50} concentrations. Statistical output is given as p-value and F-statistic including the degrees of freedom. Significant p-values are highlighted in red.

3.3.4. Apoptosis assay

Cardiomyocytes were treated with two concentrations of *C. fleckeri,* CTF-α, CTF-β and CTF-γ and analysed by flow cytometry to test for the presence of the apoptotic indicators caspase-3 and phosphatidylserine (PS). During early apoptosis pro-caspase-3 is activated to caspase-3, thus detection of caspase-3 is an indicator for early apoptosis [25]. During the mid/late stages of apoptosis, PS (a cytosolic component of the cell membrane) is expressed on the outer cell

membrane, allowing detection of apoptosis with the non-cell permeant annexin-V stain, which has a high affinity for PS [26].

The fluorescent signal intensity was tested for normality using a quantile plot (data not shown) and revealed an approximate normal distribution (the sample size was a limiting factor). The two dependent variables (annexin-V and caspase-3) were also at least somewhat correlated (data not shown) and therefore a MANOVA was conducted to test if there was a significant difference between the fluorescent signals for annexin-V and caspase-3, followed by an ANOVA including a Tukey's comparison of the mean values for each tested venom type.

The results indicate significant differences in fluorescent signal expression for annexin-V (PS-binding) and caspase-3 among the treatment groups (*C. fleckeri ,* CTF-α, CTF-β and CTF-γ) for both concentrations ($p < 0.0001$, $F_{Dfn, Dfd} = 11.011_{18, 40}$). In detail, at 20 ng/mL there was a significant overall difference (i.e. cumulative fluorescent signal intensity of annexin-V and caspase-3 dye) between treatment groups ($p = 0.03404$ $F_{Dfn, Dfd} = 2.7029_{8, 20}$) and accordingly a significant difference in annexin-V ($p < 0.001$, $F_{Df} = 12.893_{4}$) and caspase-3 fluorescent signal intensity ($p < 0.0001$, $F_{Df} = 721.01_{4}$). Similarly, the treatment groups differed significantly at 100 ng/mL in the overall fluorescent signal intensity ($p = 0.03404$ $F_{Dfn, Dfd} = 2.7029_{8, 20}$) as well as for the signal for annexin-V ($p < 0.001$, $F_{Df} = 12.94_{4}$) and caspase-3 ($p < 0.0001$, $F_{Df} = 130_{4}$) (Figure 6-9). Unfractionated *C. fleckeri* venom did not differ from the control for either concentration (Figure 6). At the lower concentration, only CTF-γ induced a significant increase in the annexin-V and caspase-3 fluorescent signal intensity, more so for the latter than for the former (Figure 9). At 100 ng/mL, compared to the control, CTF-α induced a significant increase in the annexin-V signal intensity, but no caspase-3 was detected (Figure 7). CTF-β (Figure 8) had the reverse effect to CTF-α and did not induce an increase in the annexin-V signal intensity but appeared to induce caspase-3 activation. Of all tested treatments, CTF-γ

induced the most significant increase in the annexin-V signal intensity and (more so) in caspase-3 activation in cardiomyocytes at both concentrations (Figure 10 and 11). The results of the Tukey's multiple comparison test are given in Table 6 and 7.

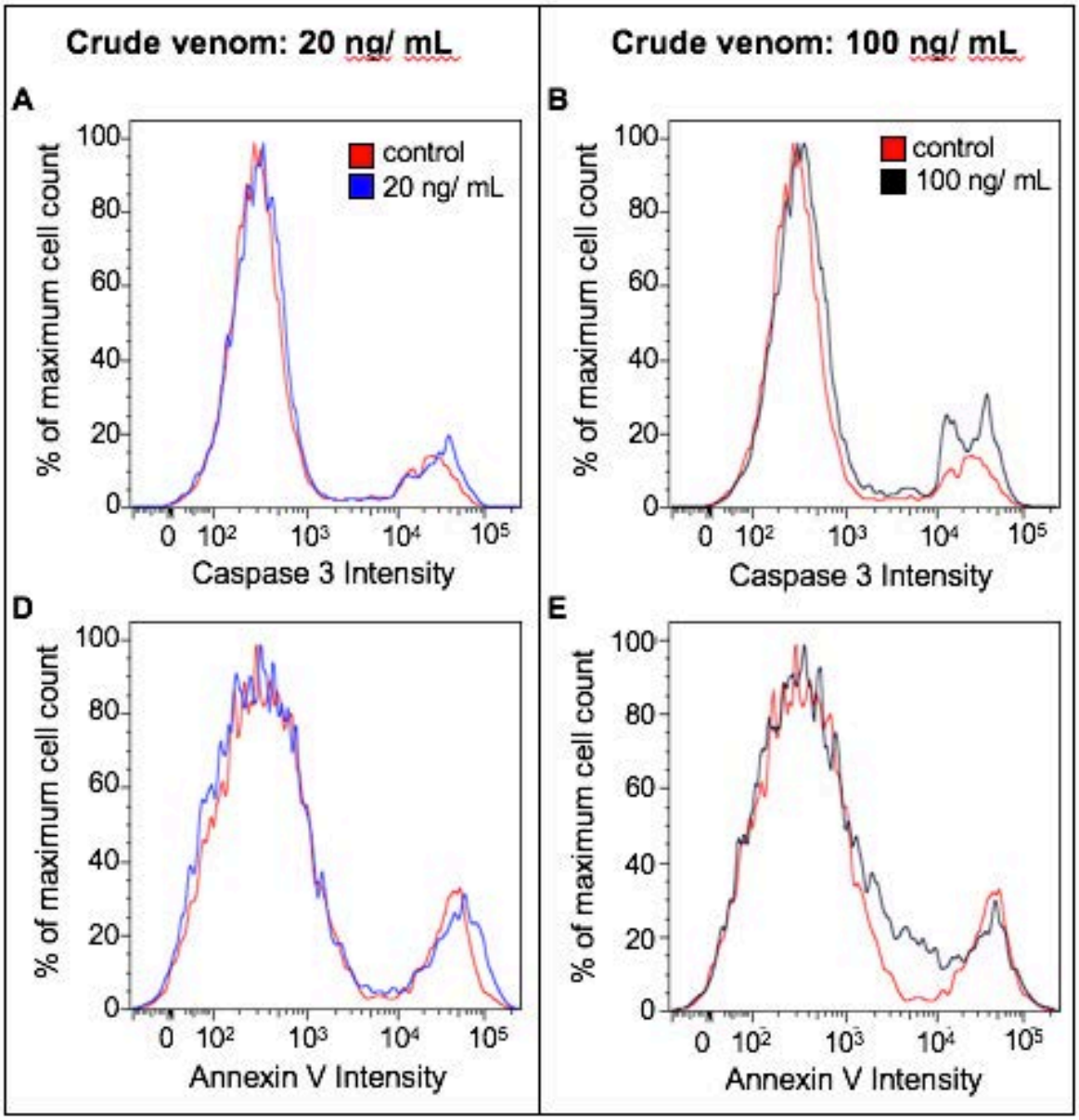

Figure 6: *C. fleckeri* venom effect on cardiomyocytes exhibiting fluorescent signal intensities of caspase-3 and annexin-V at 2 concentrations: 20 ng/mL (blue) and 100 ng/mL (black). The control is indicated in red. Healthy cells exhibit low fluorescent signal intensities for both dyes of up to approximately 10^3. Apoptotic cells are in the fluorescent signal intensity range of 10^4 – 10^5. Both cell populations (healthy and apoptotic) are present for all treatments (including the control), with the no increase in the number of apoptotic cells compared to the control when exposed to 20 ng/mL or 100 ng/mL of *C. fleckeri* venom.

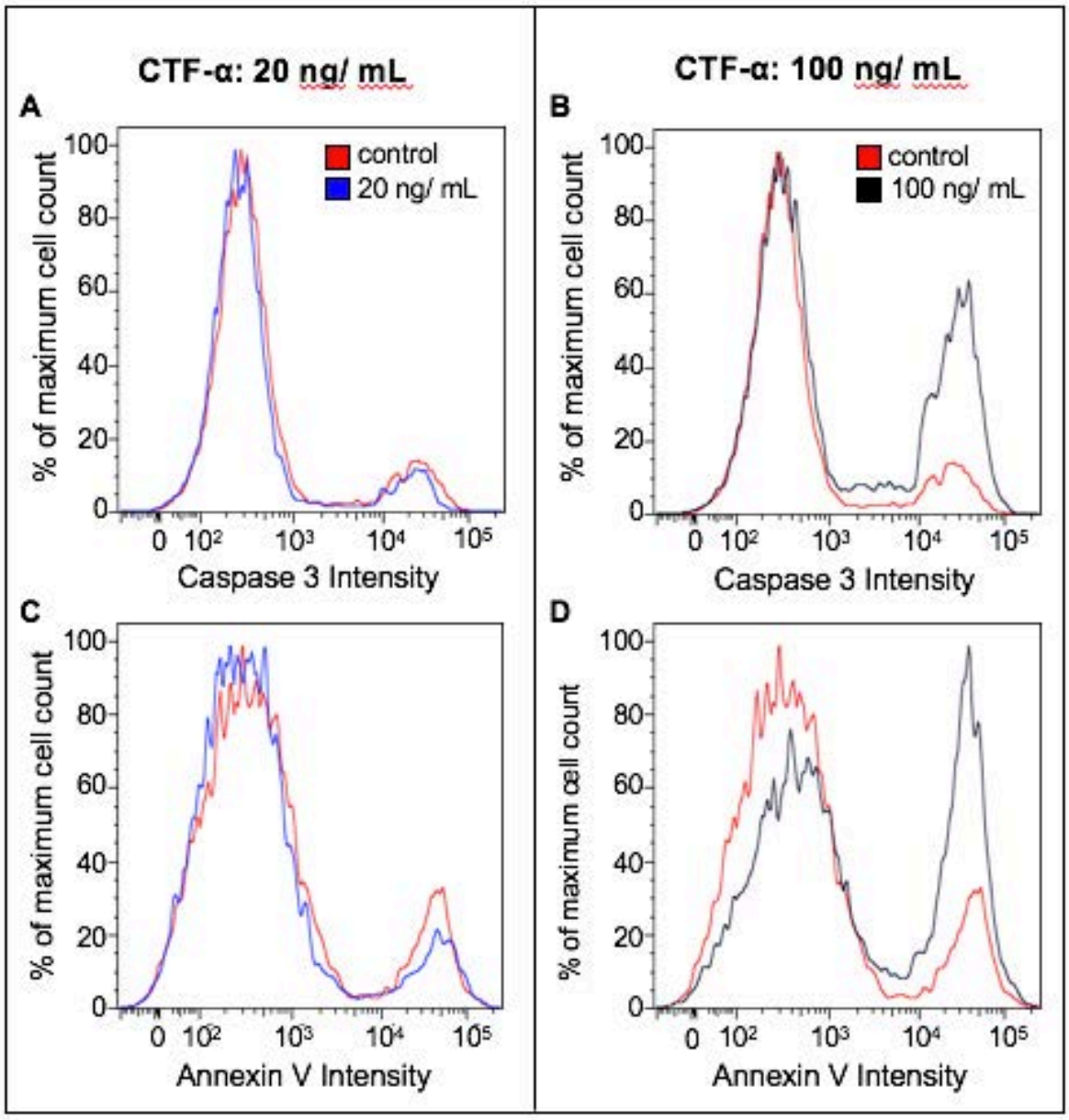

Figure 7: CTF-α effect on cardiomyocytes exhibiting fluorescent signal intensities of caspase-3 and annexin-V (binds to PS) at 2 concentrations: 20 ng/mL (blue) and 100 ng/mL (black). The control is indicated in red. Healthy cells exhibit low fluorescent signal intensities for both dyes of up to approximately 10^3. Apoptotic cells are in the fluorescent signal intensity range of 10^4 – 10^5. Both cell populations (healthy and apoptotic) are present for all treatments (including the control), with the number of apoptotic cells increasing compared to the control when exposed to 100 ng/mL, but not 20 ng/mL, of CTF-α.

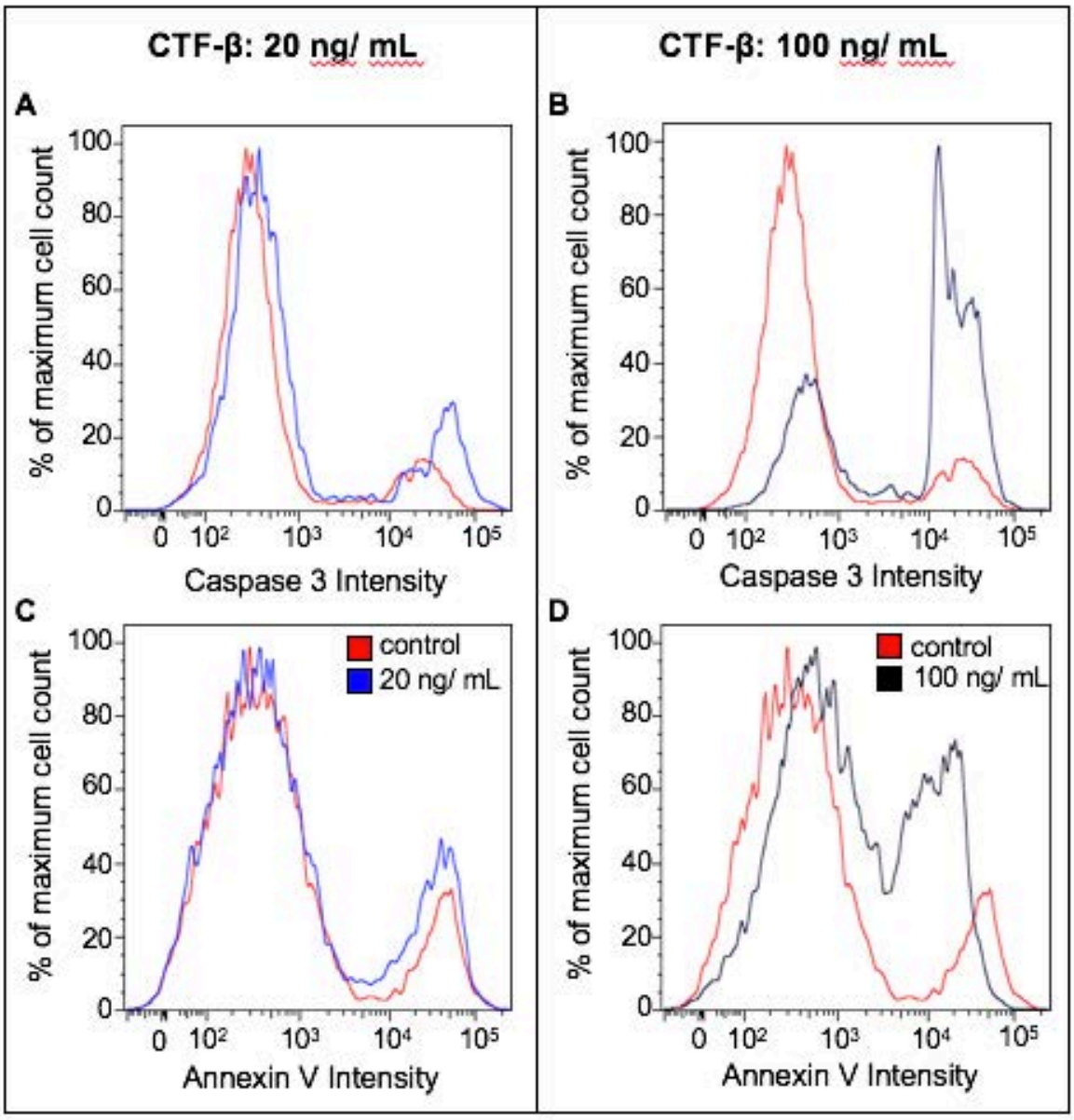

Figure 8: CTF-β effect on cardiomyocytes exhibiting fluorescent signal intensities of caspase-3 and annexin-V at 2 concentrations: 20 ng/mL (blue) and 100 ng/mL (black). The control is indicated in red. Healthy cells exhibit low fluorescent signal intensities for both dyes of up to approximately 10^3. Apoptotic cells are in the fluorescent signal intensity range of 10^4 – 10^5. Both cell populations (healthy and apoptotic) are present for all treatments (including the control), with the number of apoptotic cells increasing compared to the control when exposed to 100 ng/mL, but not 20 ng/mL, of CTF-β.

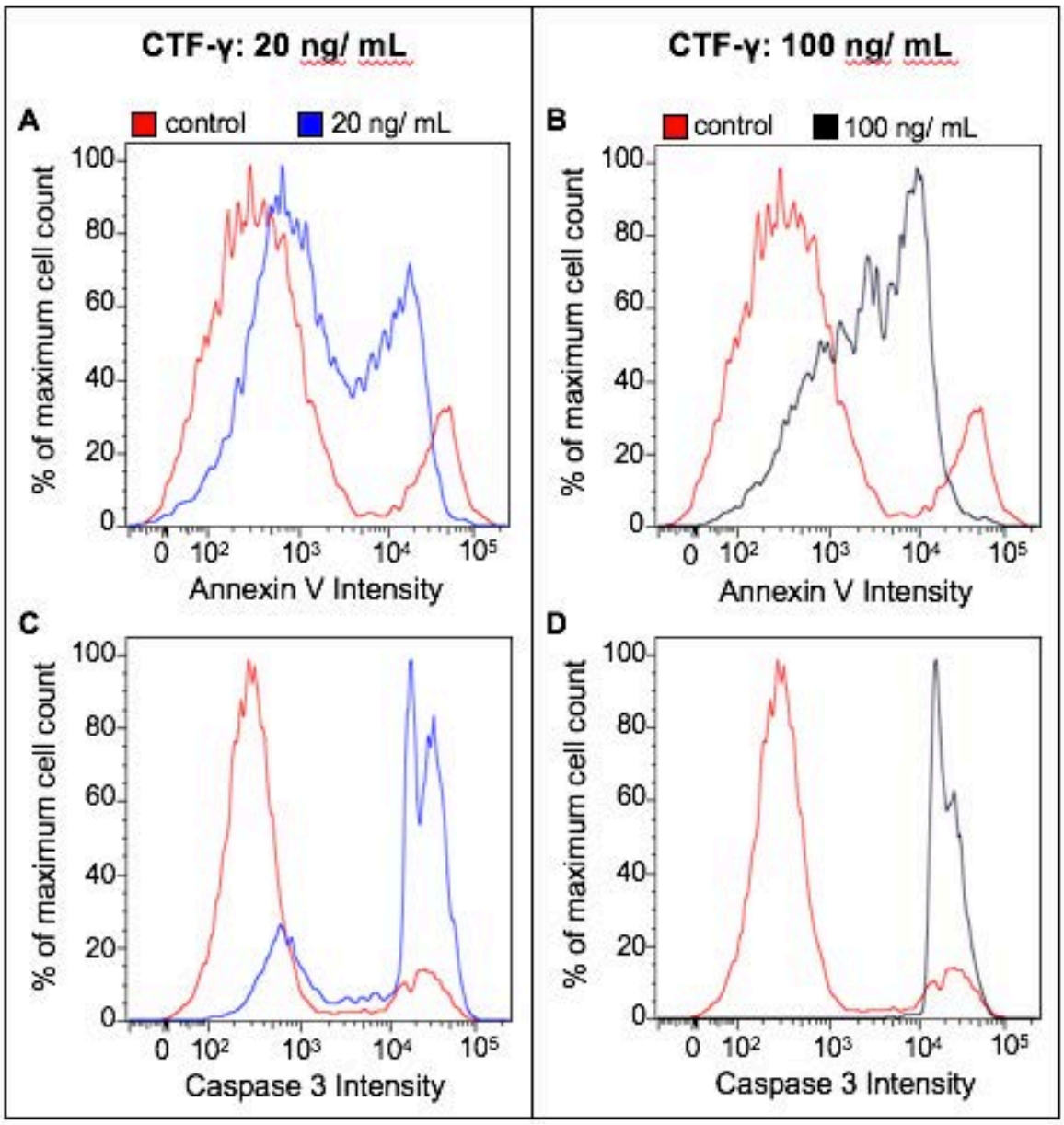

Figure 9: CTF-γ effect on cardiomyocytes exhibiting fluorescent signal intensities of caspase-3 and annexin-V at 2 concentrations: 20 ng/mL (blue) and 100 ng/mL (black). The control is indicated in red. Healthy cells exhibit low fluorescent signal intensities for both dyes of up to approximately 10^3. Apoptotic cells are in the fluorescent signal intensity range of 10^4 – 10^5. Both cell populations (healthy and apoptotic) are present for all treatments (including the control), with the number of apoptotic cells increasing compared to the control when exposed to either concentration of CTF-γ.

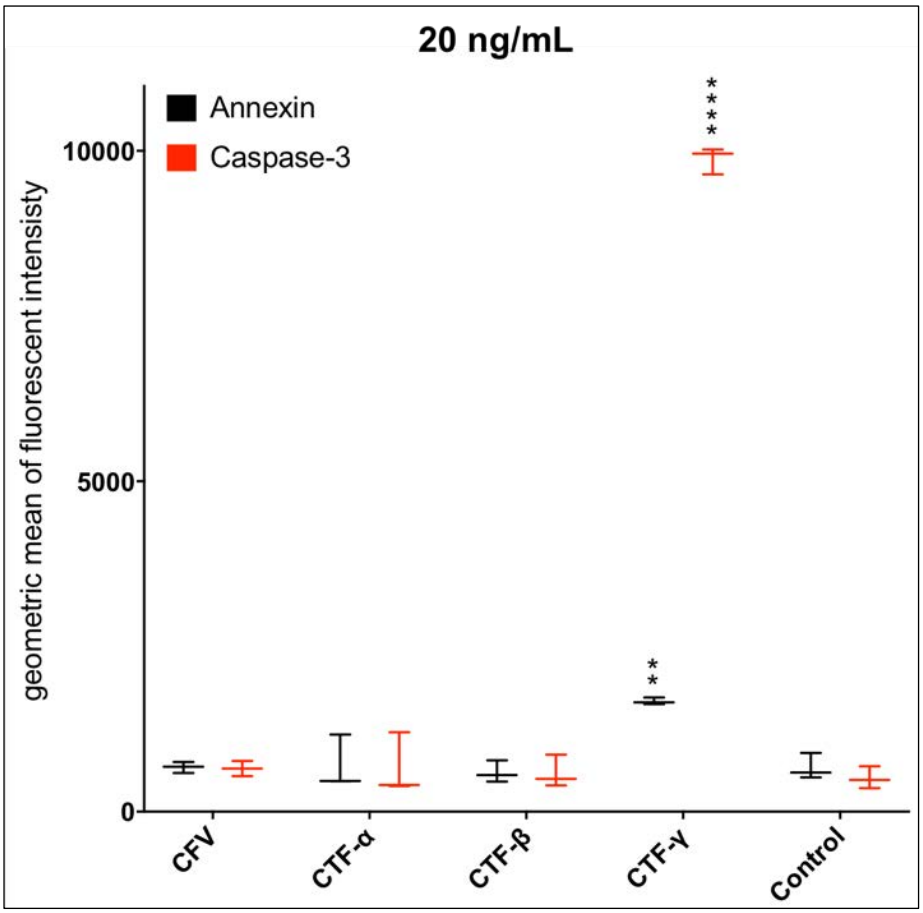

Figure 10: Geometric means of fluorescent signal intensities from the annexin-V (black) and caspase-3 (red) fluorescent signals in cardiomyocytes exposed to 20 ng/mL of *C. fleckeri* venom (CFV), CTF-α, CTF-β, CTF-γ and a control (100 % Milli-Q-water). The y-axis represents the geometric means and the x-axis represents the different venom compounds. The error bars represent the standard deviation. Significant increases in fluorescent signal intensity compared to the control are represented by ** ($p < 0.01$) and **** ($p < 0.0001$).

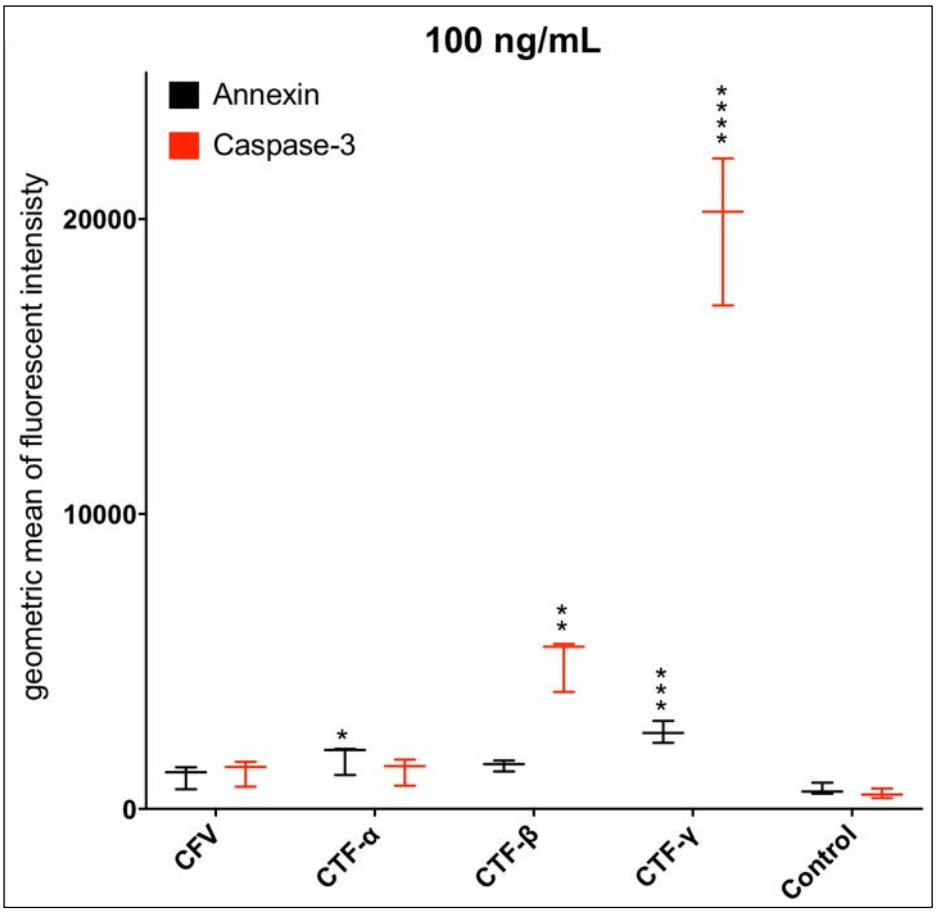

Figure 11: Geometric means of fluorescent signal intensities from the annexin-V (black) and caspase-3 (red) fluorescent signals in cardiomyocytes exposed to 100 ng/mL of *C. fleckeri* venom (CFV), CTF-α, CTF-β, CTF-γ and a control (100 % Milli-Q-water). The y-axis represents the geometric means and the x-axis represents the different venom compounds. The error bars represent the standard deviation. Significant increases in fluorescent signal intensity compared to the control are represented by * ($p < 0.05$), ** ($p < 0.01$), *** ($p < 0.001$) and **** ($p < 0.0001$).

Table 6: Summary of p-values (9 5 % CI) for Tukey's comparison of means of annexin-V and caspase-3 fluorescent signal intensities induced by 20 ng/ mL of *C. fleckeri*, CTF-α, CTF-β and CTF-γ.

Compared samples (20 ng/ mL)	Annexin-V			Caspase-3		
	p-value	Difference	95 % CI	p-value	Difference	95 % CI
Control - *C. fleckeri* venom	0.9999	-7.3	-596.0 – 581.3	0.9609	-144.0	-862.8 – 574.8
Control - CTF-α	0.9997	-32.3	-621.0 – 556.3	0.9492	-155.3	-874.2 – 563.5
Control - CTF-β	0.9942	70.0	-518.7 – 658.7	0.996	-77.7	-796.5 – 641.2
Control - CTF-γ	0.0016	-1,004.3	-1,593.9 – -415.7	<0.0001	-9,366.3	-10,085.2 – -8,647.5
C. fleckeri venom - CTF-α	0.9999	-25.0	-613.7 – 563.7	< 1	-11.3	-730.2 – 707.5
C. fleckeri venom - CTF-β	0.9916	77.3	-511.3 – 666.0	0.9978	66.3	-652.5 – 785.2
C. fleckeri venom - CTF-γ	0.0017	-997.0	-1,585.6 – -408.4	< 0.0001	-9,222.3	-9,941.2 – -8,503.5
CTF-α - CTF-β	0.9763	102.3	-486.3 – 691.0	0.996	77.7	-641.2 – 796.5
CTF-α - CTF-γ	0.0020	-972.0	-1,560.7 – -383.4	< 0.0001	-9,211.0	-9,929.8 – -8,492.2
CTF-β - CTF-γ	0.001	-1074.3	-1,663.0 – -485.7	< 0.0001	-9,288.7	-10,007.5 – -8,569.8

Table 7: Summary of p-values (95 % CI) for Tukey's comparison of means of annexin-V and caspase-3 fluorescent signal intensities induced by 100 ng/ mL of *C. fleckeri*, CTF-α, CTF-β and CTF-γ.

Compared samples (100 ng/ mL)	Annexin-V			Caspase-3		
	p-value	difference	95 % CI	p-value	difference	95 % CI
Control - *C. fleckeri* venom	0.5558	-443.3	-1,383.9 – 497.2	0.9423	-745.7	-4,068.2 – 2,576.8
Control - CTF-α	0.026	-1,061.3	-2,001.9 – 120.8	0.9301	-789.7	-4,1112.2 – 2,532.8
Control - CTF-β	0.1002	-811.7	-1,752.2 – 128.8	0.0083	-4,503.7	-7,826.2 – -1,181.2
Control - CTF-γ	0.0004	-1,936.0	-2,876.5 – -995.5	< 0.0001	-19,278.0	-22,600.5 – -15,955.5
C. fleckeri venom - CTF-α	0.2678	-618.0	-1,558.5 – 322.5	< 1	-44.0	-3,366.5 – 3,278.5
C. fleckeri venom - CTF-β	0.7035	-368.3	-1,308.8 – 572.2	0.0256	-3,758.0	-7,080.5 – -435
C. fleckeri venom - CTF-γ	0.0028	-1,492.7	-2,433.2 – -552.1	< 0.0001	-18,532.3	-21,854.8 – -15,209.8
CTF-α - CTF-β	0.9002	249.7	-690.9 – 1,190.2	0.0274	-3,714.0	-7,036.5– -391.5
CTF-α - CTF-γ	0.0714	-874.7	-690.9 – 1,190.2	< 0.0001	-18,488.3	-21,810.8 – -15,165.8
CTF-β - CTF-γ	0.0185	-1,124.3	-2,064.9 – -183.8	< 0.0001	-14,774.3	-18,096.8 – -11,451.8

3.4. Discussion

The present characterisation of the fractions CTF-α, CTF-β and CTF-γ has provided further insight into *C. fleckeri* venom proteins and their cytotoxic effects. CTF-α, CTF-β and CTF-γ show a similar composition of cubozoan venom proteins with variation in abundance of these proteins and thus varying cytotoxic effects that are induced through potentially distinct molecular pathways.

3.4.1. Toxin identification of CTF-α, CTF-β and CTF-γ

The top five protein hits of the three fractions included the *C. fleckeri* toxins CfTX-1, CfTX-2, CfTX-A and CfTX-B. Interestingly, they also abundantly included other cnidarian toxins, namely CaTX-A (*C. alata*), CrTX-A (*C. rastoni*) and CqTX-A (*C. yamaguchii*). In fact, while the most abundant hit for CTF-α was a *C. fleckeri* toxin (i.e. CfTX-1), for CTF-β it was the *C. alata* toxin CaTX-A (albeit along with toxins CfTX-A and -B), and for CTF-γ it was the *C. rastoni* toxin CrTX-A, each counting at least 160 unique peptides and a minimum of 66 % sequence coverage. These matches all came from the *C. fleckeri* database [7], as none of the matches from the toxins or the *C. barnesi* database (J. Potriquet) counted more than 20 unique peptides (data not shown). Due to the high level of homology across cnidarian protein toxins [7], it is not clear if the protein hits indicate the actual presence of these proteins or if the fractions contain unidentified toxins that are highly homologous to these hits. Without the assembly of the transcripts into a transcriptome reference library [7] this cannot be clarified.

Additional proteins were also predicted to be present in the fractions, for example protein disulfide isomerase 2, which is found in many organisms; 41 unique peptides were matched with approximately 50 % sequence coverage to this protein from the roundworm

Caenorhabditis elegans. In cone snails, protein disulfide isomerase aids conotoxin folding [27], thus it may be of relevance in *C. fleckeri* venom. However, the venom extraction method could lead to contamination, and given that *C. elegans* is widely distributed in Australia, it is not clear whether this match represents a contamination or an actual match. To avoid misinterpretation of the relevance of such matches, the data presented here stem from a conservative selection process.

3.4.1.1. CTF-α

CTF-α appears to be primarily composed of the potently cardiotoxic and haemolytic proteins CfTX-1 and CfTX-2. Despite the presence of these proteins, the IC_{50} of CTF-α indicated that it was the least potent fraction tested. The IC_{50} concentration for CTF-α at ten minutes post administration for human cardiomyocytes was greater than 12 µg/mL. The cardiomyocyte IC_{50} value (at the same time point) for CTF-α in the literature was approximately 20 times more potent (250 ng/mL) [5]. Further, CfTX-1 and CfTX-2 are thought to be responsible for the cardiovascular effects in vivo [8,9,28], therefore fractions containing predominantly these toxins were expected to display higher cardiotoxicity than other fractions. It is well documented that *C. fleckeri* venom, similar to other venomous animals [29], varies in toxicity depending on the size, the geographical location and the year the animal was collected [30]. While the venom used in the previous study [5] was collected from the same location and from similar sized animals, it was collected from different individuals in a different year and may contribute to weaker CTF-α toxicity as observed in the present study.

3.4.1.2. CTF-β

The most abundant protein in CTF-β were the *C. alata* toxin CaTX-A (412 unique peptides), a 43 kDa haemo- and cytolysin [31] and the *C. fleckeri* toxins CfTX-A and CfTX-B (409 and 397 unique peptides, respectively). CTF-β displayed the highest haemolytic activity of all the

tested fractions, with an HU_{50} concentration for mice of < 0.5 ng/mL, a concentration ten times higher than previously reported for fractions containing CfTX-A and -B [8]. CTF-β had a cardiomyocyte IC_{50} value of 0.6 μg/mL, which is consistent with previous data on this fraction [5].

3.4.1.3. CTF-γ

The top two hits for CTF-γ were the toxin CrTX-A from the box jellyfish *C. rastoni* [32] with 168 unique peptides followed by CfTX-A with 89 unique peptides. CrTX-A is a haemolysin that has been shown to be a more potent than CaTX-A [32], the top hit in fraction CTF-β. Although our results showed that CTF-β was more haemolytic than CTF-γ, it is likely that the concentration of CaTX-A in CTF-β is higher than the concentration of CrTX-A in CTF-γ, based on the number of unique peptides for those two proteins (412 and 168, respectively). Similarly, fraction CTF-β likely also contained a higher concentration of the potently haemolytic toxins CfTX-A and CfTX-B than CTF-γ, thus providing a logical rationale for the greater haemolytic activity observed in CTF-β.

3.4.1.4. Molecular weights of the CTF-toxins

The molecular weights previously reported for CTF-α, CTF-β and CTF-γ, based on size exclusion chromatography, are only partially consistent with the toxins identified in these fractions. The top-five toxins hits all have molecular weights between 40-45 kDa. The fact that the proportions of these toxins vary in the fractions, suggests that the individual toxins behave distinctly when passing through the size-exclusion column. For example, CTF-α was estimated at 75-85 kDa [5] and the top two hits for this fraction were CfTX-1 (~43 kDa) and CfTX-2 (~45 kDa), this suggests that CfTX-1 and/or -2 may be present in a dimerized form in the CTF-α fraction (oligomerisation of the CfTX-toxins has been previously suggested [8]). By contrast,

CTF-β was estimated at 35-45 kDa [5], which is consistent with all toxins in their monomeric state. The high presence of CaTX-A (43 kDa), CfTX-A (40 kDa) and CfTX-B (42 kDa) in this fraction, could suggest that these proteins may form predominantly monomers under the buffer conditions used. Similarly, CTF-γ, estimated to be below 15 kDa [5], may be composed of breakdown products of these toxins; the high presence of CrTX-A in this fraction may suggest that, under presented conditions CrTX-A fragments, and further, that these fragments are bioactive. More research is required to determine if the "separation" achieved by the size-exclusion chromatography of jellyfish venoms is perhaps influenced more by the dimeric/monomeric/fragmented state of the proteins under set conditions than by the actual molecular weight of the different jellyfish toxins.

3.4.2. Bioactivity of *C. fleckeri* venom

3.4.2.1. Lack of cardiospecificity of C. fleckeri venom

Previous data suggested that CTF-α and CTF-β may be composed of cardiospecific toxins because they were more toxic to human cardiomyocytes than to skeletal muscle cells [5]. The present study highlights the importance of assessing toxicity on a range of cell lines, as there was no indication that these two fractions were more toxic to human cardiomyocytes than to fibroblasts. As mentioned above, only CTF-γ, previously characterised as non-cardiospecific [5], was more toxic to the cardiomyocytes than to fibroblasts. In addition, all fractions were potently haemolytic, indicating that although *C. fleckeri* venom is highly cardiotoxic, it does not appear to be specific to cardiac cells when compared to skin derived fibroblast cells.

3.4.2.2. Comparison of haemolytic effects in mouse and human erythrocytes

Despite several studies showing haemolytic activity of the venom of *C. fleckeri in vitro* and *in vivo* (i.e. laboratory animals), haemolysis has not been reported in human envenomation victims [8,13-15]. The present HU_{50} comparison of human and mouse cells exposed to *C. fleckeri* venom, indicates that mouse erythrocytes are significantly (47-fold) more susceptible to the venom than human erythrocytes, with HU_{50} concentrations of approximately 1.2 ng/mL and 59 ng/mL, respectively. Discrepancies between laboratory animals and humans are well documented, and the differences in venom potencies might (at least somewhat) explain why haemolysis is seen in some laboratory animals but not in humans. However, many studies on *C. fleckeri* venom were conducted on rats [11,12] and the present results should not be extrapolated.

3.4.3. Molecular pathways to cardiac cell death – Dual apoptosis assay

The proteins present in the *C. fleckeri* venom fractions (CTF-α, CTF-β and CTF-γ) appear to act via distinct molecular pathways. Analysis of apoptotic indicators caspase-3 and PS expression (binds to annexin-V) showed that the different fractions had differing effects. The increase of PS binding without caspase-3 activity observed for CTF-α might indicate that CfTX-1 and CfTX-2, the most abundant proteins present, act via a pathway that is independent of caspase-3. There are a number of newly discovered pathways to cell death that are currently being investigated, some of which induce apoptosis independently from caspase-3 activation, however these pathways are not well documented yet [26,33]. Alternatively, the fluorescently labelled annexin-V (which binds to PS), is a non-permeant dye and can only bind to PS once it is translocated to the outer membrane. However, this dye does not distinguish between cytoplasmic and extracellular PS, and thus may bind to cytoplasmic PS if the cell membrane is compromised from e.g. necrosis or pore formation [34].

By contrast, during most caspase-dependent apoptotic processes, pro-caspase-3 is activated to caspase-3 before the translocation of PS to the surface of the cell membrane [33]. Thus, the activation of caspase-3 without PS binding for CTF-β indicates that the cardiomyocytes were in the early apoptotic stages, whereas the presence of both indicators for CTF-γ indicated a mid/late stage of apoptosis.

Interestingly, despite cell death occurring at 100 ng/mL (data not shown), *C. fleckeri* venom did not induce apoptosis, suggesting that although apoptotic cell death is induced by some toxins in *C. fleckeri* venom (i.e toxins in CTF-γ), it does not appear to be the primary cause of cell death during *C. fleckeri* envenomation. Some toxins are able to induce both apoptosis and necrosis, where the type of cell death depends on the concentration of the toxin [25,26]. For

example, cobra venom cytotoxins exhibited apoptotic anticancer activity in a limited range of toxin concentrations and at higher concentrations necrosis was observed [35]. The current assay represents a first step into identifying the types of cell death at play during *C. fleckeri* envenomation; more extensive apoptosis and necrosis assays are required to determine the primary pathways and the biochemical factors influencing their occurrence.

3.5. Conclusion

In the current study, we have shown that fractions enriched for various cubozoan toxins have distinct effects on cell lines, erythrocytes and apoptosis. Further research on these fractions is required to determine the active constituents with more confidence. In addition, we show distinct differences between mouse and human erythrocytes upon treatment with *C. fleckeri* venom and fractions, which has implications for the interpretation of previous studies.

3.6. References

1. Learmont, S.A. *Chironex fleckeri* (box jellyfish) envenomation: a case study. *Australasian Emergency Nursing Journal* **2006**, *9*, 49-56.
2. Maguire, E. *Chironex fleckeri* ("sea wasp") sting. *The Medical journal of Australia* **1968**, *2*, 1137.
3. O'Reilly, G.M.; Isbister, G.K.; Lawrie, P.M.; Treston, G.T.; Currie, B.J. Prospective study of jellyfish stings from tropical Australia, including the major box jellyfish *Chironex fleckeri*. *The Medical journal of Australia* **2000**, *175*, 652-655.
4. Saggiomo, S.L.; Seymour, J.E. Cardiotoxic effects of venom fractions from the Australian box jellyfish *Chironex fleckeri* on human myocardiocytes. *Toxicon* **2012**, *60*, 391-395.
5. Chaousis, S.; Smout, M.; Wilson, D.; Loukas, A.; Mulvenna, J.; Seymour, J. Rapid short term and gradual permanent cardiotoxic effects of vertebrate toxins from *Chironex fleckeri* (Australian box jellyfish) venom. *Toxicon* **2014**, *80*, 17-26.
6. Kintner, A.H.; Seymour, J.E.; Edwards, S.L. Variation in lethality and effects of two Australian chirodropid jellyfish venoms in fish. *Toxicon* **2005**, *46*, 699-708.
7. Brinkman, D.L.; Jia, X.; Potriquet, J.; Kumar, D.; Dash, D.; Kvaskoff, D.; Mulvenna, J. Transcriptome and venom proteome of the box jellyfish *Chironex fleckeri*. *BMC Genomics* **2015**, *16*, 407.
8. Brinkman, D.L.; Konstantakopoulos, N.; McInerney, B.V.; Mulvenna, J.; Seymour, J.E.; Isbister, G.K.; Hodgson, W.C. *Chironex fleckeri* (box jellyfish) venom proteins expansion of a cnidarian toxin family that elicits variable cytolytic and cardiovascular effects. *Journal of Biological Chemistry* **2014**, *289*, 4798-4812.
9. Brinkman, D.; Burnell, J. Identification, cloning and sequencing of two major venom proteins from the box jellyfish, *Chironex fleckeri*. *Toxicon* **2007**, *50*, 850-860.
10. Pereira, P.; Seymour, J.E. In vitro effects on human heart and skeletal cells of the venom from two cubozoans, *Chironex fleckeri* and *Carukia barnesi*. *Toxicon* **2013**, *76*, 310-315.
11. Ramasamy, S.; Isbister, G.K.; Seymour, J.E.; Hodgson, W.C. Pharmacologically distinct cardiovascular effects of box jellyfish (*Chironex fleckeri*) venom and a tentacle-only extract in rats. *Toxicology Letters* **2005**, *155*, 219-226.
12. Ramasamy, S.; Isbister, G.K.; Seymour, J.E.; Hodgson, W.C. The in vivo cardiovascular effects of box jellyfish *Chironex fleckeri* venom in rats: Efficacy of pre-treatment with antivenom, verapamil and magnesium sulphate. *Toxicon* **2004**, *43*, 685-690.
13. Yanagihara, A.A.; Shohet, R.V. Cubozoan venom-induced cardiovascular collapse is caused by hyperkalemia and prevented by zinc gluconate in mice. *Plos one* **2012,** *7* (12), e51368.

14. Bailey, P.M.; Bakker, A.J.; Seymour, J.E.; Wilce, J.A. A functional comparison of the venom of three Australian jellyfish - *Chironex fleckeri*, *Chiropsalmus sp*., and *Carybdea xaymacana* - on cytosolic Ca^{2+}, haemolysis and *Artemia sp*. lethality. *Toxicon* **2005**, *45*, 233-242.
15. Baxter, E.; Marr, A. Sea wasp (*Chironex fleckeri*) venom: lethal, haemolytic and dermonecrotic properties. *Toxicon* **1969**, *7*, 195-210.
16. Martignoni, M.; Groothuis, G.; De Kanter, R. Species differences between mouse, rat, dog, monkey and human cyp-mediated drug metabolism, inhibition and induction. *Expert Opinion on Drug Metabolism* **2006**, *2*, 875-894.
17. Eizirik, D.L.; Pipeleers, D.G.; Ling, Z.; Welsh, N.; Hellerström, C.; Andersson, A. Major species differences between humans and rodents in the susceptibility to pancreatic beta-cell injury. *Proceedings of the National Academy of Sciences* **1994**, *91*, 9253-9256.
18. Roymans, D.; Annaert, P.; Van Houdt, J.; Weygers, A.; Noukens, J.; Sensenhauser, C.; Silva, J.; Van Looveren, C.; Hendrickx, J.; Mannens, G.*, et al.* Expression and induction potential of cytochromes p450 in human cryopreserved hepatocytes. *Drug Metabolism and Disposition* **2005**, *33*, 1004.
19. Diaz, D.; Fabrev, I.; Daujat, M.; Aubert, B.S.; Bories, P.; Michel, H.; Maurel, P. Omeprazole is an aryl hydrocarbon-like inducer of human hepatic cytochrome p450. *Gastroenterology* **1990**, *99*, 737-747.
20. O'Connell, K.E.; Mikkola, A.M.; Stepanek, A.M.; Vernet, A.; Hall, C.D.; Sun, C.C.; Yildirim, E.; Staropoli, J.F.; Lee, J.T.; Brown, D.E. Practical murine hematopathology: a comparative review and implications for research. *Comparative Medicine* **2015**, *65*, 96-113.
21. Bloom, D.A.; Burnett, J.W.; Alderslade, P. Partial purification of box jellyfish (*Chironex fleckeri*) nematocyst venom isolated at the beachside. *Toxicon* **1998**, *36*, 1075-1085.
22. Carrette, T.; Seymour, J. A rapid and repeatable method for venom extraction from cubozoan nematocysts. *Toxicon* **2004**, *44*, 135-139.
23. Gao, J., Friedrichs, M.S., Dongre, A.R. and Opiteck, G.J. Guidelines for the routine application of the peptides hits technique. *Journal of the American Society for Mass Spectrometry* **2005,** 16, 1231-1238.
24. Liu, H., Sadygov, R.G. and Yates, R.J. A model for random sampling and estimation of relative protein abundance in shotgun proteomics. *Analytical Chemistry* **2004**, 76 (14), 4193-201.
25. Orrenius, S.; Nicotera, P.; Zhivotovsky, B. Cell death mechanisms and their implications in toxicology. *Toxicoligal Sciences* **2011**, *119*, 3-19.
26. Elmore, S. Apoptosis: A review of programmed cell death. *Toxicologic Pathology* **2007**, *35*, 495-516.
27. Price-Carter, M.; Gray, W.R.; Goldenberg, D.P. Folding of ω-conotoxins. 2. Influence of precursor sequences and protein disulfide isomerase. *Biochemistry* **1996**, *35*, 15547-15557.

28. Brinkman, D.; Burnell, J. Partial purification of cytolytic venom proteins from the box jellyfish, *Chironex fleckeri*. *Toxicon* **2008**, *51*, 853-863.
29. Sunagar, K.; Undheim, E.A.B.; Scheib, H.; Gren, E.C.K.; Cochran, C.; Person, C.E.; Koludarov, I.; Kelln, W.; Hayes, W.K.; King, G.F.; Antunes, A. Intraspecific venom variation in the medically significant southern pacific rattlesnake (*Crotalus oreganus helleri*): biodiscovery, clinical and evolutionary implications. *Journal of Proteomics* **2014**, *99*, 68-83.
30. Winter, K.L.; Isbister, G.K.; McGowan, S.; Konstantakopoulos, N.; Seymour, J.E.; Hodgson, W.C. A pharmacological and biochemical examination of the geographical variation of *Chironex fleckeri* venom. *Toxicology letters* **2010**, *192*, 419-424.
31. Nagai, H.; Takuwa, K.; Nakao, M.; Sakamoto, B.; Crow, G.L.; Nakajima, T. Isolation and characterization of a novel protein toxin from the hawaiian box jellyfish (sea wasp) *Carybdea alata*. *Biochemical Biophysical Research Communications* **2000**, *275*, 589-594.
32. Nagai, H.; Takuwa, K.; Nakao, M.; Ito, E.; Miyake, M.; Noda, M.; Nakajima, T. Novel proteinaceous toxins from the box jellyfish (sea wasp) *Carybdea rastoni*. *Biochemical Biophysical Research Communications* **2000**, *275*, 582-588.
33. Kroemer, G.; Martin, S.J. Caspase-independent cell death. *Nature Medicine* **2005**, *11*, 725-730.
34. Crowley, L.C.; Marfell, B.J.; Scott, A.P.; Waterhouse, N.J. Quantitation of apoptosis and necrosis by annexin-V binding, propidium iodide uptake, and flow cytometry. *Cold Spring Harbor Protocols* **2016**, *11*, doi: 10.1101/pdb.prot087288.
35. Ebrahim, K.; Shirazi, F.H.; Mirakabadi, A.Z.; Vatanpour, H. Cobra venom cytotoxins; apoptotic or necrotic agents? *Toxicon* **2015**, *108*, 134-140.

CHAPTER 4

Structural characterisation of predicted helical regions in the *Chironex fleckeri* CfTX-1 toxin

4.1. Introduction

The Australian box jellyfish, *Chironex fleckeri*, belongs to a family of cubozoan jellyfish that are known for their potent venoms [1-3]. In the northern half of the Australian continent, *C. fleckeri* envenomations, ranging from mostly minor to occasionally life threatening, occur frequently, particularly during October-June [4]. Envenomation symptoms include immediate severe pain, cutaneous inflammation, cardiovascular distress and dysfunction, loss of consciousness and potential cardiac arrest [5,6].

The venom of *C. fleckeri* is of particular clinical relevance as rapid cardiovascular collapse followed by death can occur within minutes [6,7]. The majority of the venom toxins are proteins with a variety of distinct functions. These protein toxins include CfTX-like proteins, a variety of enzymes such as proteases and oxido-reductases, CRISP-toxins, an alpha-macroglobulin and a protease inhibitor [8]. The most abundant CfTX protein toxins in the venom are CfTX-1 and -2 and CfTX-A and -B. Fractions with predominantly the CfTX-1/2 or CfTX-A/B toxins both have potent hemolytic activity (HU50 ≤161 ng/mL), with the latter toxins being more potent (HU50 5 ng/mL) [9-11]. By contrast, fractions with the CfTX-1/-2 toxins induce a rapid fatal cardiovascular collapse in rats, whereas fractions with CfTX-A and -B have only minor cardiotoxic effects [9]. Phylogenetic analysis of the amino acid sequences of these venom proteins indicates the toxins belong to two functionally and structurally distinct subfamilies; Type I (CfTX-1 and -2) and Type II (CfTx-A and B) [9]. Thus far, the potent Type I cardiotoxins CfTX-1 and -2 have only been found in *C. fleckeri* , suggesting that these proteins are likely the cause of the rapid cardiovascular collapse observed in severe envenomations and hence, potentially the reason why this species is considered the most dangerous of its family [9].

There is no experimental structural information on *C. fleckeri* toxins. However, secondary structure analysis on CfTX-1 and 2 has predicted that the first 300 amino acids are dominated by α-helices and loop structures, including an amphiphilic α-helix in the N-terminal region that is followed by a transmembrane spanning region, which is also predicted to be helical [11]. Predicted amphiphilic α-helices in the N-terminal region of toxin sequences of other cubozoan jellyfish (*Chiropsalmus quadrigatus, Carybdea rastoni, Alatina alata (previously Carybdea alata* [12]), have been suggested to be associated with their hemolytic activity [13,14]. In addition, the predicted transmembrane spanning region consists of a series of highly conserved amino acids in CfTX-1 and -2 as well as the related jellyfish toxins CqTX-A, CrTXs and CaTX-A [11], and has also been implicated in the mechanism of action of these toxins. Transmembrane spanning regions are commonly seen in pore-forming toxins [15,16], thus suggesting that the cardiotoxicity of CfTX-1 and -2 might result from the transmembrane spanning region integrating itself into the membrane of the cardiomyocytes and creating pores in the process. This would create a rational for previously observed non-specific ion leakage into the cardiac cell, followed by increased calcium levels. This increase has been suggested to induce irregular contractions of the single cardiomyocyte, leading to a communal flagging of contractions of cardiac cells overall, and thus resulting in cardiovascular collapse [17]. The locations of the predicted amphiphilic α-helix and transmembrane spanning region in CfTX-1 are shown in Figure 1. There is no experimental evidence for the existence of the putative structures of these two regions and therefore conclusions on the function of these regions remain hypothetic. Experimental evidence on these putative structures is imperative to provide a baseline for future studies directed towards developing effective treatment of *C. fleckeri* envenomation but is also likely to provide insight into the development of bioactive peptides that might have potential for the development of *C. fleckeri* venom derived drugs.

α-Helices have been shown to form in isolation [reviewed in 18] and can either be derived from larger proteins or present in small naturally occurring peptides such venom derived peptides. The aim of the current study was to determine if regions associated with the predicted helical regions in the CfTX-1 toxin can form well-defined structures in solution. The results of this study provide insight into the structural architecture of CfTX-1 and provide a foundation for future structural analysis on *C. fleckeri* toxins.

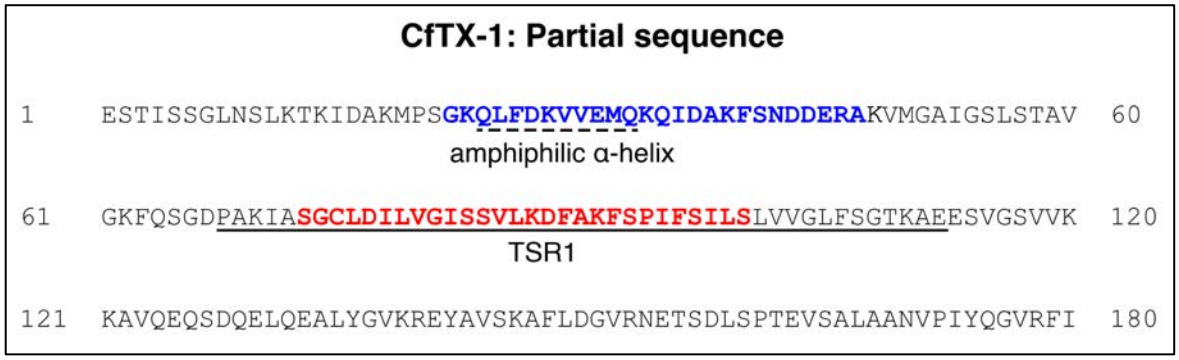

Figure 1: N-terminal region of *C. fleckeri* toxin CfTX-1. The predicted amphiphilic α-helix and the transmembrane spanning region (TSR1) as defined by Brinkman and Burnell [11] are indicated by a dotted and continuous underline, respectively. The sequences of the two peptides synthesized in the current study include the complete amphiphilic α-helix (blue) and part of the TSR1 (red), respectively.

4.2. Materials and Methods

4.2.1. Peptide synthesis and purification

Peptides were synthesised by solid-phase peptide synthesis on an automated PS3™ peptide synthesizer (Protein Technologies Inc.) using fluorenylmethyloxycarbonyl (Fmoc) chemistry on a 0.1 mmole scale. Peptides were assembled on 2-chlorotrityl chloride resin (Auspep, Australia). Amino acids were activated in peptide grade dimethylformamide (DMF, Auspep, Australia) using 2-(1H-benzotriazol-1-yl)-1,1,3,3-tetramethyluronium hexafluorophosphate (HBTU, Iris Germany). The first amino acid was coupled manually. Peptides were cleaved in a trifluoroacetic acid (TFA)/H_2O/triisopropylsilane (TIPS) (95:2.5:2.5) mixture for 2 h. After

cleavage, the TFA was evaporated with nitrogen and the peptides were precipitated in cold diethyl ether (4°C). The ether was removed by filtration and the precipitated peptides were solubilised in a mixture of acetonitrile (ACN)/H_2O/TFA (CfTX-1_{22-47}: 5:94.95:0.05; CfTX-1_{73-100}: 25:74.95:0.05) and then lyophilised. The resulting peptides were purified by reversed phase high performance liquid chromatography (RP-HPLC) (Agilent 1200 Infinity series, Agilent Technologies, Inc.) on a semi-preparative C-18 column (Jupiter 4 µm C_{18} Proteo 90 A° 250 mm x 10.00 mm, Penomenex, Inc.). The peptides were eluted using a 1 %/ min gradient of solvent B (solvent A: 0.05 % TFA, solvent B: 90 % ACN, 0.05 % TFA) starting at 0 % and 25 % solvent B for CfTX-1_{22-47} and CfTX-1_{73-100}, respectively and finishing at 90 % solvent B. Absorbance traces of the effluent were collected at 214 and 280 nm. The purity of the eluted peptide was verified by analytical RP-HPLC (Agilent 1260 Infinity series, Agilent Technologies, Inc.) with a C-18 column (Eclipse Plus 3.5 µm 4.6 mm x 100 mm, Agilent Technologies, Inc.) and the mass was analysed using MALDI mass spectrometry.

4.2.2. NMR Spectroscopy and Structure Determination

The purified peptides were dissolved in a mixture of 89.9%H_2O:10%D_2O:0.1%TFA and 69.9 % H_2O:20%ACN:10%D_2O:0.1%. A 600 MHz AVANCE III NMR spectrometer (Bruker, Karlsruhe, Germany) with a cryogenically cooled probe was used to acquire two-dimensional (2D) ^{1}H- ^{1}H TOCSY and ^{1}H- ^{1}H NOESY spectra at 303 K. 4,4-dimethyl-4-silapentane-1-sulfonic acid was used as a chemical shift reference. NMR spectra were also collected for both peptides in 100 mM SDS 90% H_2O:10%D_2O. All spectra were recorded with an interscan delay of 1 s. NOESY spectra were acquired with mixing times of 200-300 ms, and TOCSY spectra were acquired with isotropic mixing period of 80 ms. Standard Bruker pulse sequences were used with an excitation sculpting scheme for solvent suppression. Assignments were made

based on the procedure described by [30]. Slowly exchanging amide protons were detected by acquiring a series of one-dimensional and TOCSY spectra after dissolution of the peptides in 100 mM SDS in D_2O.

Three-dimensional structures were determined with the program CYANA [22]. Non-intra residue peaks in the NOESY spectra were automatically assigned and an ensemble of structures calculated. Dihedral angle restraints derived from TALOS+ [31] were used in the structure calculations. Hydrogen bonds predicted from preliminary structures, that were consistent with the slowly exchanging amide protons, were subsequently included in the structure calculations. A final ensemble of 100 structures was calculated and the 20 structures with the lowest target functions chosen to represent the structures of CfTX-$1_{22\text{-}47}$ and CfTX-$1_{73\text{-}100}$. The structure statistics were calculated with CYANA and MOLMOL [23].

4.2.3. Structural predictions for CfTX-1, CfTX-$1_{22\text{-}47}$, CfTX-$1_{73\text{-}100}$

iTASSER [24] was used to generate a three-dimensional structure model of CfTX-1. PrDOS [25] was used to predict natively disordered regions of CfTX-1, CfTX-$1_{22\text{-}47}$ and CfTX-$1_{73\text{-}100}$. PrDOS is a protein disorder prediction system that is based on two predictors: 1) the amino acid sequence of the protein being analysed (implemented using support vector machine) and 2) template proteins or homologues with available structural information (implemented using PSI-BLAST and PrDOS measure of disorder. The method was assessed by the CASP benchmark and achieved high performance, in particular for short disordered regions.

4.3. Results

4.2.1. CfTX-1 peptides – design and synthesis

The peptide design was based primarily on the predicted helical regions in CfTX-1 (Figure 1) [11]. The length of the predicted amphipathic helix in CfTX-1 involves residues 24-33 whereas the putative transmembrane spanning region with at least one helix, although not precisely defined, was located within residues 68-112. An intermediate length (approximately 25 residues) was chosen for both peptides as peptides of this length are more likely to have secondary structure than smaller peptides (for example see [19]) and are less likely to have significant overlap in the NMR spectra, which can be present in relatively large peptides (for example see [20]). The termini of the synthetic peptides were chosen based on sequence similarity with related toxins including CfTX-2, CqTX-A, CrTXs and CaTX-1 [11]. The sequences of the synthetic peptides, termed CfTX-$1_{22\text{-}47}$ and CfTX-$1_{73\text{-}100}$ to designate the residue numbering for the N- and C-termini, are shown in Figure 1. Henceforth, the residue numbers for each of the two synthetic peptides will be referred to in numerical order starting with 1, e.g. the first residue of CfTX-$1_{22\text{-}47}$ will be referred to as residue 1 of CfTX-$1_{22\text{-}47}$.

The peptides were synthesized using Fmoc chemistry, purified using RP-HPLC and characterized using mass spectrometry. CfTX-$1_{73\text{-}100}$ was significantly more hydrophobic than CfTX-$1_{22\text{-}47}$ based on the retention time on RP-HPLC; 66 min (59.9 % acetonitrile - ACN) and 33.5 min (30 % ACN) on a 1 % gradient, respectively.

4.2.2. Structural analysis using NMR spectroscopy

NMR spectroscopy was used for the structural analysis of the two peptides. The one-dimensional spectra of CfTX-1_{22-47} had limited chemical shift dispersion in the amide region. Resonances were assigned using two-dimensional TOCSY and NOESY spectra and the secondary shifts were calculated by subtracting random coil shifts [21] from the αH shifts. The secondary shifts for CfTX-1_{22-47} are close to random coil values as shown in Figure 2, indicating that the peptide lacks structure in an aqueous environment.

CfTX-1_{73-100} was insoluble in aqueous solution but soluble in 20 % acetonitrile. However, the one-dimensional spectrum of CfTX-1_{73-100} in 20 % acetonitrile showed broad peaks, indicating that the peptide is aggregating under these conditions. Given the apparent aggregation of CfTX-1_{73-100} and the lack of structure for CfTX-1_{22-47}, the NMR data was therefore repeated for both peptides in the presence of deuterated sodium dodecyl sulfate (SDS) micelles. In SDS, both peptides had enhanced chemical shift dispersion in the amide region and the secondary shifts of CfTX-1_{22-47} and CfTX-1_{73-100} were consistent with helical structure based on the consecutive negative shifts (more negative than -0.1), as shown in Figure 2.

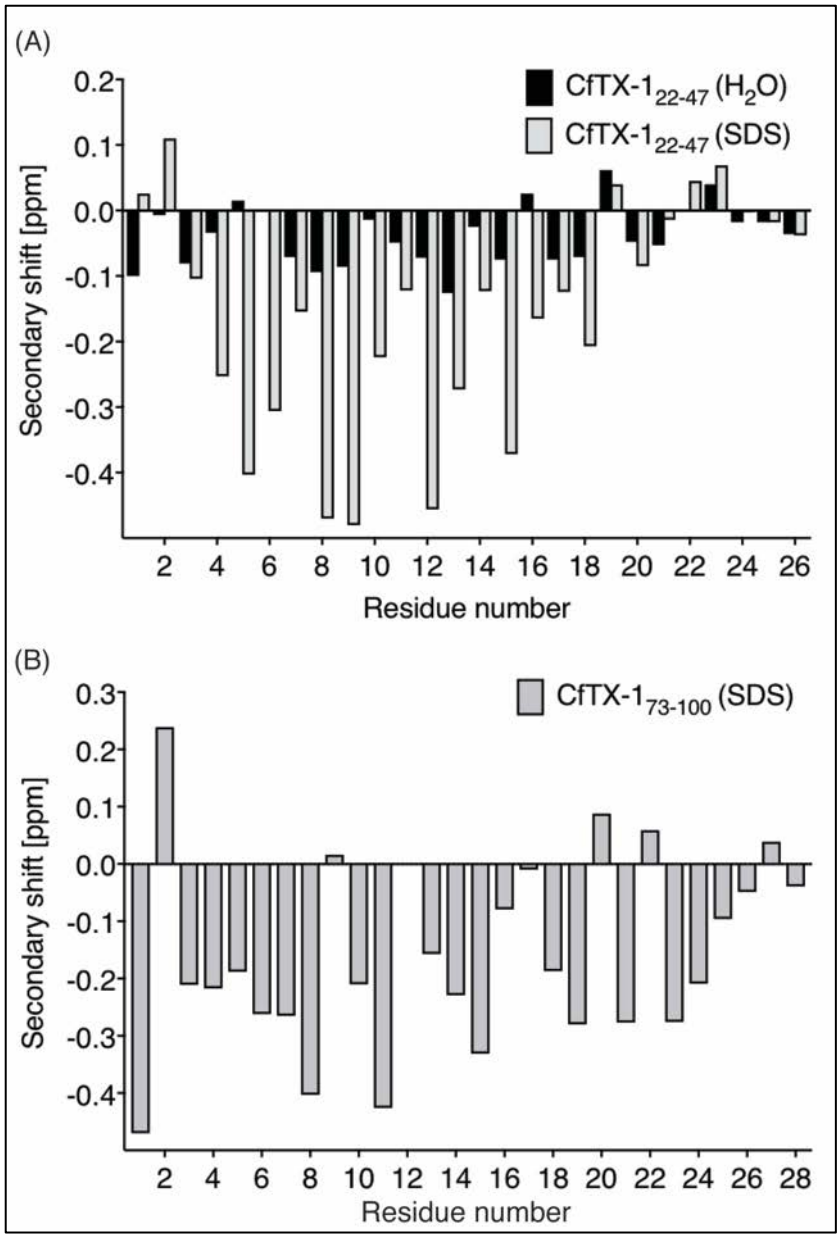

Figure 2: Secondary α-H shifts of CfTX-122-47 and CfTX-173-100. (A) Secondary α-proton shifts for CfTX-122-47 in H2O (black bars) and in 100 mM SDS (grey bars with black border). Secondary shift values of CfTX-122-47 in an aqueous environment are generally within ±0.1, indicating lack of structure; whereas the values of CfTX-122-47 in SDS are lower than -0.1ppm between residues 4 and 19 (corresponding to residues 25 and 40 in the full-length protein), indicating an α-helical structure in this environment. (B) Secondary α-proton shifts for CfTX-173-100 in SDS. All secondary shift values between residues 3 and 20 (corresponding to residues 75 and 92 in the full-length protein), except residue 9, 12 and 17 (corresponding to residues 81, 84 and 89 in the full-length protein) are below -0.1ppm indicating a helical structure. Residue 12 (corresponding to residue 84 in the full-length protein) could not be assigned due to overlap with other NOEs.

The three-dimensional structures of both peptides were determined using the program CYANA [22]. The structures of CfTX-1_{22-47} were determined based on 263 NOEs and 43 dihedral angle restraints. Secondary structure analysis using MOLMOL [23] indicated that an α-helix was

present between residues 4 to 19 (corresponding to residues 25 to 40 in the full-length protein). The structures of CfTX-$1_{73\text{-}100}$ were determined based on 437 NOEs and 45 dihedral angle restraints. Secondary structure analysis using MOLMOL indicated that an α-helix was present between residues 3-20 (corresponding to residues 75-92 in the full-length protein). The structural statistics for the peptides are given in Table 1 and an overlay of the 20 lowest energy structures given in Figure 3. The greater number of NOEs for CfTX-$1_{73\text{-}100}$ appears to be related to more overlap in the amide region of CfTX-$1_{22\text{-}47}$. A surface structure representation for both peptides is given in Figure 4.

Table 1. Structural statistics for CfTX-$1_{22\text{-}47}$ and CfTX-$1_{73\text{-}100}$.

	Peptide	
	CfTX-$1_{22\text{-}47}$	**CfTX-$1_{73\text{-}100}$**
Experimental restraints		
Interproton distance restraints	263	437
Intraresidue, |i-j|=0	122	145
Sequential, |i-j|=1	82	158
Medium range, 1 <|i-j| < 5	59	134
Dihedral-angle restraints	43	45
R.m.s. deviations from mean coordinate structure (Å)		
Backbone atoms (indicated)	0.32 ± 0.12 (res. 4-19)	0.43 ± 0.17 (res.3-20)
All heavy atoms (indicated)	1.48 ± 0.23 (res. 4-19)	1.06 ± 0.25 (res. 3-20)
Backbone atoms (all)	2.19 ± 0.79	0.89 ± 0.32
All heavy atoms (all)	3.18 ± 0.87	1.36 ± 0.32
Ramachandran (%)		
Residues in most favoured regions	85.8	91.3
Residues in additionally allowed regions	14.2	8.7

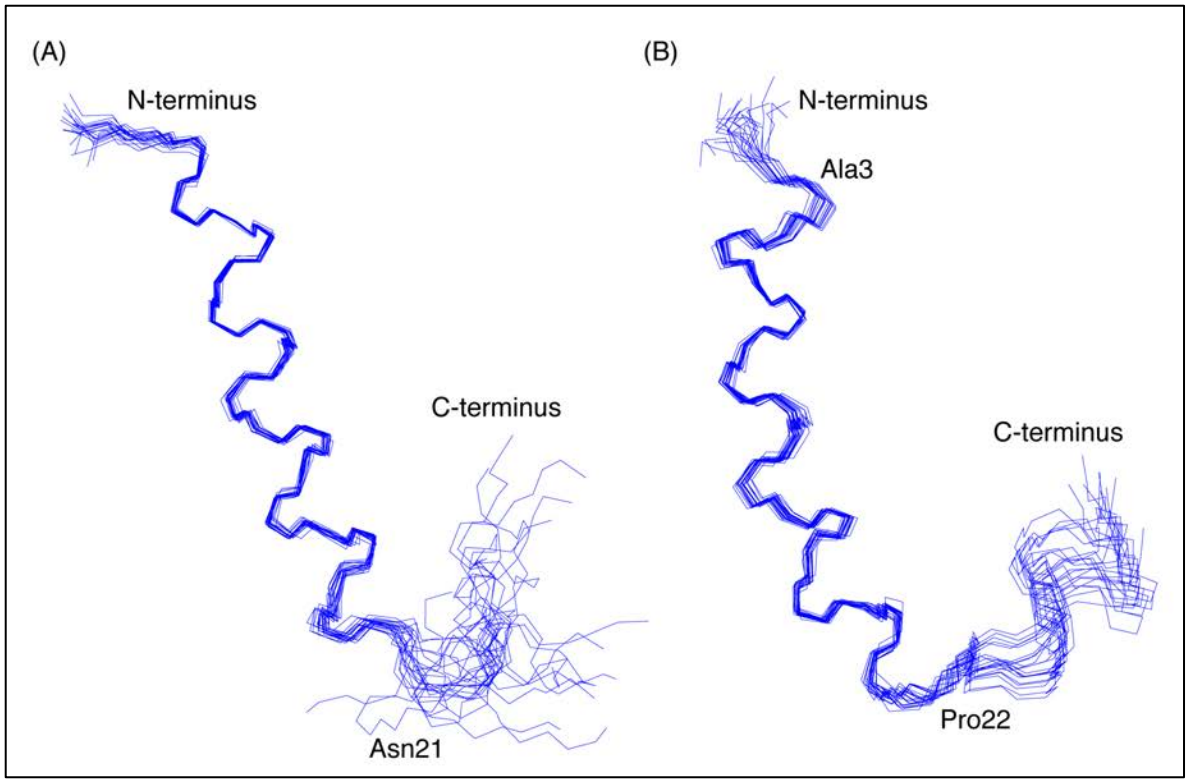

Figure 3: Structural analysis of CfTX-1 derived peptides. The three-dimensional structure of the 20 lowest energy structures of (A) CfTX-$1_{22\text{-}47}$ and (B) CfTX-$1_{73\text{-}100}$ highlighting the well-defined helical region between residues 4-19 and 3-20 (corresponding to residues 25-40 and 75-92 in the full-length protein), respectively, as well as the less defined C-terminus. (B) Cys3 (corresponding to Cys75 in the full-length protein) was substituted for an alanine residue (Ala3) to prevent disulfide bridge formation. Asn21 and Pro22 (corresponding to Asn42 and Pro94 in the full-length protein) indicate the region of the turn in CfTX-$1_{22\text{-}47}$ and CfTX-$1_{73\text{-}100}$, respectively. The figure was created in MOLMOL [23].

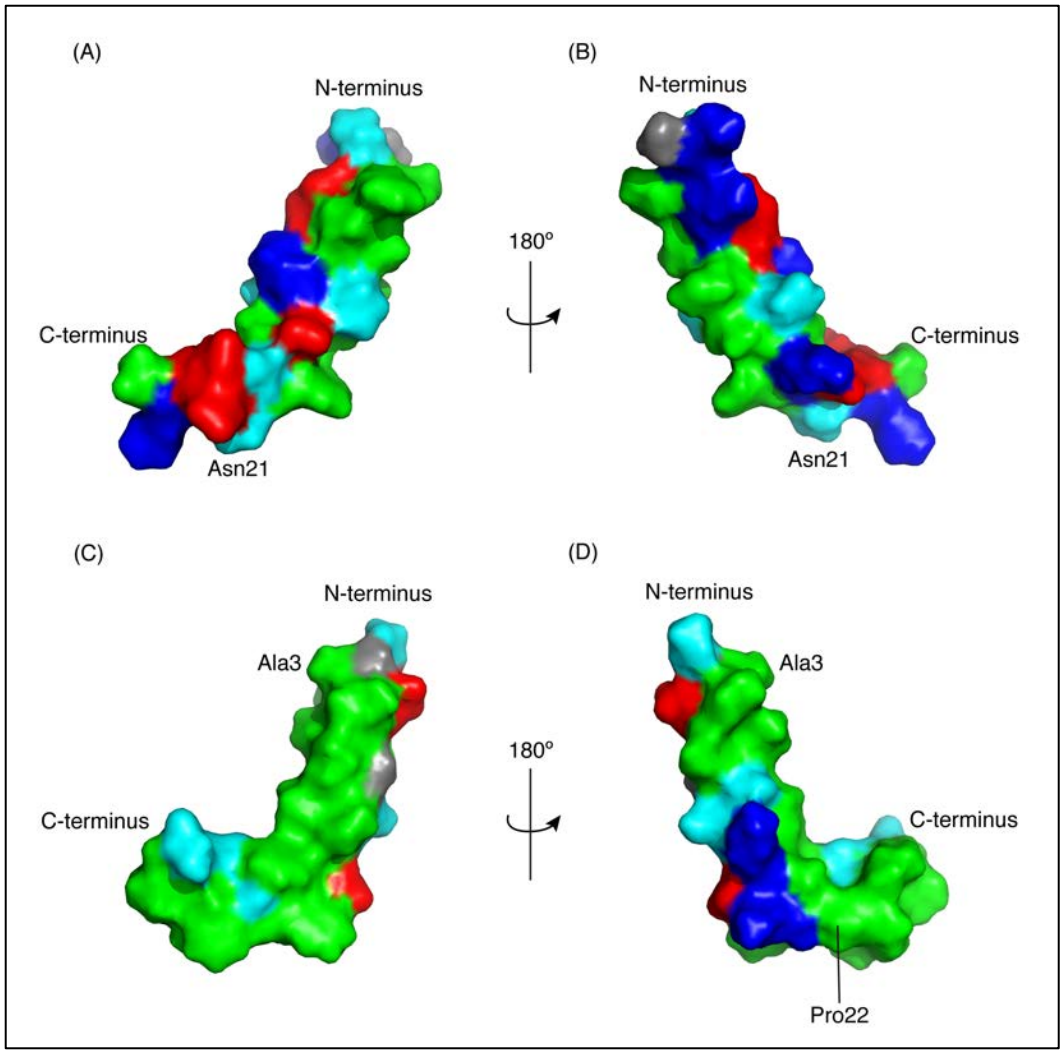

Figure 4 Surface representation of CfTX-1 derived peptides. Hydrophobic residues are represented in green, polar residues in cyan, glycine residues in grey, positively and negatively charged residues in dark blue and red, respectively. The charge states represent expected states at physiological conditions based on generic pKa values for glutamic acid and aspartic acid residues (~4) and lysine and arginine residues (>10). CfTX-$1_{22\text{-}47}$ has a cluster of positively and negatively charged residues on one face of the molecule and a cluster of hydrophobic residues on the other face. CfTX-$1_{73\text{-}100}$ shows an extended patch of hydrophobic residues. The arrow pivoting around the axis in the top and bottom center represents the 180º turn between figure (A), (C) and (B), (D), respectively. The figure was generated in PyMol (Schrödinger, Inc.).

4.2.3. Structure predictions for CfTX-1

As there is no experimental structure available for CfTX-1 we used iTASSER [24] to produce a model to compare our peptide structures with the predicted structure of the full-length protein. The highest-ranking protein structure is shown in Figure 5. The structure was based on the crystal structure of an insecticidal δ-endotoxin Cry8Ea1 from *Bacillus thuringiensis*, which has 25 % sequence identity with CfTX-1. The iTASSER score was -3.12. The first 373 residues of the model are dominated by α-helices whereas the remaining 83 residues are a mix of helices, coil structures, bends and β-sheets.

The regions corresponding to the peptides CfTX-$1_{22\text{-}47}$ and CfTX-$1_{73\text{-}100}$ are shown on the model in green and red respectively. Overall, the structures of the peptides in SDS are consistent with the iTASSER model of CfTX-1, however, the terminal regions of the peptides differ from the model in that they are not well defined. Further, the "bend" in the helix of CfTX-$1_{73\text{-}100}$ rotates the C-terminal residues into a slightly different orientation from that present in the CfTX-1 model.

Given the lack of structure of CfTX-$1_{22\text{-}47}$ in aqueous solution we analyzed the propensity of CfTX-1 to have disordered structure using the program PrDOS [25]. This analysis indicated that the majority of the protein is structured (Figure 6), consistent with the iTASSER model. Interestingly, there are small regions predicted to be disordered including residues 20-65 which encompasses the sequence of CfTX-$1_{22\text{-}47}$. The isolated sequence of CfTX-$1_{22\text{-}47}$ was also predicted to be disordered by PrDOS (Figure 6A). By contrast, CfTX-$1_{73\text{-}100}$ was predicted to be structured (Figure 6B). The NMR data for CfTX-$1_{22\text{-}47}$ solubilized in water is consistent with the PrDOS results, which indicated that the respective sequence is unstructured.

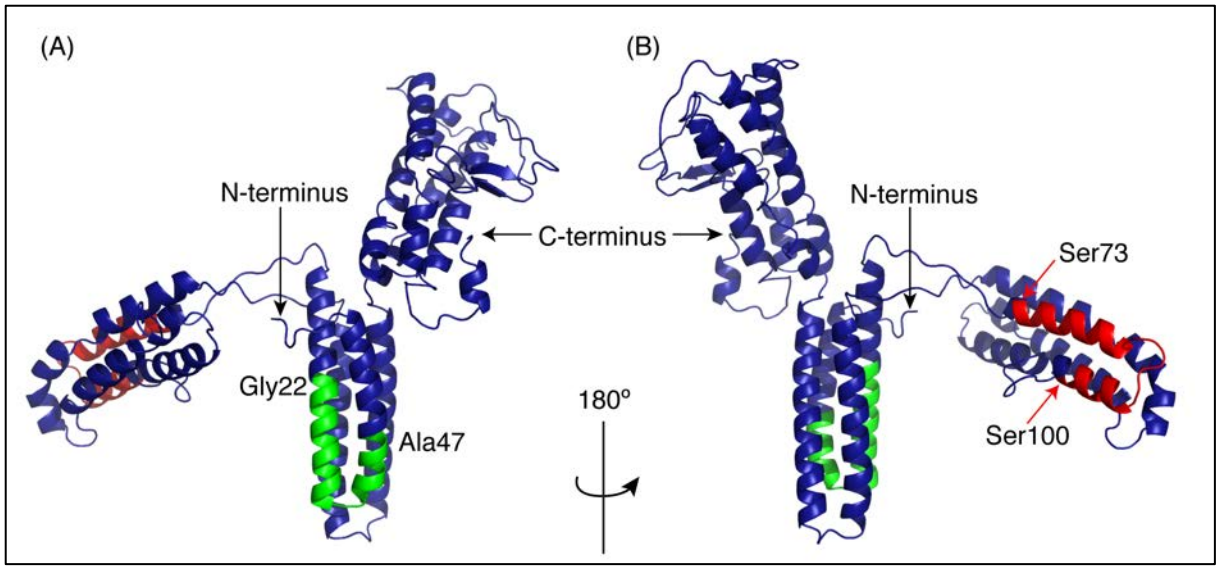

Figure 5 i-TASSER model of CfTX-1. This model represents the highest-ranking modelled protein structure. The model indicates three multi-helical regions separated by loop structures. The location of CfTX-$1_{22\text{-}47}$ is shown in green and CfTX-$1_{73\text{-}100}$ in red. (A) and (B) are rotated 180º with respect to each other. The figure was generated in PyMol (Schrödinger, Inc.).

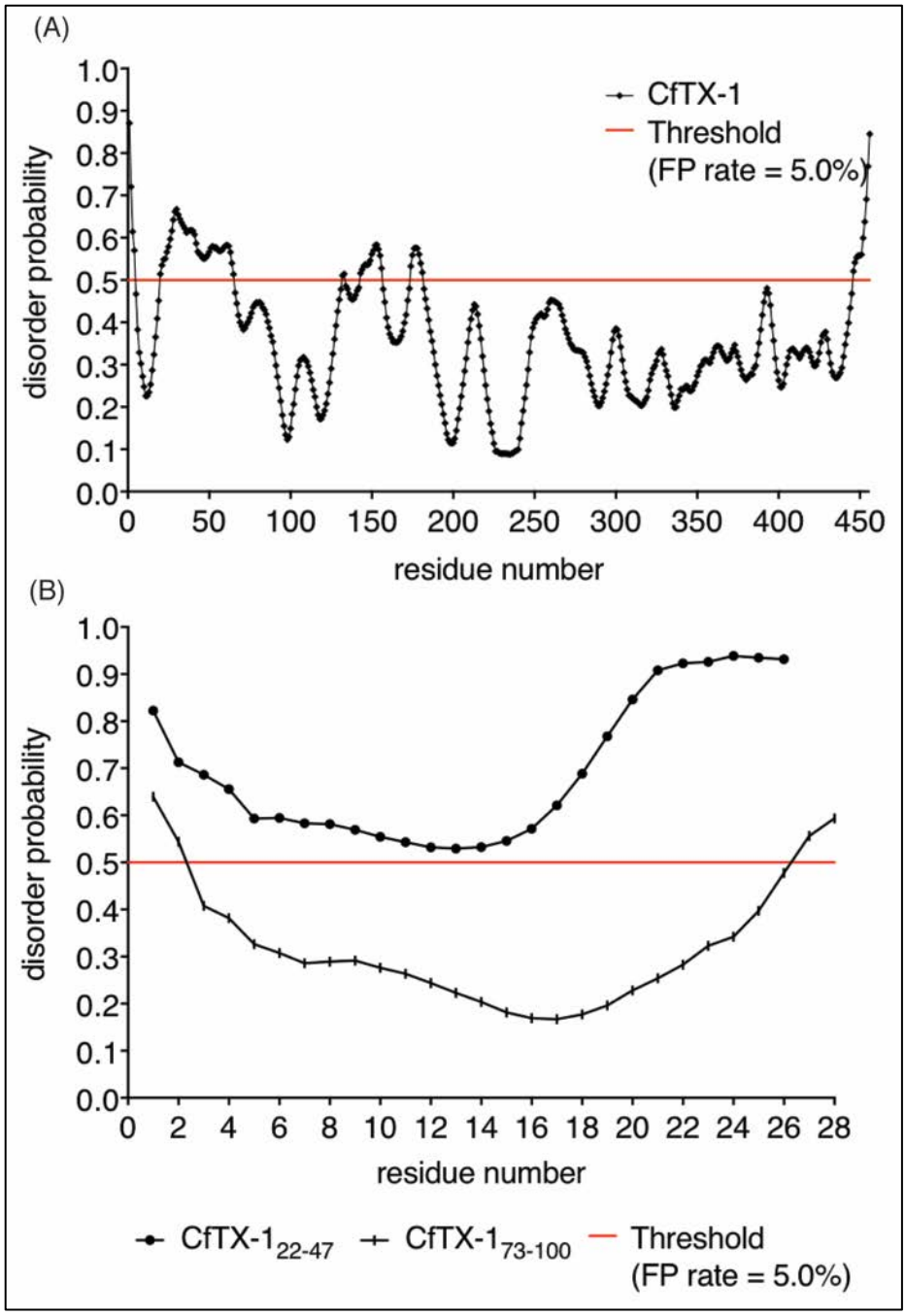

Figure 6. Protein disorder predictions. Residues above/below the threshold probability of 0.5 (red line) are classed as disordered/structured with a false positive rate of 5.0 %. (A) The disorder prediction for CfTX-1, which indicates a mostly structured protein with four disordered regions between residues 20-65 (location of CfTX-1_{22-47}), 131-132, 143-156 and 174-181. (B) This disorder prediction for CfTX-1_{22-47} and CfTX-1_{73-100}. The former appears to lack structure whereas the latter appears structured between residues 3-26 (corresponding to residues 75-98 in the full-length protein). The analysis was conducted with the online protein disorder prediction system PrDOS [25].

4.4. Discussion

This study provides the first experimental data regarding the structures of peptides derived from the putatively poreforming *C. fleckeri* toxin, CfTX-1. Two of the regions previously predicted to be involved in helices [11] behave differently in aqueous solution but both form well defined helices in the presence of SDS. Structural predictions of the full-length protein provided some context for the experimental structures.

The region predicted to form an amphiphilic α-helix in CfTX-1 (residues 25-32) appears to be disordered in aqueous solution based on the chemical shift analysis of CfTX-1_{22-47}. By contrast, the chemical shift analysis in the presence of 100 mM SDS has several consecutive negative shifts, consistent with helical structure. This helical structure was confirmed by determination of the three-dimensional structure (Figure 2). SDS-micelles have previously been shown to stabilise helical structures, likely because the micelles solvate the hydrophobic regions of the peptide (for example see [26]). The helix formed in the presence of SDS has an amphiphilic nature as one face contains mainly charged residues whereas the opposite face is significantly more hydrophobic. The model of CFTX-1 predicted using iTasser shows that residues 22-47 are involved in a helical structure (including a turn centered at residue 33) but analysis of the intrinsic disorder using PrDOS suggests that this region is unstructured in the full-length protein, as well as in the isolated peptide. Our NMR results in aqueous solution are consistent with the PrDOS results, however the propensity of the peptide to form helical structure, albeit in the presence of a detergent, is consistent with the modelled structure and the predicted secondary structure [11]. An experimental structure of the full-length protein is required to answer the question of whether this region is structured in the protein or not.

CfTX-1_{73-100} encompasses many of the residues previously predicted to be involved in a transmembrane helix in CfTX-1 which was suggested to be involved in the putatively pore

2005 forming mechanism of the protein [11]. CfTX-$1_{73\text{-}100}$ is significantly more hydrophobic than
2006 CfTX-$1_{22\text{-}47}$, is insoluble in aqueous solution and appears to aggregate in a water/acetonitrile
2007 solution. However, in the presence of SDS the peptide is soluble, gives relatively sharp peak
2008 in the NMR spectra, and has a well-defined helical structure for most of the peptide. Our
2009 experimental structure of CfTX-$1_{73\text{-}100}$ in SDS is largely consistent with the model of CfTX-1.
2010 Residues 73-100 in the model have predominantly helical structure with a bend region before
2011 a proline residue. The terminal regions of the peptide are disordered, as is often present in
2012 small, unconstrained peptides. The orientation of the bend region of CfTX-$1_{73\text{-}100}$ also slightly
2013 differs from the model. Overall, our analyses on CfTX-$1_{73\text{-}100}$ are consistent with this region of
2014 the protein being involved in membrane spanning [11]. Transmembrane peptides are generally
2015 hydrophobic, aggregate in aqueous solutions and form helices under certain conditions [27],
2016 similar to what we have observed for CfTX-$1_{73\text{-}100}$. Based on our structural data it is interesting
2017 to speculate that this helical region is involved with the putative pore formation that appears to
2018 be associated with *C. fleckeri* toxins [17, 28]. Transmembrane regions are commonly observed
2019 in toxins that operate by pore formation [29]. However, further research into the structure of
2020 *C. fleckeri* toxins and their mechanism is required to draw a definitive conclusion.
2021 In summary, this study represents the first structural characterization of isolated regions of
2022 CfTX-1. Amphiphilic helices have been predicted for the N-terminal region of several jellyfish
2023 toxins, including CfTX-1, but the present data suggest this region does not have an intrinsic
2024 propensity to form an α-helix in isolation. By contrast, the experimental data are consistent
2025 with the structural predictions for the putative transmembrane spanning region. The current
2026 study also provides information on the chemical and physical properties of these peptides,
2027 which might facilitate the development of effective treatment and/or venom-derived drug
2028 development. More research into the structures and bioactivity of the full-length protein is
2029 needed to elucidate the mode of action of *C. fleckeri* toxins.

4.5. References

1. Brinkman, D.L.; Aziz, A.; Loukas, A.; Potriquet, J.; Seymour, J.; Mulvenna, J. Venom proteome of the box jellyfish *Chironex fleckeri*. *PLoS One* **2012**, *7*, e47866.
2. Brinkman, D.L.; Burnell, J.N. Biochemical and molecular characterisation of cubozoan protein toxins. *Toxicon* **2009**, *54*, 1162-1173.
3. Pereira, P.; Seymour, J.E. In vitro effects on human heart and skeletal cells of the venom from two cubozoans, *Chironex fleckeri* and *Carukia barnesi*. *Toxicon* **2013**, *76*, 310-315.
4. Currie, B.J.; Jacups, S.P. Prospective study of *Chironex fleckeri* and other box jellyfish stings in the "Top End" of Australia's Northern Territory. *Medical Journal Australia* **2005**, *183*, 631-636.
5. O'Reilly, G.M.; Isbister, G.K.; Lawrie, P.M.; Treston, G.T.; Currie, B.J. Prospective study of jellyfish stings from tropical Australia, including the major box jellyfish *Chironex fleckeri*. *Medical Journal Australia.* **2000**, *175*, 652-655.
6. Beadnell, C.; Rider, T.; Williamson, J.; Fenner, P. Management of a major box jellyfish (*Chironex fleckeri*) sting. Lessons from the first minutes and hours. *Medical Journal Australia* **1992**, *156*, 655-658.
7. Currie, B. Clinical implications of research on the box-jellyfish *Chironex fleckeri*. *Toxicon* **1994**, *32*, 1305-1313.
8. Brinkman, D.L.; Jia, X.; Potriquet, J.; Kumar, D.; Dash, D.; Kvaskoff, D.; Mulvenna, J. Transcriptome and venom proteome of the box jellyfish *Chironex fleckeri*. *BMC Genomics* **2015**, *16*, 407.
9. Brinkman, D.L.; Konstantakopoulos, N.; McInerney, B.V.; Mulvenna, J.; Seymour, J.E.; Isbister, G.K.; Hodgson, W.C. *Chironex fleckeri* (box jellyfish) venom proteins expansion of a cnidarian toxin family that elicits variable cytolytic and cardiovascular effects. *Journal of Biological Chemistry* **2014**, *289*, 4798-4812.
10. Brinkman, D.; Burnell, J. Partial purification of cytolytic venom proteins from the box jellyfish, *Chironex fleckeri*. *Toxicon* **2008**, *51*, 853-863.
11. Brinkman, D.; Burnell, J. Identification, cloning and sequencing of two major venom proteins from the box jellyfish, *Chironex fleckeri*. *Toxicon* **2007**, *50*, 850-860.
12. Lewis, C.; Bentlage, B.; Yanagihara, A.; Gillan, W.; Van Blerk, J.; Keil, D.P.; Bely, A.E.; Collins, A.G. Redescription of *Alatina alata* (Reynaud, 1830) (cnidaria: Cubozoa) from Bonaire, Dutch Caribbean. *Zootaxa* **2013**, *3737*, 473-487.
13. Nagai, H.; Takuwa, K.; Nakao, M.; Sakamoto, B.; Crow, G.L.; Nakajima, T. Isolation and characterization of a novel protein toxin from the Hawaiian box jellyfish (sea wasp) *Carybdea alata*. *Biochemical and Biophysical Research Communications* **2000**, *275*, 589-594.

14. Nagai, H.; Takuwa-Kuroda, K.; Nakao, M.; Oshiro, N.; Iwanaga, S.; Nakajima, T. A novel protein toxin from the deadly box jellyfish (sea wasp, habu-kurage) *Chiropsalmus quadrigatus*. *Bioscience, Biotechnologoy and Biochemistry* **2002**, *66*, 97-102.
15. Krause, G.; Protze, J.; Piontek, J. Assembly and function of claudins: Structure-function relationships based on homology models and crystal structures. *Seminars in Cell and Developmental Biology* **2015**, *42*, 3-12.
16. Tilley, S.J.; Saibil, H.R. The mechanism of pore formation by bacterial toxins. *Current Opinion in Structural Biology* **2006**, *16*, 230-236.
17. Mustafa, M.; White, E.; Hongo, K.; Othman, I.; Orchard, C. The mechanism underlying the cardiotoxic effect of the toxin from the jellyfish *Chironex fleckeri*. *Toxicology and Applied Pharmacology* **1995**, *133*, 196-206.
18. Swanson, C.J.; Sivaramakrishnan, S. Harnessing the unique structural properties of isolated α-helices. *Journal of Biological Chemistry* **2014**, *289*, 25460-25467.
19. Wu, C.; Hoang, H.N.; Liu, L.; Fairlie, D.P. Glucuronic acid as a helix-inducing linker in short peptides. *Chemical Communications* **2018**, *54*, 2162-2165.
20. Nielsen, J.T.; Nielsen, N.C. VirtualSpectrum, a tool for simulating peak list for multidimensional NMR spectra. *Journal of Biomolecular NMR* **2014**, *60(1)*, 51-66.
21. Wishart, D.S.; Bigam, C.G.; Holm, A.; Hodges, R.S.; Sykes, B.D. ^{1}H, ^{13}C and ^{15}N random coil NMR chemical shifts of the common amino acids. I. Investigations of nearest-neighbor effects. *Journal of Biomolecular NMR* **1995**, *5*, 67-81.
22. Güntert, P. Automated NMR structure calculation with CYANA. *Methods in Molecular Biology* 2004, 278, 353-378
23. Koradi, R.; Billeter, M.; Wüthrich, K. MOLMOL: A program for display and analysis of macromolecular structures. *Journal of Molecular Graphics* **1996**, *14*, 51-55.
24. Zhang, C.; Mortuza, S.M.; He, B.; Wang, Y.; Zhang, Y. Template-based and free modeling of i-TASSER and quark pipelines using predicted contact maps in casp12. *Proteins* **2017**, 1-16.
25. Ishida, T.; Kinoshita, K. PrDOS: Prediction of disordered protein regions from amino acid sequence. *Nucleic Acids Research* **2007**, *35*, W460-W464.
26. Coles, M.; Bicknell, W.; Watson, A.A.; Fairlie, D.P.; Craik, D.J. Solution structure of amyloid β-peptide(1−40) in a water−micelle environment. Is the membrane-spanning domain where we think it is? *Biochemistry* **1998**, *37*, 11064-11077.
27. Bordag, N.; Keller, S. A-helical transmembrane peptides: A “divide and conquer” approach to membrane proteins. *Chemistry and Physics of Lipids* **2010**, *163*, 1-26.
28. Bailey, P.M.; Bakker, A.J.; Seymour, J.E.; Wilce, J.A. A functional comparison of the venom of three Australian jellyfish - *Chironex fleckeri*, *Chiropsalmus sp*., and *Carybdea xaymacana* - on cytosolic Ca^{2+}, haemolysis and *Artemia sp*. lethality. *Toxicon* **2005**, 45, 233-242.

29. Xu, C.; Wang, B.-C.; Yu, Z.; Sun, M. Structural Insights into *Bacillus thuringiensis* Cry, Cyt and Parasporin Toxins. *Toxins* **2014,** 6 (9), 2732-2770. doi:10.3390/toxins6092732.
30. Wüthrich, K. *NMR of Proteins and Nucleic Acids.* Wiley-Interscience: New York, USA, **1986**.
31. Shen, Y.; Delaglio, F.; Cornilescu, G.; Bax A. TALOS+: a hybrid method for predicting protein backbone torsion angles from NMR chemical shifts. *Journal of Biomolecular NMR* **2009**, 44, 213-223.

CHAPTER 5

Conclusions and Future directions

5.1. Conclusions

The analysis and characterisation of the components involved in *C. fleckeri* envenomation has been a research target for many years [1-3]. This thesis has presented new insights into the bioactivity and potential modes of actions of the venom as well as a first structural analysis of a major *C. fleckeri* toxin.

Cubozoan jellyfish envenomations are a recurring problem for bathers in tropical areas all over the world [4-7]. These jellyfish are known for their potent cytotoxic, haemolytic and potentially lethal toxins that are unique to the cubozoan family [8]. The toxin composition of the venoms across many cubozoan species appears to be similar [9] and thus the research presented in this thesis on the venom of *C. fleckeri* is also of relevance for these related species.

Chapter 2 was based on the premise that severe *C. fleckeri* envenomations can lead to cardiovascular collapse due to the cardiotoxic properties in the venom. The specific aim of this chapter was to analyse the cardiotoxic effects of crude *C. fleckeri* venom on a cellular and, more specifically, on an intracellular level. The expected outcomes were the visualisation of the cell organelles and compartments affected by *C. fleckeri* venom with the aim of determining their relevance in the cardiomyocyte death during *C. fleckeri* envenomation.

The microscopy method used for Chapter 2 required adequate adherence of the cardiomyocyte to the bottom of specialised cell culture slides. Despite several attempts to improve cell adherence, through use of specialised chamber slides and optimisation of the staining protocol, the necessary cell adherence for a systematic evaluation of the experiments was not achieved. However, the experiments in Chapter 2 consistently indicated three events during *C. fleckeri* envenomation, 1) loss of cell adherence, 2) “condensed” nuclei and 3) loss of membrane

integrity. Loss of cell adherence and loss of membrane integrity following *C. fleckeri* envenomation have already been described, to some degree, in the literature [10-12]. By contrast, this is the first study to report nuclear condensation in the cardiomyocyte (or any other cell type) post *C. fleckeri* venom exposure. It was this nuclear condensation in combination with the loss of adherent properties that prompted the idea to conduct an apoptosis FACS assay in Chapter 3. The apoptosis assay was of particular interest because thus far only necrosis (of the skin), in accordance with the loss of membrane integrity, had been reported for *C. fleckeri* envenomation. However, the loss of membrane integrity in the Chapter 2 study was a conclusion drawn from the presence of propidium iodide (non-permeant cell stain) in the envenomed cardiomyocyte. Due to the putatively pore-forming properties of the venom, it was not clear if the propidium iodide entered the cells through the pores or because of necrosis induced cell membrane rupture. In an attempt to shed some light on whether the cells were undergoing necrosis or apoptosis (as suggested by the nuclear condensation) or perhaps neither following *C. fleckeri* envenomation, the apoptosis assay was carried out in Chapter 3. In conclusion, fluorescence microscopy is not an effective technique for analysing the effects of *C. fleckeri* venom on live cardiomyocytes, but indicated that apoptosis might be occurring, which was explored using flow cytometry in Chapter 3.

The overall objective of Chapter 3 was the characterisation of the toxins in the previously determined bioactive fractions CTF-α, CTF-β and CTF-γ from *C. fleckeri* venom. The specific aims of this chapter were 1) identifying whether or not the cardiotoxic *C. fleckeri* proteins CfTX-1 and -2 were present in these fractions, 2) conducting bioactivity assays to compare the effects of the venom and the fractions on different cell lines, 3) determining if apoptosis is a relevant type of cell death in *C. fleckeri* envenomation. This chapter was expected to provide

some of the missing links between previous proteomic and bioactivity studies on *C. fleckeri* venom and to identify potential molecular pathways of the different toxins.

All aims for chapter 3 were successfully completed and the study provided several new insights in terms of composition, bioactivity and molecular pathways impacted by *C. fleckeri* venom. The first aim, the characterization of the *C. fleckeri* fractions CTF-α, CTF-β and CTF-γ was performed by using Fast Protein Liquid Chromatography (FPLC) and mass spectrometry with a subsequent database search. The top two hits were CfTX-1 (176 unique peptides (UPs)) and CfTX-2 (145 UPs) for CTF-α, CaTX-A (340 UPs) and CfTX-1 (78 UPs) for CTF-β and CrTX-A (169 UPs) and CaTX-A (91 UPs) for CTF-γ. CTF-α showed the least toxic activity of all the fractions, despite the abundant presence of CfTX-1 and CfTX-2; two proteins suggested to be highly toxic [13]. CTF-β was the most cardiotoxic and CTF-γ the most haemolytic out of the tested fractions. The high abundance of CaTX-A in CTF-β suggests that this protein is responsible for the cardiotoxic activity, and similarly, the high abundance of CrTX-A in CTF-γ appears to be responsible for the haemolytic activity. Interestingly, all three fractions had the same top five database hits in differing order of abundance, all of which were proteins unique to the phylum Cnidaria. It appeared this difference in abundance of the top five proteins was the underlying cause for the differences observed amongst the fractions in the subsequent bioactivity assays, suggesting that each of these toxins has a distinct mode of action. However, the fact that the top hits were the same across fractions also suggests that the size exclusion column used on the FPLC may not be adequate in fully separating these proteins, most likely as a result of the similar molecular weights of the toxins. Additionally, it has been suggested that *C. fleckeri* toxins may form oligomeric complexes [8], which would likely contribute to molecular weight discrepancies and separation problems through size-exclusion. Further separation based on hydrophobicity or cation/anion exchange chromatography might improve

the separation, but was beyond the scope of the current study, as this study used a single (limited) source of venom for consistency and consequently further purification was not feasible at this stage of the project.

The second aim of chapter 3 was to explore the bioactivity of *C. fleckeri* venom and the three CTF-fractions. These bioactivity experiments were designed to answer two specific questions: a) Does *C. fleckeri* venom have a higher specificity for cardiac cells than other cells? b) Is *C. fleckeri* venom more toxic to murine blood than to human blood? These questions were successfully answered by showing that neither *C. fleckeri* venom, CTF-α nor CTF-β had a greater effect on cardiac cells compared to fibroblasts. Surprisingly, the CTF-γ fraction, that was previously described as non-cardiotoxic, displayed greater toxicity in cardiomyocytes than in fibroblasts. Further, it appears *C. fleckeri* venom is more toxic to murine than human erythrocytes, which provides the first experimental explanation for the haemolytic in vivo effects observed in mice but not in humans. The successful completion of this aim provided essential knowledge for the experimental designs and interpretation of future *C. fleckeri* venom studies.

The third aim of chapter 3 was to investigate the molecular pathways involved in *C. fleckeri* induced cardiomyocyte death using flow cytometry. The primary pathway investigated was apoptosis by screening for the presence of the apoptotic markers caspase-3 and phosphatidylserine (PS). The only fraction that tested positive for both caspase-3 activity and PS-binding, was CTF-γ, indicating the cells exposed to this fraction were apoptotic. CTF-α induced cell death appeared to act through caspase-3-independent pathways, thus not apoptosis. In contrast, CTF-β showed caspase-3 activity but no PS-binding suggesting the cardiomyocytes were in the early stages of apoptosis. Interestingly, *C. fleckeri* venom did not indicate caspase-3 activity, or PS-binding, suggesting that the primary molecular pathway of

C. fleckeri venom inducing cardiomyocyte death is not apoptosis at the concentrations and time point tested. While the primary cell death mechanism of the venom remains to be fully elucidated, the results from this chapter suggest that several cell death pathways are occurring during *C. fleckeri* envenomation, likely because of the many different toxins in the venom.

There are two reasons the focus was laid on apoptosis as a cell death pathway. Firstly, the results of chapter 2 suggested that this cell death pathway was worth investigating (e.g. nuclear condensation) and secondly, the knowledge on other types of cell death is still emerging, and consequently available tests are limited. Nevertheless, several new types of cell death are currently being defined [14-16], revealing new ways of investigation as research is progressing.

Chapter 4 focused on the structural characterization of two regions of *C. fleckeri* venom protein CfTX-1 that, based on sequence analysis, were predicted to form helical structures and suggested to be involved in membrane pore-formation during the envenomation process. The aim of this chapter was to validate these predictions by conducting the first structural analysis of regions of a *C. fleckeri* toxin.

The structural analysis in Chapter 4 was successfully carried out with the use of nuclear magnetic resonance spectroscopy (NMR-spectroscopy). The two predicted helical regions were synthesised into the peptides CfTX-$1_{22\text{-}47}$ and CfTX-$1_{73\text{-}100}$. The peptides were initially put in an aqueous solution, however CfTX-$1_{22\text{-}47}$ did not form a helical structure under these conditions and CfTX-$1_{73\text{-}100}$ appeared to aggregate. Two alternative solvents were available for the subsequent experiments; dimethyl sulfoxide (DMSO) and sodium dodecyl sulfate (SDS). The advantage of using DMSO is that this solvent can be used for bioactivity studies, but it does not provide the membrane-mimicking environment of SDS. Previous studies predicted that the region of CfTX-1 corresponding to CfTX-$1_{73\text{-}100}$ was a trans-membrane-spanning

region and thus SDS, also with its membrane-mimicking properties, was considered the more relevant solvent for this structural analysis. The resulting structures of CfTX-1_{22-47} and CfTX-1_{73-100} in SDS were indeed of helical nature, and thus provided the first experimental structural evidence towards a potentially pore-forming mode of action for CfTX-1.

In summary, my thesis has illustrated the complexity of working with *C. fleckeri* venom and has provided several links across studies in the existing literature. My thesis has also provided a first experimental structural analysis, the results of which should facilitate future attempts of structural characterisation of *C. fleckeri* (and other cnidarian) toxins.

5.2. Future directions

Perhaps the most critical future direction is the assembly of the transcripts from the *C. fleckeri* transcriptome analysis in order to create a publicly available library *C. fleckeri* venom proteins. This would enable the confident identification of relevant toxins of bioactive fractions such as the CTF's in Chapter 3 and consequently help identify key protein toxins for the mechanism of action of *C. fleckeri* venom. Further, it would perhaps be beneficial to conduct a series of transcriptome analysis on *C. fleckeri* venom from different geographical locations, thereby enabling the further description of geographical differences amongst venom samples. This might have implications for future studies and in particular, for antivenom production.

Another avenue that may be of benefit to explore, would be the sequencing of the *C. fleckeri* genome. The application of the *C. fleckeri* genome would be influential in many research fields that affect the management of this species. Phylogenetic studies could finally address the missing links relating to the evolution of the potent toxins found in cubozoan venoms. Life cycle studies would gain a better understanding of the different developmental stages of *C.*

fleckeri and potentially provide some clues to the environmental requirements of these stages. Currently very little is known about where *C. fleckeri* jellyfish are when they are not in the medusa stage. Such information would greatly facilitate the management of the species and, perhaps more importantly, it would open the door for captive breeding programs, which are helpful for genetic manipulation studies on venom expression.

Another possible direction for *C. fleckeri* venom studies could be the use of recombinant protein expression systems. Protein expression systems would eliminate the need to separate the complex *C. fleckeri* venom sample by chromatography. However, Dr. Diane Brinkman attempted the expression of CfTX-1 and -2 in an *Escherichia coli* system during her PhD and while the expression was completed, the yield of the recombinant proteins was too low to conduct subsequent functional and structural studies. She also raised the issue that expressed proteins formed insoluble inclusion bodies that would have to be solubilised and then refolded prior their use in bioactivity studies.

In terms of structural studies, many avenues are still to be unexplored. Chapter 4 illustrated some of the potential challenges associated with the successful structural analysis of *C. fleckeri* toxins by NMR spectroscopy, but it particularly highlighted the need for method expansion of such studies. Perhaps NMR spectroscopy could be combined with X-ray crystallography and *de novo* structure predictions.

Finally, for the elucidation of the molecular pathways of *C. fleckeri* venom, SWATH-mass spectrometry could be a method worth exploring. SWATH (Sequential Window Acquisition of all THeoretical spectra) is a mass spectrometry method with the capacity to analyse inherently dynamic biological processes in perturbed systems (e.g. the cell) [17]. SWATH is

able to generate accurate, reproducible and complete data on complex protein networks [17] by producing a permanent record of almost every single peptide fragment in the sample [18]. Thus, SWATH is a only high-throughput method that can reliably quantify temporal changes in protein networks. Recently, the expression of over 3600 proteins in uninfected and HIV-1 infected monocyte-derived macrophages was successfully identified and quantified, while revealing that 420 of these proteins were severely altered upon HIV infection [17]. This HIV study indicates that SWATH methods hold strong potential to analyse the effects of *C. fleckeri* venom treatment on heart cells. Although SWATH currently requires a high level of expertise, it is developing into an accessible pipeline for systems biology studies and is worth testing in other biological fields such as toxicology.

A greater understanding of the components in *C. flekeri* venom and their roles in the envenomation process could ultimately lead to better treatments. Furthermore, the discovery of novel toxins will add to the expanding library of bioactive marine toxins, which is proving to be a valuable resource for dissecting pharmacological pathways and developing novel drug leads.

5.3. References

1. Baxter, E.; Marr, A. Sea wasp (*Chironex fleckeri*) venom: lethal, haemolytic and dermonecrotic properties. *Toxicon* **1969**, *7*, 195-210.
2. Mustafa, M.; White, E.; Hongo, K.; Othman, I.; Orchard, C. The mechanism underlying the cardiotoxic effect of the toxin from the jellyfish *Chironex fleckeri*. *Toxicology and Applied Pharmacology* **1995**, *133*, 196-206.
3. Saggiomo, S.L.; Seymour, J.E. Cardiotoxic effects of venom fractions from the Australian box jellyfish *Chironex fleckeri* on human myocardiocytes. *Toxicon* **2012**, *60*, 391-395.
4. Bordehore, C.; Nogué, S.; Gili, J.M.; Acevedo, M.J.; Fuentes, V.L. *Carybdea marsupialis* (Cubozoa) in the mediterranean sea: the first case of a sting causing cutaneous and systemic manifestations. *Journal of Travel Medicine* **2015**, *22*, 61-63.
5. Brinkman, D.L.; Burnell, J.N. Biochemical and molecular characterisation of cubozoan protein toxins. *Toxicon* **2009**, *54*, 1162-1173.
6. Nagai, H.; Takuwa-Kuroda, K.; Nakao, M.; Oshiro, N.; Iwanaga, S.; Nakajima, T. A novel protein toxin from the deadly box jellyfish (sea wasp, habu-kurage) *Chiropsalmus quadrigatus*. *Bioscience Biotechnology and Biochemistry* **2002**, *66*, 97-102.
7. Yanagihara, A.A.; Shohet, R.V. Cubozoan venom-induced cardiovascular collapse is caused by hyperkalemia and prevented by zinc gluconate in mice. *Plos one* **2012,** *7(12),* e51368.
8. Brinkman, D.L.; Konstantakopoulos, N.; McInerney, B.V.; Mulvenna, J.; Seymour, J.E.; Isbister, G.K.; Hodgson, W.C. *Chironex fleckeri* (box jellyfish) venom proteins expansion of a cnidarian toxin family that elicits variable cytolytic and cardiovascular effects. *Journal of Biological Chemistry* **2014**, *289*, 4798-4812.
9. Brinkman, D.L.; Jia, X.; Potriquet, J.; Kumar, D.; Dash, D.; Kvaskoff, D.; Mulvenna, J. Transcriptome and venom proteome of the box jellyfish *Chironex fleckeri*. *BMC Genomics* **2015**, *16*, 407.
10. Chaousis, S.; Smout, M.; Wilson, D.; Loukas, A.; Mulvenna, J.; Seymour, J. Rapid short term and gradual permanent cardiotoxic effects of vertebrate toxins from *Chironex fleckeri* (Australian box jellyfish) venom. *Toxicon* **2014**, *80*, 17-26.
11. Andreosso, A.; Smout, M.J.; Seymour, J.E. Dose and time dependence of box jellyfish antivenom. *Journal of Venomous Animals and Toxins including Tropical Diseases* **2014**, *20*, 34.
12. Bailey, P.M.; Bakker, A.J.; Seymour, J.E.; Wilce, J.A. A functional comparison of the venom of three Australian jellyfish - *Chironex fleckeri*, *Chiropsalmus sp.*, and *Carybdea xaymacana* - on cytosolic Ca^{2+}, haemolysis and *Artemia sp.* lethality. *Toxicon* **2005**, *45*, 233-242.
13. Brinkman, D.; Burnell, J. Identification, cloning and sequencing of two major venom proteins from the box jellyfish, *Chironex fleckeri*. *Toxicon* **2007**, *50*, 850-860.

14. Elmore, S. Apoptosis: A review of programmed cell death. *Toxicological Pathology* **2007**, *35*, 495-516.
15. Kroemer, G.; Martin, S.J. Caspase-independent cell death. *Nature Medicine* **2005**, *11*, 725-730.
16. Orrenius, S.; Nicotera, P.; Zhivotovsky, B. Cell death mechanisms and their implications in toxicology. *Toxicological Sciences* **2011**, *119*, 3-19.
17. Haverland, N.A.; Fox, H.S.; Ciborowski, P. Quantitative proteomics by SWATH-MS reveals altered expression of nucleic acid binding and regulatory proteins in HIV-1-infected macrophages. *Journal of Proteome Research* **2014**, *13*, 2109-2119.
18. Marx, V. Targeted proteomics. *Nature Methods* **2013**, *10*, 19-22.

Appendix

Appendix 1. Sequences of *C. fleckeri* toxins CfTX-1 and CfTX-2. The sequences were aligned to visualize the level of homology (71%) between the sequences. The signal peptide sequences are highlighted in grey.

```
CfTX-1 MVKMLFFAFLPLLFMTGIAAESTISSGLNSLKTKIDAKMPSGKQLFDKVVEMQKQIDAKF 60
CfTX-2 ---MILVSLLPLLFMTGIASESTISSGLASLKAKIDIKKPTGKQLFDKVKSMEQALENKF 57
          *:::.::**********:******** ***:*** * *:******** .*:: :: **

CfTX-1 SNDDERAKVMGAIGSLSTAVGKFQSGDPAKIASGCLDILVGISSVLKDFAKFSPIFSILS 120
CfTX-2 SDDDERAKVMGAIGSLGTAIGKFQSGDPASIASGCLDILVGISSVLKDFAKFSPVFSILS 117
       *:**************.**:*********.*************************:*****

CfTX-1 LVVGLFSGTKAEESVGSVVKKAVQEQSDQELQEALYGVKREYAVSKAFLDGVRNETSDLS 180
CfTX-2 LVVGLFSGTKAEESVSSVVTKAIQEQSDQELQEALYGVKREFAVSKAFLDGVRNEESDLR 177
       ***************.***.**:******************:************* ***

CfTX-1 PTEVSALAANVPIYQGVRFIAMVVQRIKYIKPKTESEIKRMLTMLELFTDLCSLRDLILL 240
CfTX-2 PTEVSALAANIPVYQGVRFIAMVVQRIKYIKPKTESEIKRMLTMLELFTDLCSIRDLILL 237
       **********:*:*******************************************:******

CfTX-1 DLYQLVATPGHSPNIASGIKEVSNLGREEYKKVFEDLLKNDDKETYLFLSYLYPREKNEQ 300
CfTX-2 DLHQLIATPGHSPNIASGIKEVTSLGREEYQRVFEDLLKTDDEETFLFLSYLYPKEKNEQ 297
       **:**:****************:.******::*******.**:**:********:*****

CfTX-1 SRKIFNFFDLMKVKYDDRLKQDLTGVKIFSNVHWPNYFMCSSNDYLALICTKPYGSLKLD 360
CfTX-2 SRKIFKFFDLIEVKYDDRFKLDLSGGQALSTLQWPNYYLCPHNDYLANNCHDLRVGLKLE 357
       *****:****::*******:* **:* : :*.::****::*  *****  * .   .***:

CfTX-1 KLNDGYYSIKTTQHDPKICHRYGNYILFTHKRNDDLEKFNFVPVKLEKREIYLLSSKESP 420
CfTX-2 KLSDGFYTIKTYGRDPRTCYWTDDYVKISSTSNGELEKFSFVPVQVKGQKAYLLSTKKWP 417
       **.**:*:***  :**: *:  .:*: :: . *.:****.****::: :: ****:*: *

CfTX-1 NKFAYVPQNADGALFFVDGIPSKVGYGNQGYFTLVE--------- 456
CfTX-2 HNFAYSQKTANGLLSILKDVPSKLGYGNQGFFTISTYSNPKNRHA 462
       ::***  :.*:* * ::..:***:******:**:
```

–	(dash) indicates an introduced gap for better alignment
*	(asterix) indicates positions which have a single, fully conserved residue.
:	(colon) indicates conservation between groups of strongly similar properties - scoring > 0.5 in the Gonnet PAM 250 matrix
.	(period) indicates conservation between groups of weakly similar properties - scoring =< 0.5 in the Gonnet PAM 250 matrix.